Doctoral Dissertation (Shinshu University)

Study on development of highly conductive materials via electroless deposition technique for advance wearable devices

(先端ウェアラブル機器のための無電解蒸着技術を通じた高伝導性材料の開発に関する研究)

September 2021

HUSSAIN NADIR

Abstract

Study on development of highly conductive materials via electroless deposition technique for advance wearable devices.

Recently, characteristics and synthesis of nanomaterials specially nanofibers into membrane are getting intensive attraction to explore potential applications that can work under mechanical deformation such as medical implants, flexible and wearable electronics, energy storage, electronic skins, sensors, biological actuators, deformable capacitors, and antennas, and point of care diagnostics. Nanofibers are being widely used because of their unique characteristics, fine diameter, high surface area and multifunctional properties such as biomedical, surgical, filtration, tissue engineering, membranes engineering, sensors, but their electrical properties such as electroconductive properties has remain challenge for researcher. In the past a wide range of polymers and facile techniques are used to fabricated high-performance conductive materials. However, in consideration of electroconductive performance, low cost, metal has remains first choice of materials.

In the view of above, the most effective approaches have been used to fabricate the conductive material. Here in, we report a versatile, novel, and easy approach to fabricate highly durable and electrically conductive aramid nanofibers (ANFs). The ANFs were firstly fabricated via electrospinning and afterward, the conductive ANFs were prepared using electroless deposition (ELD) technique. The copper (Cu) metal was used to prepare conductive ANFs due to its significant advantages i.e. conductance. During the ELD process, parameters including time and temperature were studied to optimize proper deposition and performance. The optimized ANFs samples were characterized by FE-SEM, EDX, XRD, XPS, FTIR, TGA, water contact angle, and electrical conductance. Copper (Cu) deposition on ANFs achieved high electrical conductivity. The as ANFs shows good candidate for copper (Cu) deposition and provide good stability in terms of electrical conductance. The as-prepared Cu-ANFs could

be used in various applications such as wearable electronics, flexible displays, and energy storage.

Plastic bottles are generally recycled by remolding them into numerous products. In this study, waste from plastic bottles was used to fabricate recycled polyethylene terephthalate (r-PET) nanofibers via the electrospinning technique, and high-performance conductive polyethylene terephthalate nanofibers (r-PET nanofibers) were prepared followed by copper deposition using the electroless deposition (ELD) method. Firstly, the electrospun r-PET nanofibers were chemically modified with silane molecules and polymerized with 2-(methacryloyloxy) ethyl trime-thylammonium chloride (METAC) solution. Finally, the copper deposition was achieved on the surface of chemically modified r-PET nanofibers by simple chemical/ion attraction. The water contact angle of r-PET nanofibers, chemically modified r-PET nanofibers, and copper deposited nanofibers were 140o, 80o, and 138o, respectively. The r-PET nanofibers retained their fibrous morphology after copper deposition, and EDX results confirmed the presence of copper on the surface of r-PET nanofibers. XPS was performed to analyze chemical changes before and after copper deposition on r-PET nanofibers. The successful deposition of copper one r-PET nanofibers showed an excellent electrical resistance of 0.1 ohms/cm and good mechanical strength according to ASTM D-638.

On other hand, we report the synthesis of conductive Nylon 6 nanofibers (N6 NFs) using the electroless deposition (ELD) method. We fabricated the N6 NFs by electrospinning technique and modified the surface with [2-(methacryloyloxy) ethyl] trimethylammonium chloride (PMETAC). After surface modification of N6 NFs, copper metal was successfully deposited using the ELD process. Parameters including time, temperature, volume, and pH concentration were optimized for copper deposition. SEM images revealed smooth morphology of neat N6 NFs and copper-coated N6 NFs. EDX spectrum was performed on neat N6 NFs and copper-coated N6 NFs to ensure the qualitative and quantitative presence of copper

nanoparticles. Furthermore, advance characterization methods such as FTIR, XPS, water contact angle, and tensile strength were performed to analyze the successful copper deposition on N6 NFs.

One of the contributions of nanotechnology to our daily life is the preparation of a large variety of polymer-based nanofibers which could be the basis of future wearable devices. Wearable electronics are a great part of smart textiles research. Herein, we have reported an easy method to fabricate electrically conductive cellulose nanofibers (CNFs). To fabricate CNFs, we firstly prepared cellulose acetate nanofibers (CANFs) by using the electrospinning technique and later, the deacetylation process was done to obtain the CNFs. The electroless deposition (ELD) technique was then used to create the conductive nanofibers. Copper (Cu) was used to coat the CNFs because of their high conductivity and low cost. The ELD process parameters including time, temperature, volume, and pH were optimized to obtain a nanofiber with higher conductivity. The optimized condition was temperature: 40℃, time: 10 min, volume: 600 ml, and pH: 13 to obtain a nanofiber web with 983.5 S/cm conductivity. Cu coated CNFs were characterized by Scanning Electron Microscope (SEM), Energy-dispersive X-ray spectroscopy (EDS), Fourier-transform infrared spectroscopy (FTIR), water contact angle (WCA), antibacterial activity, tensile, and electrical conductivity. The bending cycle test was performed to quantitatively demonstrate the durability and flexibility of the Cu coated nanofibers. Cu-coated CNFs exhibited great performance to be used as a conductive layer with antibacterial activity..

TABLE OF CONTENTS

Study on Development of Highly Conductive Materials Via Electroless Deposition Technique for Advance Wearable Devices.

List of figures

List of tables

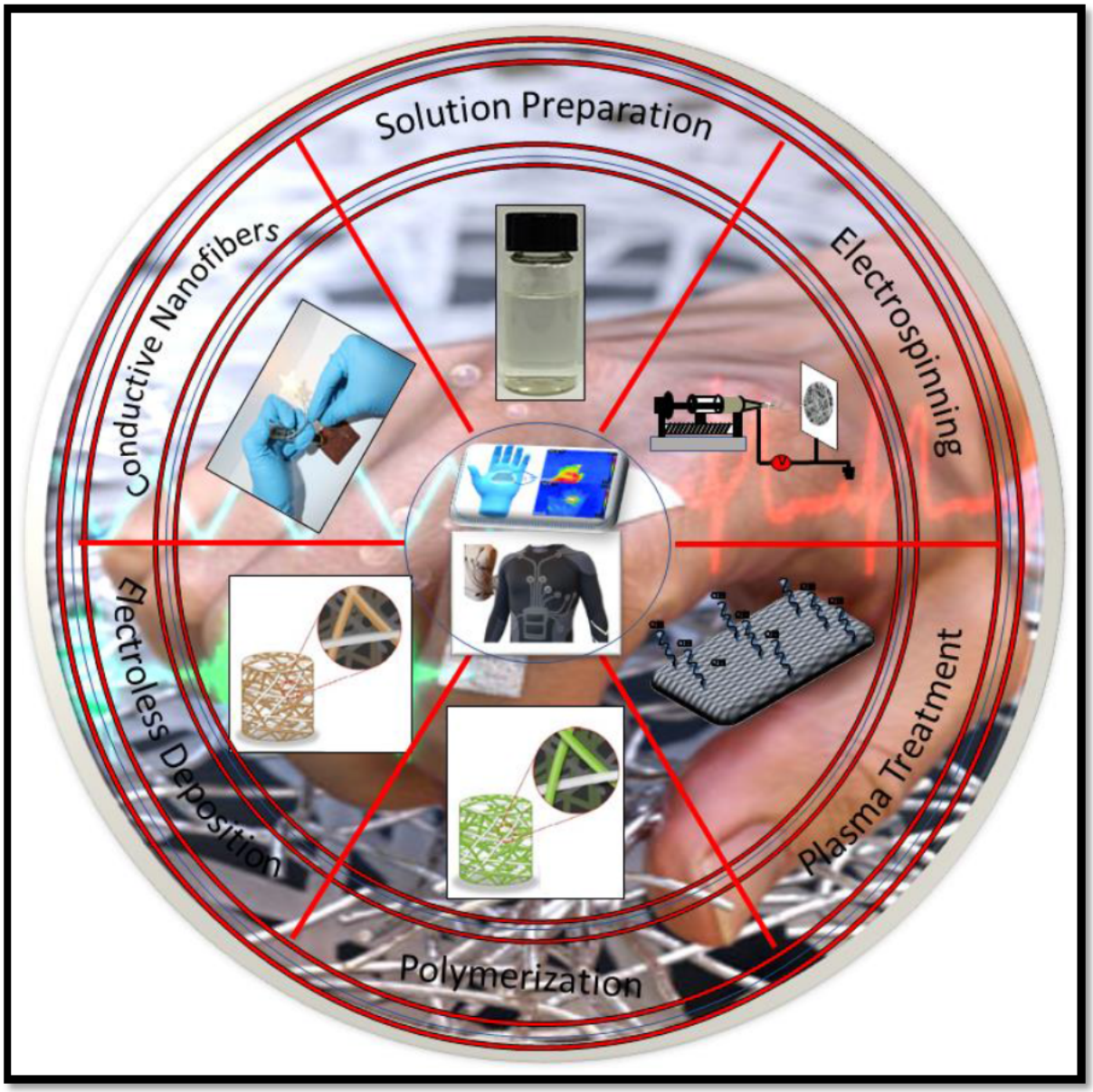

Figure 1. Scheme diagram of Conductive Materials Via Electroless Deposition Technique

Recently, high performance technologies in the field of energy and advanced electronics demands the ability to control features at the nanoscale 10^{-9} m [1]. Automotive, aerospace, sports, cosmetics, , and smart textiles require the use of such materials with suitable properties viz. Chemical/heat/corrosion resistance, mechanical strength, and presence of funtional groups on the surface to perfom/assess the significant funtional applications [2-8].

To improve materials performance a substantial flexiblity with suitable electroconductivity is required to prepare a wearable electronics with functions such as energy storage, skin implantable electronics, sensors, biological actuators, and deformable capacitors [9-11], and in past, most research can be found mainly on incorporation of conductive materials such as metal [12], carbon materials [13], nanoparticles [14], nanowires [15], and conducting polymers into flexible, stretchable, and wearable substrates [16-18], where metals are still considered as the first choice of material to impart electroconductive properties in advanced materials because of their high conductivity, stability, and low cost [19].

Generally, metals are rigid, but they become very flexible, stretchable, and thin when structured into proper shapes. vacuum deposition [20], resist casting [21], patterning [22], pattern transfer through etching [23], and lift-off are some common approaches that had been used in past for depositing thin metal conductors on different soft substrates. When it comes to depositing thin metal conductors on polymeric substrates especially elastomers, it arose some serious challenges as such substrates have poor dimensional stability when exposed to heat, organic solvent environments, or vacuum[24].

This problem had been partially solved by researchers by using the transfer printing technique [22]. In this technique, transfer patterns that are pre-defined on a mother Si wafer to a targeted polymeric substrate in a pick-and-print manner [16]. Addiotnally, in printable electronics, some researchers have applied roll-to-roll strategies which use solution-based

processes rather than vacuum-based technologies. In this technique, low-cost printing tools such as inkjet and screen printers are used to directly deposit the thin metal conductors on different substrates such as plastics, elastomers, papers, and textiles [25].

The established technology in roll-to-roll strategies is printing inks of metal nanoparticles or precursors onto soft substrates, followed by thermal annealing and/or chemical reduction. However, drawbacks in these approaches include the need of post-thermal annealing and the difficulty in fabricating Cu interconnects with high conductivity[22]. polymer-assisted metal deposition (PAMD), has also been used to fabricate flexible, foldable, stretchable, compressible, and wearable metal (especially Cu) conductors with very high conductivity [24].

Synthetic and natural polymers and blends of these polymers can be used in this method. Nanofibers have been utilized for a variety of advanced applications. Due to their lightweight, the flexibility of function, three-dimensional structure, and ease of production using the electrospinning method [25]. Nanofibers have been utilized for aerospace, advanced wearable devices, smart electronics, advanced apparel, environmental, biomedical, sensor, agriculture, tissue engineering, filtration, batteries, cosmetics, food, pharmaceutical but there is still a big research gap to be addressed.

Textile-based flexible devices have many advantages over conventional conductive materials. But low surface area and high porosity are the main drawback of Textile based devices, which can limit metal deposition rate. On the other hand, Electrospun nanofibers can be the alternative to Textile-based flexible devices as nanofibers have a high surface area and they can create a high metal deposition which can ultimately cause our product more conductive. In addition, nanofibers also have gained adequate attention because of sufficient availability, higher mechanical strength, flexibility, thermal resistance, chemical resistance,

lightweight, and three-dimensional structure. Keeping well properties of nanofibers, the aim of this research to develop the flexible and highly conductive the nanofibers with different polymers.

1.1 Electrospun Nanofibers

There are various methods of nanofibers production. One of the most flexible and cost-effective is electrospinning. It is an efficient technique that produces continuous nanofibers with lengths in the range of 5–100 nm. These fibers are 100–10000 times smaller than fibers fabricated by solution or melt spinning [26-30]. Electrospun nanofibers are created from electrically charged jets of polymer solution or polymer melt. A typical electrospinning scheme is given in Figure 02.

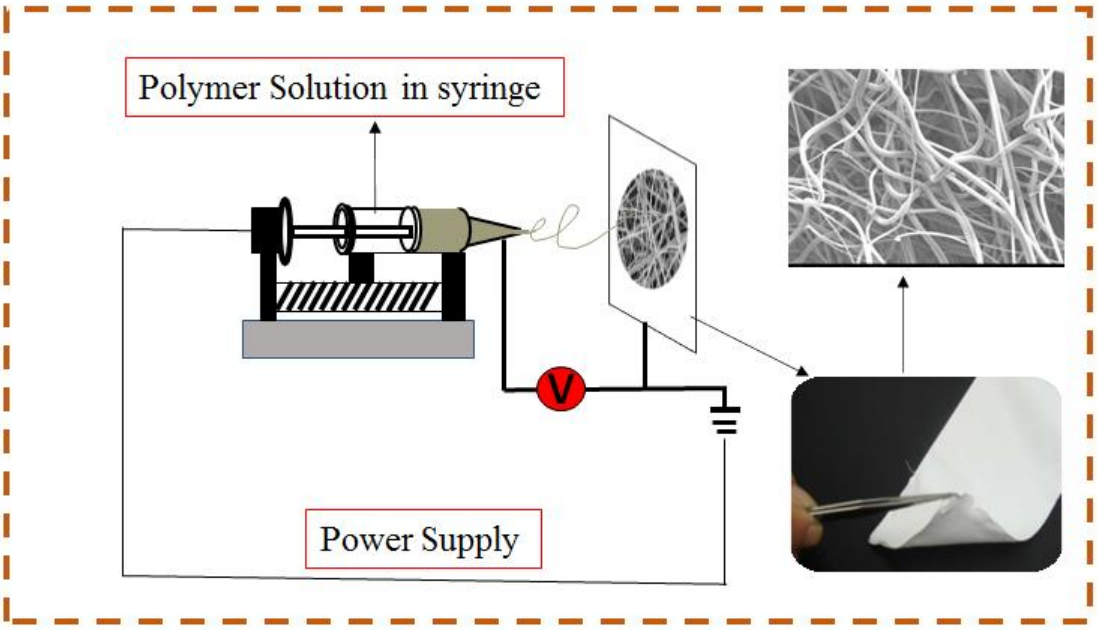

Figure 02. Scheme diagram of electrospinning

1.2 Electroless Deposition

The deposition of a metallic coating by a controlled chemical reduction that is catalyzed by the metal or alloy being deposited is called electroless deposition. In this method, selective reduction of metal ions at the surface of a catalytic substrate immersed into an aqueous solution of those metal ions is happened [24]. The deposition takes place continuously on the substrate through the catalytic action of the deposit itself. This process has been used to produce deposits of Ni, Co, Cu, and Ag as well as some alloys containing these metals plus P or B.

In the past, some common metals including gold (Au), silver (Ag), copper (Cu) and nickel (Ni) metals, were used to develop a soft device by using ELD method. The high electrical conductivity at low cost is a fundamental requirement for any metal electrode device.Considering the conductivity to cost ratio, copper metal is a better choice as compared to noble metals (Au, Ag, Pt, and Pd) [25]. The Cu is a typical transition metal, exhibiting a significantly higher electrical conductivity that is only 6% lower than Ag but has an outstanding conductivity to cost ratio. Because of these unique properties such as excellent conductivity and corrosion resistance, electroless deposition of copper is one of the most important metal that can be deposited by using ELD process [25]. Wang et al. have successfully developed conductive fabric from cotton while depositing Cu metals using the ELD technique. Coating of nanofiber surface with Cu metal as conductive material can increase the conductivity and performance of nanofibers. In this research work we have successfully developedhighly conductive nanofibers by using electroless deposition of Cu.

1.3 Conductive Nanofibers

Nanofibers from any polymer, which can be synthetic or natural can be produced by electrospinning with sizes at the nanoscale [31]. Flexible and highly conductive nanofibers will be widely applied in the flexible consumer electronics, smart clothing, energy harvesting, and sensors in the future. In the recent conductive nanofibers not only must retain their high-performance such as conductivity, flexibility, but also have light weight, low cost, and capability for large-scale manufacturing. Most importantly, these materials should have environmentally friendly features. However, traditional conductive films (such as ITO) cannot fulfill the requirements of the next-generation flexible electronic device because of low surface and high porosity. In this study, flexible conductive nanofibers have been successfully prepared with different polymers such as aramid, cellulose via ELD technique. These prepared nanofibers have been utilized for aerospace, wearable devices, advanced apparel, environmental, biomedical, sensor, solar cell, batteries, and fuel cell.

1.4 Objectives

Conclusively, the main object of our research to reduce the metal consumption from electronic and advance textile industry. Furthermore, aim of our research is to promote the fabrication, optimization, synthesis, and structural/physicochemical analysis of functionality and advancement of electrospun nanofibers related to potential applications for advance wearable devices.

The main objectives of the research are listed below;

Our research group is working on various applications of nanofibers,

1- chapter of dissertation are: A novel, and easy approach to fabricate highly durable and electrically conductive aramid nanofibers (ANFs). We successfully prepared highly durable and electrically conductive aramid nanofibers (ANFs). Copper metal particles were deposited on aramid nanofibers by electroless deposition. This study was approach in wearable electronics, flexible displays, and energy storage.

2- Chapter of dissertation are: Plastic bottles are generally recycled by remolding them into numerous products. In this study, Synthesis of Highly Conductive Electrospun r-PET Nanofibers. Waste from plastic bottles was used to fabricate recycled polyethylene terephthalate (r-PET) nanofibers via the electrospinning technique, and high-performance conductive polyethylene terephthalate nanofibers (r-PET nanofibers) were prepared followed by copper deposition using the electroless deposition (ELD) method. It would be greatly helpful towards the environmental issue of waste drinking bottles and played significant role in the field of electronic technology.

3- Chapter of dissertation are: In this study, we tried to modify the surface properties of Nylon-6 nanofibers. And take advance of nylon 6 properties because of its ease of production, eco-friendly character, economic viability, unique molecular structure, suitable transition temperature, and mechanical properties. We report the synthesis of conductive Nylon 6 nanofibers (N6 NFs) using the electroless deposition (ELD) method and fabricated the N6 NFs by electrospinning technique and modified the surface of Nylon 6 nanofibers with [2-(methacryloyloxy) ethyl] trimethylammonium chloride (PMETAC). After surface modification of N6 NFs, copper metal was successfully deposited using the ELD process. Thus, our proposed material copper-coated N6 NFs can be used in many electrical applications such as flexible and wearable devices.

4- Chapter of dissertation are: We tried to bring the multifunctional properties such as flexible conductive and antibacterial activities on cellulose nanofibers by deposition of copper to the nanofibrous platform. Cellulose is an abundant natural polymer which has attracted more and more interest from academia and industry. The work introduces unique technique to decorate cellulose nanofibers with metal copper nanoparticles and assesses the flexible conductive and antibacterial effects of the resulted composite nanofibers. The results demonstrated that the Cu-coated cellulose nanofibers could be a great candidate for wearable electronics for biomedical application.

References

[1] Ramesh, K.T., 2009. Nanomaterials. In Nanomaterials (pp. 1-20). Springer, Boston, MA.

[2] Joshi, M. and Bhattacharyya, A., 2011. Nanotechnology–a new route to high-performance functional textiles. Textile Progress, 43(3), pp.155-233.

[3] Sabantina, L., 2021. Nanocarbons-based textiles for flexible energy storage. In Nanosensors and Nanodevices for Smart Multifunctional Textiles (pp. 163-188). Elsevier.

[4] Mazari, S.A., Ali, E., Abro, R., Khan, F.S.A., Ahmed, I., Ahmed, M., Nizamuddin, S., Siddiqui, T.H., Hossain, N., Mubarak, N.M. and Shah, A., 2021. Nanomaterials: Applications, waste-handling, environmental toxicities, and future challenges-A Review. Journal of Environmental Chemical Engineering, p.105028.

[5] Taylor, A.A., Freeman, E.L. and van der Ploeg, M.J., 2021. Regulatory developments and their impacts to the nano-industry: A case study for nano-additives in 3D printing. Ecotoxicology and Environmental Safety, 207, p.111458.

[6] Barik, T.K., Maity, G.C., Gupta, P., Mohan, L. and Santra, T.S., 2021. Nanomaterials: An Introduction. Nanomaterials and Their Biomedical Applications, 16, p.1.

[7] uzamil Khatri, Nadir Hussain, Sofia El-Ghazali, Takayuki Yamamoto, Shunichi Kobayashi, Zeeshan Khatri, Farooq Ahmed, and Ick Soo Kim "Ultrasonic-assisted dyeing of silk fibroin nanofibers: an energy-efficient coloration at room temperature" Applied Nanoscience (2019) 1-14

[8] Mujahid Mehdi, Faraz Khan Mahar, Umair Ahmed Qureshi, Muzamil Khatri, Zeeshan Khatri, Farooq Ahmed, Ick Soo Kim “Preparation of colored recycled polyethylene terephthalate nanofibers from waste bottles: Physicochemical studies” Advances in Polymer Technology (2018), 37 (8), 2820-2827

[9] Li, X., Chen, X., Jin, Z., Li, P. and Xiao, D., 2021. Recent progress in conductive polymers for advanced fiber-shaped electrochemical energy storage devices. Materials Chemistry Frontiers, 5(3), pp.1140-1163.

[10] Wang, H., Biswas, S.K., Zhu, S., Lu, Y., Yue, Y., Han, J., Xu, X., Wu, Q. and Xiao, H., 2020. Self-healable electro-conductive hydrogels based on core-shell structured nanocellulose/carbon nanotubes hybrids for use as flexible supercapacitors. Nanomaterials, 10(1), p.112.

[11] Chen, R., Huang, X., Deng, W., Zheng, R., Aftab, W., Shi, J., Xie, D., Zou, R. and Mei, Y., 2020. Facile preparation of flexible eicosane/SWCNTs phase change films via colloid aggregation for thermal energy storage. Applied Energy, 260, p.114320.

[12] Yoon, S., Kim, Y.J., Lee, Y.R., Lee, N.E., Won, Y., Gandla, S., Kim, S. and Kim, H.K., 2021. Highly stretchable metal-polymer hybrid conductors for wearable and self-cleaning sensors. NPG Asia Materials, 13(1), pp.1-14.

[13] Sedighi, A., Taheri, R.A. and Montazer, M., 2020. High-Performance Electromagnetic Interference Shielding Electrodes/Substrates for Wearable Electronics. Industrial & Engineering Chemistry Research, 59(28), pp.12774-12783.

[14] Chiu, C.W., Li, J.W., Huang, C.Y., Yang, S.S., Soong, Y.C., Lin, C.L., Lee, J.C.M., Sanchez, W.A.L., Cheng, C.C. and Suen, M.C., 2020. Controlling the structures, flexibility, conductivity stability of three-dimensional conductive networks of silver nanoparticles/carbon-based nanomaterials with nanodispersion and their application in wearable electronic sensors. Nanomaterials, 10(5), p.1009.

[15] Tao, T., Liu, X., Islam, A., Wu, J., Ni, Y., Huang, L., Chen, L., Ouyang, X. and Li, J., 2020. Flexible and Conductive Cellulose Substrate by Layered Growth of Silver Nanowires and Indium-doped Tin Oxide. BioResources, 15(3), pp.4699-4710.

[16] Baeg, K.J. and Lee, J., 2020. Flexible Electronic Systems on Plastic Substrates and Textiles for Smart Wearable Technologies. Advanced Materials Technologies, 5(7), p.2000071.

[17] Kraft, U., Molina-Lopez, F., Son, D., Bao, Z. and Murmann, B., 2020. Ink development and printing of conducting polymers for intrinsically stretchable interconnects and circuits. Advanced Electronic Materials, 6(1), p.1900681.

[18] Sedighi, A., Taheri, R.A. and Montazer, M., 2020. High-Performance Electromagnetic Interference Shielding Electrodes/Substrates for Wearable Electronics. Industrial & Engineering Chemistry Research, 59(28), pp.12774-12783.

[19] Baeg, K.J. and Lee, J., 2020. Flexible Electronic Systems on Plastic Substrates and Textiles for Smart Wearable Technologies. Advanced Materials Technologies, 5(7), p.2000071.

[20] Shin, J., Jeong, B., Kim, J., Nam, V.B., Yoon, Y., Jung, J., Hong, S., Lee, H., Eom, H., Yeo, J. and Choi, J., 2020. Sensitive wearable temperature sensor with seamless monolithic integration. Advanced Materials, 32(2), p.1905527.

[21] Garg, A., Nam, W. and Zhou, W., 2020. Reusable Surface-Enhanced Raman Spectroscopy Membranes and Textiles via Template-Assisted Self-Assembly and Micro/Nanoimprinting. ACS Applied Materials & Interfaces.

[22] Matzeu, G., Mogas-Soldevila, L., Li, W., Naidu, A., Turner, T.H., Gu, R., Blumeris, P.R., Song, P., Pascal, D.G., Guidetti, G. and Li, M., 2020. Large-Scale Patterning of Reactive Surfaces for Wearable and Environmentally Deployable Sensors. Advanced Materials, 32(28), p.2001258.

[23] Jo, S., Cho, S., Yang, U.J., Hwang, G.S., Baek, S., Kim, S.H., Heo, S.H., Kim, J.Y., Choi, M.K. and Son, J.S., 2021. Solution-Processed Stretchable Ag2S Semiconductor Thin Films for Wearable Self-Powered Nonvolatile Memory. Advanced Materials, p.2100066.

[24] Hussain, F., Jeong, J., Park, S., Jeong, E., Kang, S.J., Yoon, K. and Kim, J., 2020. Fabrication and characterization of a novel terpolyester film: An alternative substrate polymer for flexible electronic devices. Polymer, 210, p.123019.

[25] Yu, Y., Yan, C. and Zheng, Z., 2014. Polymer-Assisted Metal Deposition (PAMD): A Full-Solution Strategy for Flexible, Stretchable, Compressible, and Wearable Metal Conductors. Advanced Materials, 26(31), pp.5508-5516.

[26] Hussain, N., Mehdi, M., Yousif, M., Ali, A., Ullah, S., Hussain Siyal, S., Hussain, T. and Kim, I.S., 2021. Synthesis of Highly Conductive Electrospun Recycled Polyethylene Terephthalate Nanofibers Using the Electroless Deposition Method. Nanomaterials, 11(2), p.531.

[27] Hussain, N., Yousif, M., Ali, A., Mehdi, M., Ullah, S., Ullah, A., Mahar, F.K. and Kim, I.S., 2020. A facile approach to synthesize highly conductive electrospun aramid nanofibers via electroless deposition. Materials Chemistry and Physics, 255, p.123614.

[28] Hussain, N., Ullah, S., Sarwar, M.N., Hashmi, M., Khatri, M., Yamaguchi, T., Khatri, Z. and Kim, I.S., 2020. Fabrication and Characterization of Novel Antibacterial Ultrafine Nylon-6 Nanofibers Impregnated by Garlic Sour. Fibers and Polymers, 21(12), pp.2780-2787.

[29] Ullah, S., Hashmi, M., Hussain, N., Ullah, A., Sarwar, M.N., Saito, Y., Kim, S.H. and Kim, I.S., 2020. Stabilized nanofibers of polyvinyl alcohol (PVA) crosslinked by unique method for efficient removal of heavy metal ions. Journal of Water Process Engineering, 33, p.101111.

[30] Hashmi, M., Ullah, S., Ullah, A., Khan, M.Q., Hussain, N., Khatri, M., Bie, X., Lee, J. and Kim, I.S., 2020. An optimistic approach “from hydrophobic to super hydrophilic nanofibers” for enhanced absorption properties. Polymer Testing, 90, p.106683.

[31] Muzamil Khatri, Nadir Hussain, Sofia El-Ghazali, Takayuki Yamamoto, Shunichi Kobayashi, Zeeshan Khatri, Farooq Ahmed, and Ick Soo Kim "Ultrasonic-assisted dyeing of silk fibroin nanofibers: an energy-efficient coloration at room temperature" Applied Nanoscience (2019) 1-14

CHAPTER 2

A Facile Approach to Synthesize Highly Conductive Electrospun Aramid Nanofibers via Electroless Deposition

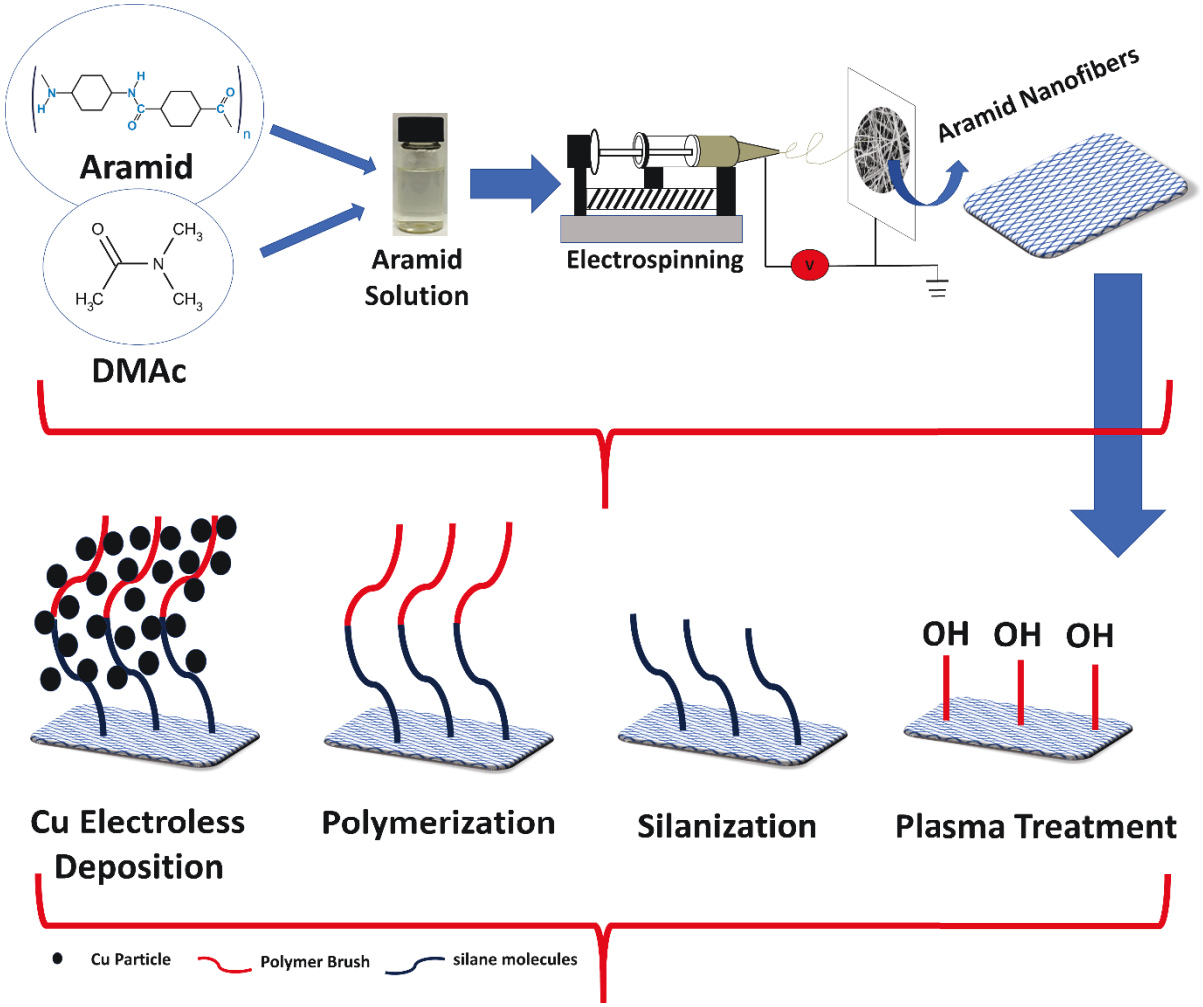

Scheme 1. Fabrication process of the conductive ANFs

2.1 Introduction

Flexible electronics are being promoted and show much demand due to their wide range of new applications that can work under mechanical deformation such as medical implants, flexible and wearable electronics, energy storage, electronic skins, sensors, biological actuators, deformable capacitors and antennas, and point of care diagnostics. [1-7]. A key challenge of these acquiescent flexible devices are to produce high efficiency of conductive interconnections, contacts, and electrodes that are known to be one of the most important components with stable conductivity (i.e. bending, twisting, folding, compressing and folding) [8]. Recently many researchers have put their efforts to improve the properties of flexible electronics. Various organic and inorganic conductive materials were investigated to improve industrial growth including metals, carbon materials, nanoparticles, nanowires, and composite polymers into wearable, flexible, and stretchable conductive substrate [9]. Nonetheless, due to their extremely high conductivity and performance, metals are known as promising materials to synthesis a flexible conductive device. The fabrication and design of well-marked metal structures or thin films for flexible substrates has taken attention and many developments have been made by applying various methods of metallization, such as physical deposition of vapors, [10-12] chemical vapor deposition, [13] electrochemical plating and electroless deposition (ELD) of metals [14-17]. Among the above-mentioned techniques, ELD process has also got attraction due to versatility, site-selectivity, easy process-ability, low-cost, and scalability. These characteristics made the ELD process a suitable method for fabricating large scale metal structures on flexible textile surfaces. [18-21]. Many polymers thin films, paper, rubber, foils, and fabrics have been developed as a flexible electrode device [22]. Among the various available textile fabrics, polyethylene terephthalate (PET), cotton, and polyimide (PI) show much attention due to versatile available structures, low cost, lighter in weight, high strength, and readily processable [23-24]. In the past, some common metals including gold (Au), silver

(Ag), copper (Cu) and nickel (Ni) metals, were used to develop a soft device by using ELD method. The high electrical conductivity at low cost is a fundamental requirement for any metal electrode device. Considering the conductivity to cost ratio, copper metal is a better choice as compared to noble metals (Au, Ag, Pt, and Pd). The Cu is a typical transition metal, exhibiting a significantly higher electrical conductivity that is only 6% lower than Ag but has an outstanding conductivity to cost ratio[25-26]. Wang et al. have successfully developed conductive fabric from cotton while depositing Cu metals using the ELD technique [21].

Although, textile-based flexible devices have many advantages over conventional conductive materials. But few drawbacks were also identified in previous reports i.e. low surface area and high porosity, which can limit metal deposition rate. Electrospun nanofibers gain attraction in wide applications due to its high surface area and it can create a high metal deposition which can ultimately cause our product more conductive. Among other electrospun nanofibers, aramid nanofibers (ANFs) have gained adequate attention because of sufficient availability, higher mechanical strength, flexible, thermal resistant, and chemical resistant [27]. Therefore, ANFs have a neutral fiber surface which is suitable for metal deposition using electroless deposition technique for flexible electronics.

In this work, we report the possibility of copper deposition on flexible electrospun ANFs via electroless deposition technique after surface modification of ANFs. Before the ELD process, polyelectrolyte brushes were covalently attached to the surface of ANFs. Subsequent metal particles were attached to these polymeric brushes on the surface of ANFs via the ELD technique and made AFNs conductive. The ANFs shows the lowest resistance of 1.5 ohm/cm^2.

2.2. Experimental work

2.3.1 Materials

Aramid polymer solution (20%) was purchased from Yantai Taihenxin Materials Co., Ltd. Dimethylacetamide (DMAC) was obtained from Sangon Biotech (Shanghai) Co., Ltd. Other all chemicals including 2-methoxy ethanol ($C_2H_6O_2$), ammonium tetrachloropalladate -II [$(NH_4)_2PdCl_4$], Vinyltrimethoxy silane (VTMS), [2-(methacryloyloxy) ethyl] trimethyl ammonium chloride (METAC), Potassium persulfate ($K_2S_2O_8$) KPS, Sodium hydroxide (NaOH), Copper(II) sulfate pentahydrate ($CuSO4{\cdot}5H_2O$), potassium sodium tartrate tetrahydrate ($KNaC_4H_4O_6{\cdot}4H_2O$) and formaldehyde (HCHO) were purchased from Sigma-Aldrich.

2.3.2 Fabrication of Conductive Aramid Nanofibers (ANFs)

Scheme 1 indicates the complete fabrication process of the conductive ANFs which is divided into 5 steps (electrospinning of ANFs, plasma treatment, silanization, polymerization and electroless deposition) that are explained in the experimental section.

2.3.3 Electrospinning of Aramid Nanofibers (ANFs)

Aramid nanofibers were obtained by electrospinning technique [28]. Briefly, a 13 wt% aramid polymer solution was prepared with DMAC and stirred for 1 h to ensure homogeneity. The prepared solution was placed in a 5 ml syringe attached to a 22 mm gauge needle. A positive electrode was attached to the needle and a negative electrode was attached to the rotating metallic collector. The distance between the tip of needle and metallic rotating collector was 15 cm and a high voltage of 13 kV was used to prepare the aramid nanofibers membrane at 0.3 ml/h flow rate. The nanofibers membrane was fabricated at 30.6 ±2 °C under 50-60 % relative humidity. As prepared aramid nanofibers were collected on aluminum foil wrapped around rotating metallic cylinder and finally, carefully peeled-off for further use.

2.3.4 Plasma Treatment

The electrospun ANFs are hydrophobic in nature and needed to be treated with air plasma before silanization to create functional hydroxyl groups for further reactions. ANFs were treated in plasma for 5 mins with constant pressure (30 Pa) and power (45 W).

2.3.5 Silanization

The Plasma-ANFs were immersed in an ethanol solution containing 2 % (v/v) vinyltrimethoxysilane (VTMS) for 15 min. After VTMS treatment, the surface of ANFs becomes largely hydrophobic owing to the presence of dense vinyl groups. The VTMS-ANFs were finally rinsed with DI water and immediately dried at 60 °C for 15 min.

2.3.6 Polymerization

The VTMS-ANFs sample was immersed into 100 ml of 20 % (v/v) METAC solution containing 60 mg potassium persulfate (KPS) and placed at 80 °C for 1 h to carry out the polymerization of PMETAC brushes while stirring. Finally, the polymerized samples were carefully washed with DI water and dried at 45 °C in a vacuum dryer for 2 h.

2.3.7 Electroless Deposition

The Copper (Cu) deposition via the ELD technique was followed with previously reported methods [26,13]. PMETAC-ANFs were immersed in a 5 mM $(NH_4)_2PdCl_4$ solution for 15 min for the ion-exchange process. During an ion-exchange $[PdCl_4]^{2-}$ catalytic ions were immobilized onto the quaternary ammonium groups of PMETAC polymer chains and samples were gently washed with DI before further process. ELD bath was prepared by pouring two different mixtures (A and B) with a ratio of 1.1 v/v into the bath. Briefly, solution A (13 g/l copper (II) sulfate pentahydrate, 29 g/l potassium sodium tartrate tetrahydrate, and 12 g/l sodium hydroxide) and solution B (9.5 ml/L formaldehyde in water) were mixed equally into

the ELD bath. Finally, the ANFs were immersed in the ELD bath for 15-60 min at 10 - 60 °C. Upon successful ELD process, samples were washed with DI water, ethanol, and dried before measuring the conductive ANFs performance.

2.3.8 **Characterizations**

SEM images were taken using S-4800 Hitachi Ltd japan Field emission Scanning electron microscope. EDX images and spectrum were obtained using S-3000N Hitachi Ltd Japan X-ray Spectroscopy. All the SEM and EDX samples were sputtered with Au before the examination. FTIR spectroscopy measurement was analyzed with Thermo Nicolet 5700, Thermo Fisher Scientific Inc. USA. All the FTIR samples 1-2 mg were ground with 0.1g KBr and pressed into a pellet of which transmission FTIR spectrum was measured. X-ray photoelectron spectroscopy measurement was analyzed with Axis ultra by Shimadzu equipped with a dual anode X-ray source Al/Mg and HAS hemispherical sector analyzer detector. The thermal properties of the samples were investigated by a thermal analyzer (Diamond 5700, PE Co., Ltd., USA). XRD measurements performed on the Rigaku X-ray diffractometer (D/MAX-IIB). Plasma treatment was carried out on Harrick Plasma cleaner PDC-002. An OCA -40 Contact angel instrument (Data physics Germany) was applied to determine the water contact angle. Nanofiber resistance value measured using ST-225*C multifunctional Digital 4 Probe meter.

2.3 **Results and Discussion**

2.**3.1 Water Contact Angle**

Water contact angle measurements reveal their dramatic difference in surface wettability of each process involved in the fabrication and can confirm the successful ELD process. Fig 1 indicates the water contact angle of neat ANFs, plasma-treated, silanized, polymerized, and Cu-ANFs. ANFs are hydrophobic in nature but for surface coating of VTMS on ANFs,

hydroxyl groups (hydrophilic nature) must be needed. The plasma treatment is widely used to alter the hydrophobic nature of material into hydrophilic nature by simply creating hydroxyl groups on the surface [29]. In our experiments, the original ANFs showed an angle of 138° but after plasma treatment, the water contact angle is decreased dramatically to 1.3°. This change in water contact angle indicates successful plasma treatment on our samples and creates hydroxyl groups that are helpful for the VTMS process. After plasma, the P-ANFs were immersed in 2 % (v/v) vinyltrimethoxysilane (VTMS) in ethanol which allows the reaction of silane molecules with hydroxyl groups on the surface of the substrate. The 2 % (v/v) VTMS in ethanol allows the hydroxyl groups of plasma-ANFs to make a chemical attachment with silane molecules. As VTMS nature, the material will be again giving hydrophobic nature in VTMS-ANFs and it is presented in Fig 1, VTMS-ANFs show an angle of 144° which indicates proper attachment with plasma-ANFs. This hydrophobic nature is mainly due to the presence of vinyl groups in VTMS [30]. The next step is polymerization, in which VTMS-ANFs was then immersed in a polymerization solution containing a METAC monomer and a potassium persulfate (KPS) initiator for a certain time, leading to the fabrication of PMETAC-ANF substrate. Moreover, in the polymerization step, METAC monomers and potassium persulfate (KPS) combine to bind chemically onto VTMS-ANFs. The successful surface modification was verified by consequent measurement from water contact angle and PMETAC-ANFs showed an angle of 88°. This decrease in angle is may be due to some hydroxyl groups present in PMETAC [31]. The successful surface modification of ANFs with PMETAC allows Cu particles to densely pack and cover on the surface of ANFs. The Cu-ANFs show an angle of 146° and it is mainly due to the presence of Cu particles on the surface of ANFs [32-33]. Overall results of the water contact angle are good evidence of the successful process involved in each fabrication step and ELD process.

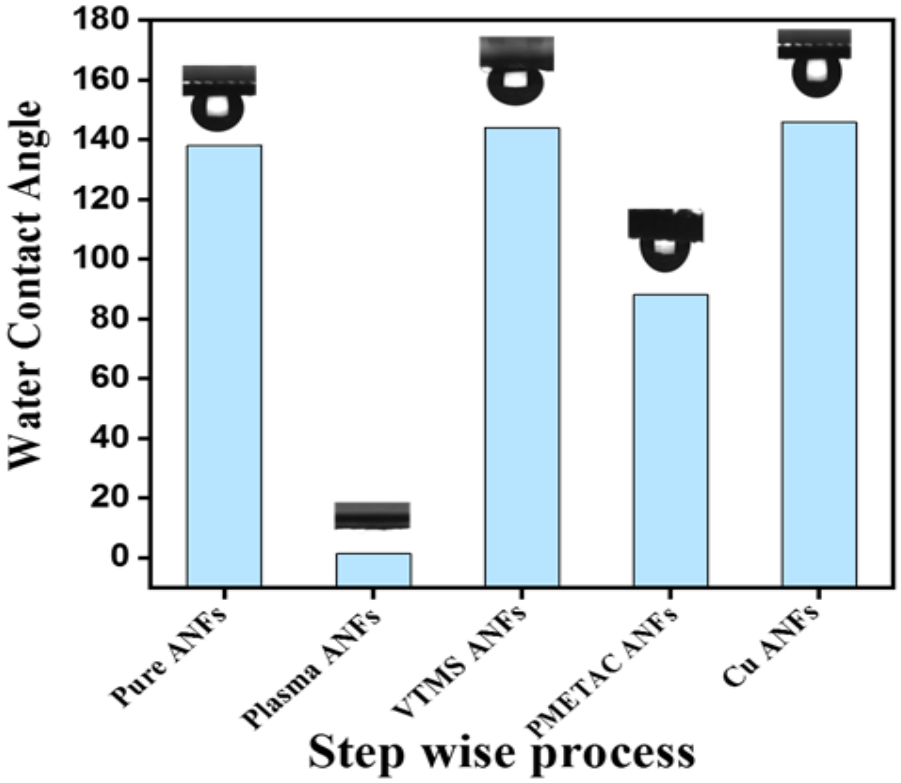

Figure 1. Water contact angel of each process involved in fabrication and electroless deposition on ANFs

2.3.2 **Surface morphology**

Surface morphology of AFNs was examined through FE-SEM. Fig 2 (A) shows the surface morphology of pure AFNs and Fig 2 (B) shows the surface morphology AFNs after the ELD process. As can be seen in Fig 2 (A), electrospun ANFs have a smooth and bead free morphology with an average diameter of 100-150 nm. Though, as anticipated, the diameter of ANFs was increased up to 200 – 250 nm after the ELD process (Fig 2B). This increase in diameter after the ELD process indicates successful deposition of Cu particles onto the surface of ANFs [34]. Fig 3 shows smooth a morphology of plasma ANFs, VTMS-ANFs, and PMETAC-ANFs. The plasma-ANFs showed negligible increasing diameter after plasma treatment. Similarly, VTMS-ANFs has shown slightly dense morphology and overall VTMS-

ANFs retained nanofibers morphology. Moreover, PMETC-ANFs has shown more dense morphology and fibers are overlapping each other. This may be due to numerous chemical interactions with ANFs. It was observed that ANFs retain its fibrous morphology after Cu deposition which can introduce flexibility in conductive Cu-ANFs membrane and a better choice in flexible devices.

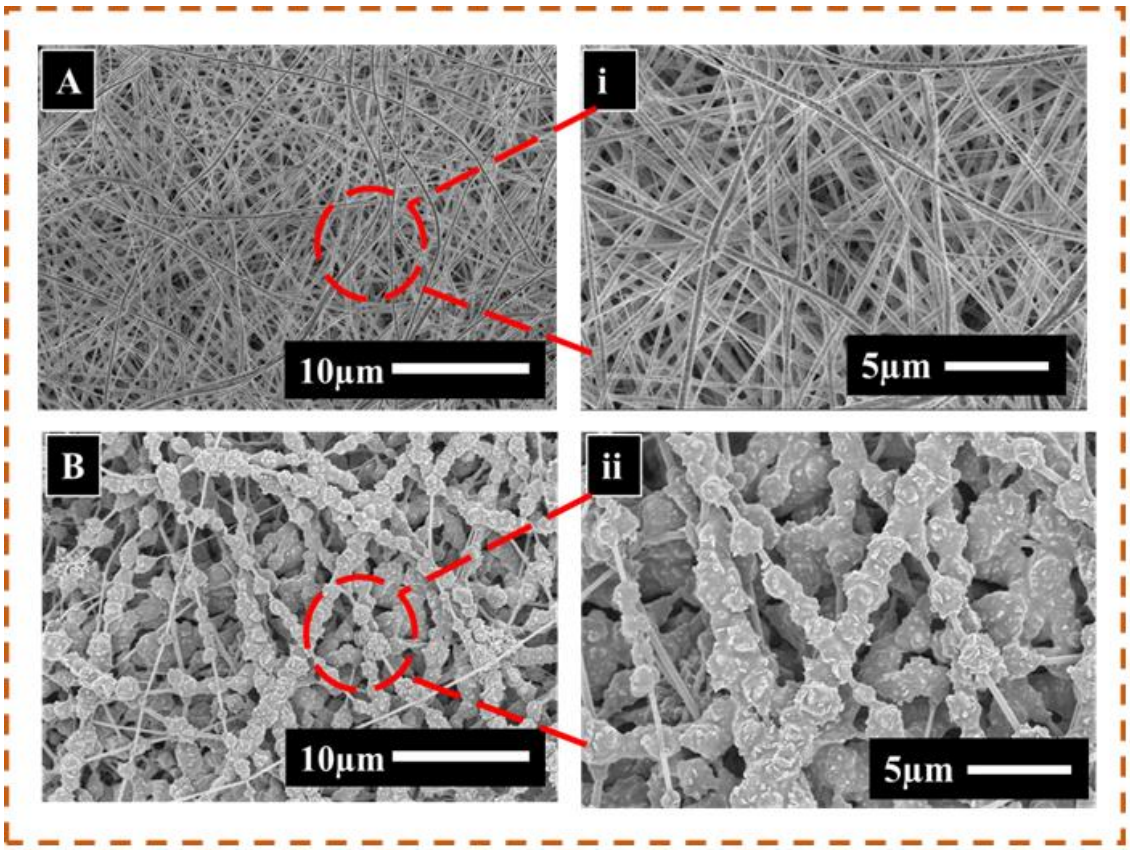

Figure 2. (A and B) Surface morphology of Pure ANFs and copper deposited ANFs. Figure 2 (i and ii) Magnified surface morphology of Pure ANFs and copper deposited ANFs.

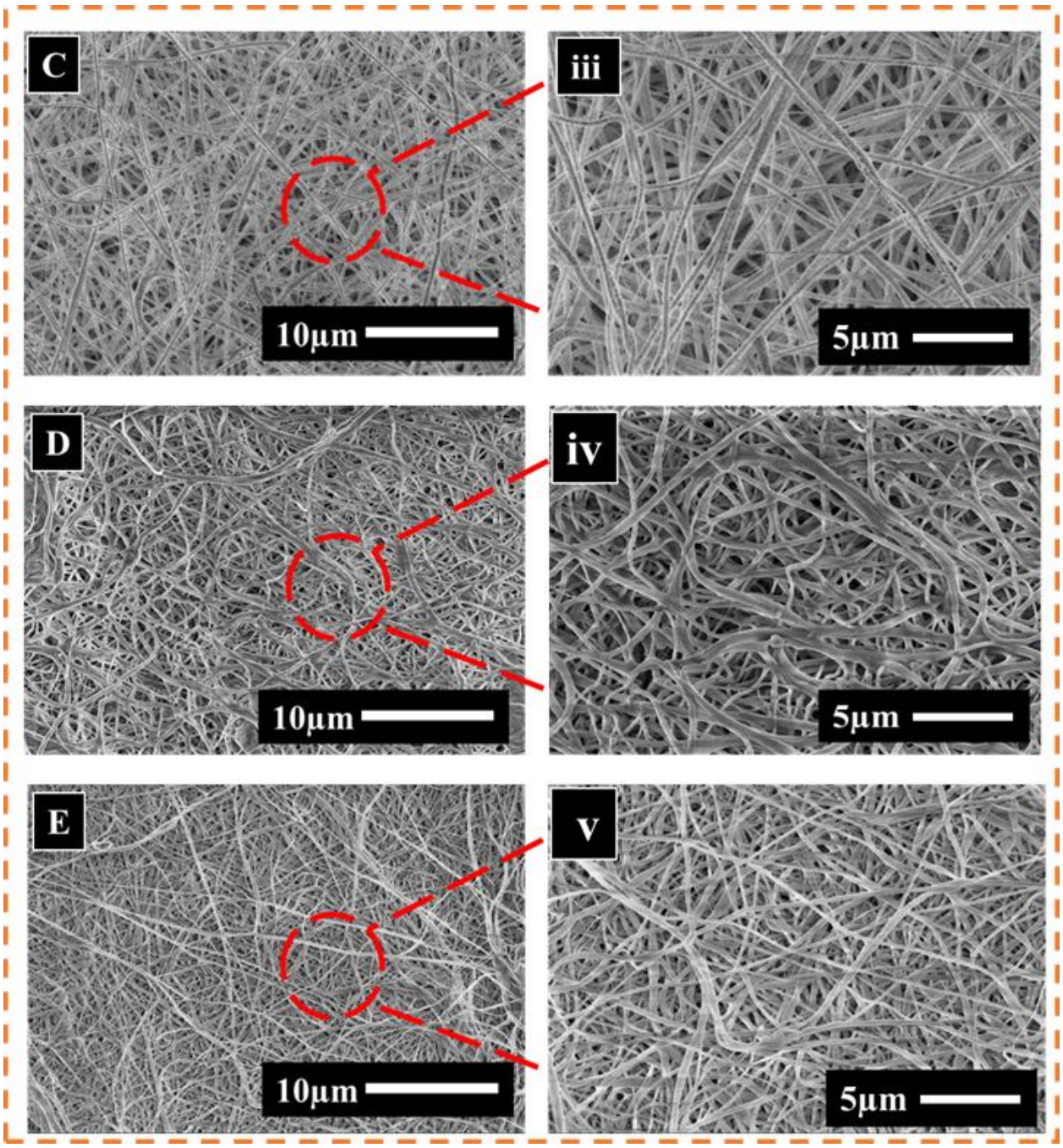

Figure 3. (C-E) Surface morphology of plasma-ANFs, VTMS-ANFs and PMETAC-ANFs. Figure 3 (iii-v) Magnified surface morphology of plasma-ANFs, VTMS-ANFs and PMETAC-ANFs.

2.3.3 Element Mapping:

The EDX was performed to confirm the presence of copper metal after electroless deposition. Fig 4 shows the EDX spectrum of Cu-ANFs and the main compositions on Cu-ANFs. The EDX spectrum confirms the rich presence of Cu particles with 69.8 % total weight of other components of ANFs. This rich presence of Cu particles on ANFs is much higher than Cu deposited on conventional textiles [35]. This higher deposition may be due to the higher surface area of ANFs [36] and it will help produce high-performance ANFs. Moreover, element mapping indicates uniform deposition of Cu particles on the surface of ANFs.

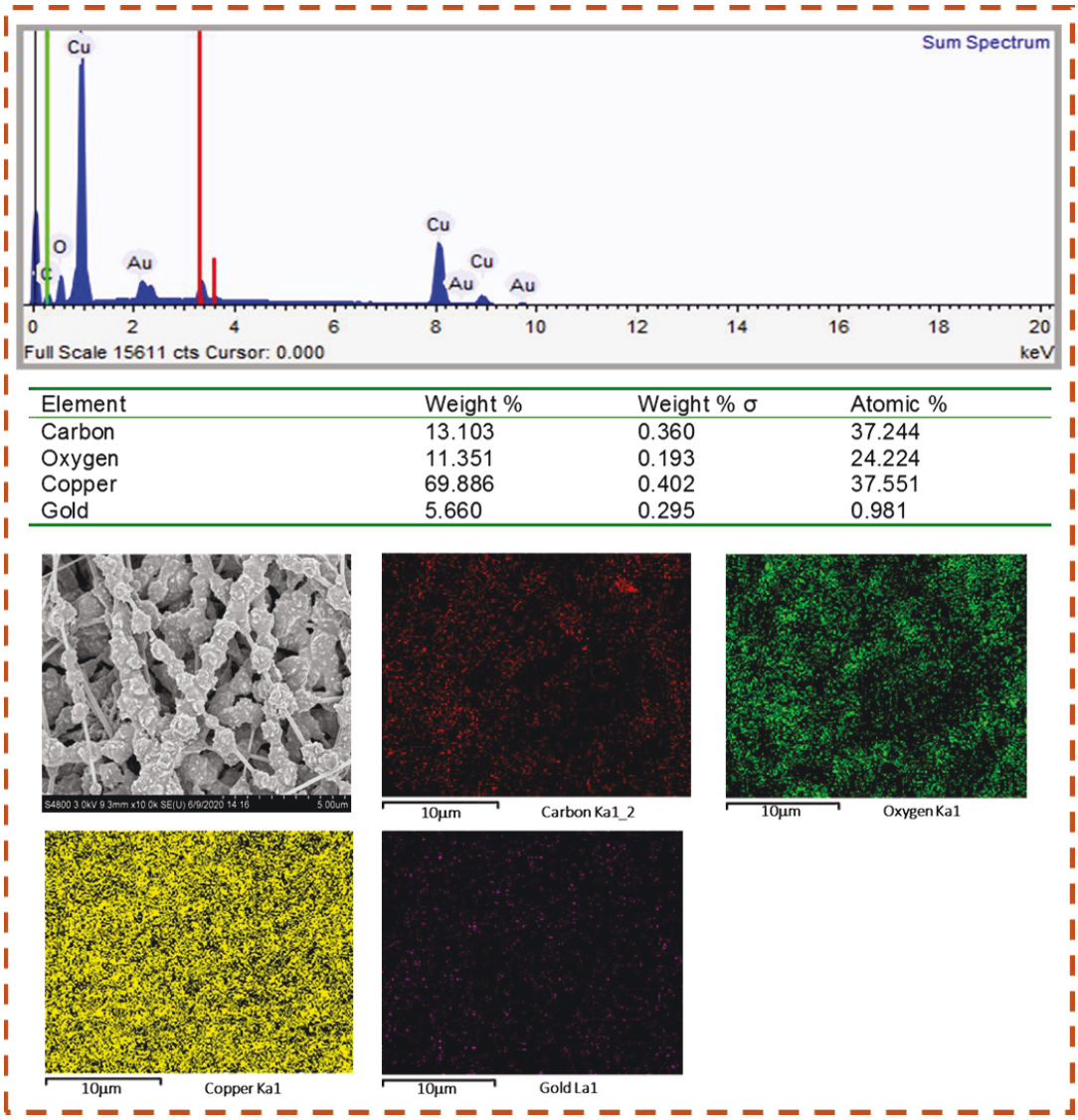

Figure 4. Energy-dispersive X-ray spectra of ANFs after electroless deposition and element mapping

2.3.4 Chemical Analysis

The FTIR was used to analyze chemical structural changes of prepared samples at different processing stages. The FTIR spectra of prepared samples at each step could be explained by the interaction of different functional groups as shown in Fig 5. The FTIR spectra of pure ANFs showed the four main peaks observed at 3320 cm^{-1}, 1540 cm^{-1}, 1340 cm^{-1}, and 780 cm^{-1}. The stretching peak observed at 3320 cm^{-1} indicates the presence of N-H group, the peak at 1540 cm^{-1} indicates the bending vibration of N-H bonding, the strong stretching peak observed at 1340 cm^{-1} is due to Ph-N vibration, and the peak observed at 780 cm^{-1} indicates intensive bending of C-C bonding which correspond to the presence of aromatic rings [37-39]. Further, the plasma-treated sample presented the same spectra with higher intensity of O-H bonding that ensures plasma treatment. Furthermore, in the third step of VTMS processing, the observed FTIR spectra showed one additional peak of 1014 cm^{-1} that indicates in-plane C-H vibration. Similarly, the FTIR spectra of PMETAC-ANFs also showed one more additional peak at 1656 cm^{-1} which indicates C=O stretching [40]. In addition, referring to Fig 5, it is proposed that the treatment of ANFs with VTMS and PMETAC helps ionize the N-H groups of ANFs nanofibers for the ELD process [41]. Finally, when the Cu was deposited after the PMETAC-ANFs stage, the FTIR spectra did not show any of the above-mentioned peaks, it may due to deposition of Cu on the surface of the sample.

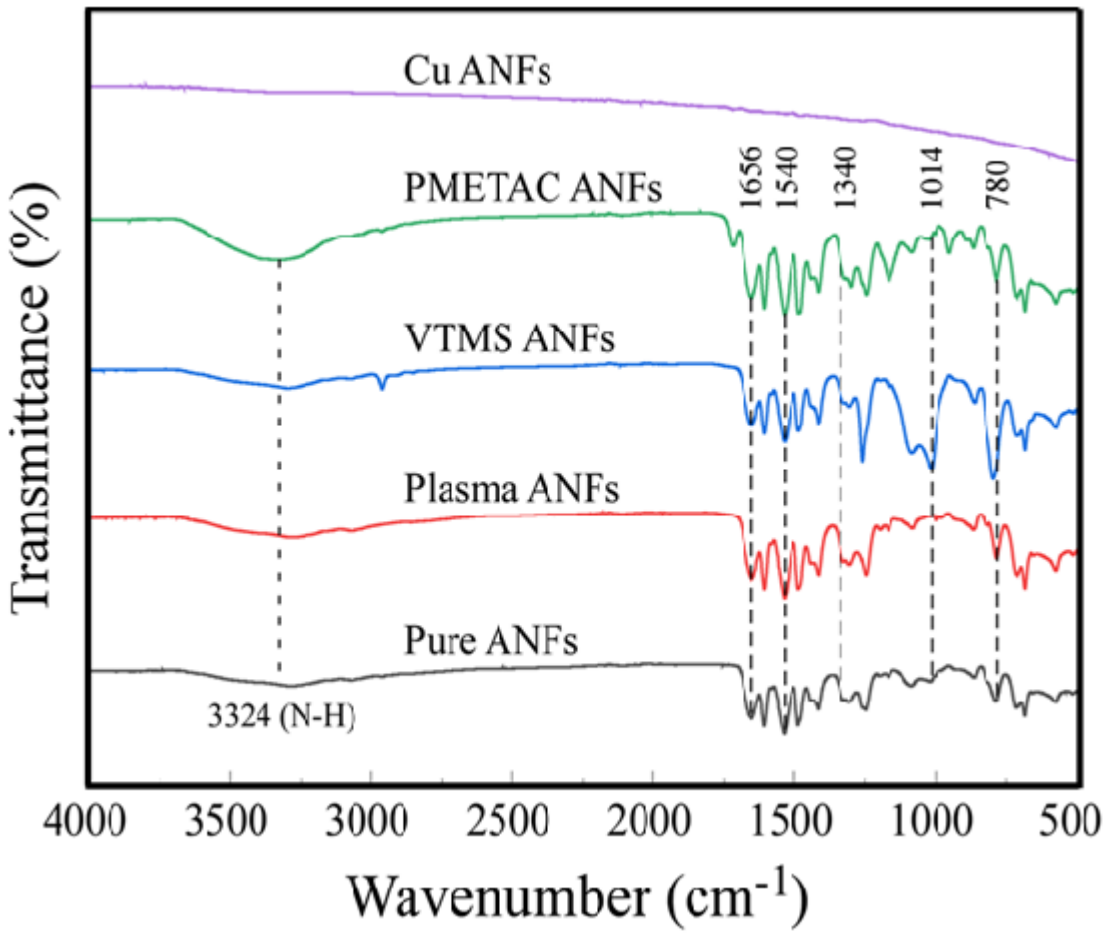

Figure 5. FTIR spectrum of ANFs fabrication and electroless deposition.

Fig 6 (a) indicates the XRD pattern of ANFs before and after ELD respectively. The diffraction peaks of as-prepared electrospun ANFs was observed at 22.5°. Whereas, Cu-ANFs showed two more new peaks exactly at 43 °and 50.5 ° that indicates the (111), (200) crystal plane of Cu [42].

We also used photoelectron spectroscopy (XPS) to further evaluate the chemical structure and identify the elemental composition of ANFs before-after copper deposition. Fig 6 (b) indicates the XPS peaks of aramid nanofibers before and after electroless deposition. The ANFs shows the main two peaks at 281 eV and 530 eV corresponds to C1s and O1s respectively; are nearly similar to those reported for ANFs [43]. Moreover, Cu-ANFs showed the same peaks at C 1s and O 1s spectrum but two new peaks appeared at 933.06 eV (Cu 2p 3/2) and 952.96 eV (Cu

2p ½) corresponds to Cu 2p. These results validate the existence of Cu particles onto ANFs [44].

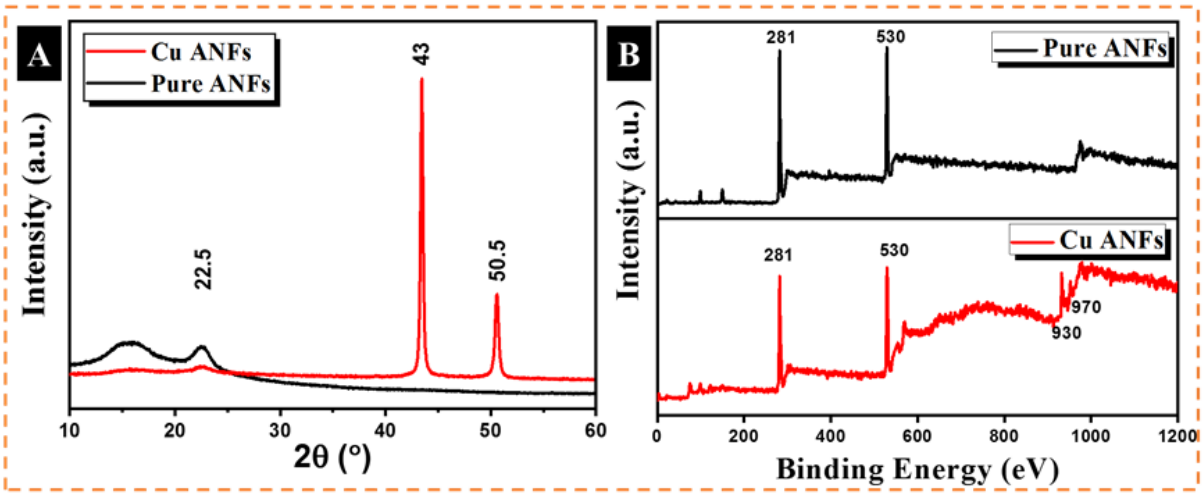

Figure 6. (A) XRD spectra of Pure ANFs and Cu deposited ANFs and (B) XPS spectra of pure ANFs and Cu deposited ANFs.

2.3.5 Thermal Gravimetric Analysis

The analysis of thermal degradation rate and total combustion of pure ANFs and Cu ANFs were performed with thermogravimetric analysis as shown in Fig 7. The thermogravimetric analysis graph is saturated in phases to demonstrates the weight percentage and temperature range. The first phase determines a small increase in weight, which transpires in the temperature range when it is increased from ambient to 120℃ due to air moisture into both nanofiber samples. However, the rate of absorbed moisture is frequently evaporated at the temperature range of 140℃. The temperature of the thermal degradation rate of pure ANFs and Cu-ANFs was found at 370℃ While, the decomposition rate proceeded up to total combustion was found at 438℃.

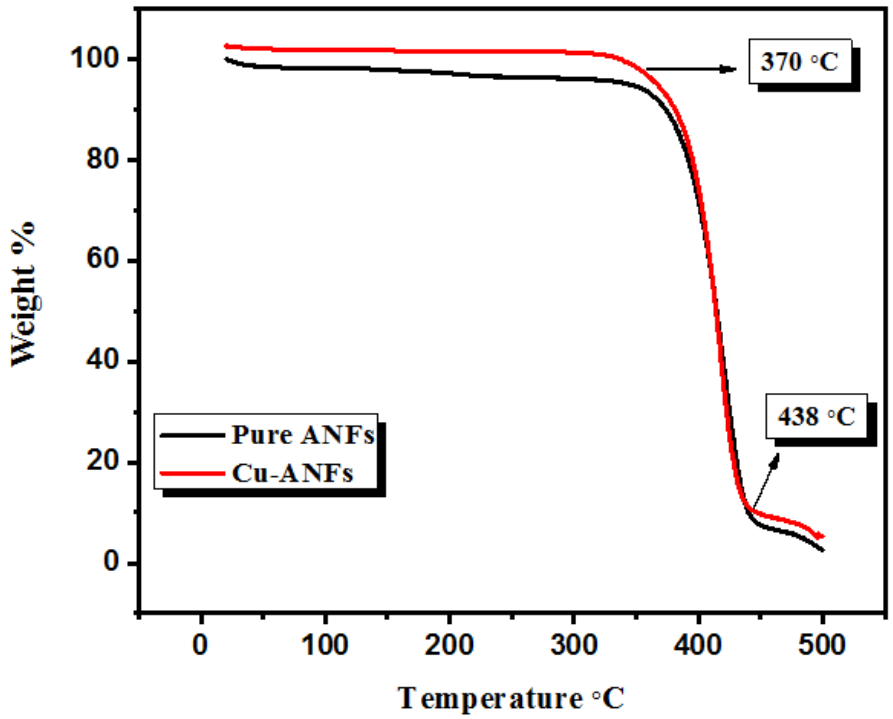

Figure 7. Thermal Gravimetric Analysis of pure ANFs and Cu deposited ANFs

2.3.6 Effect of Time and Temperature

The effect of time and temperature on the deposition rate of copper on ANFs was optimized Fig 8. The results were compared with plasma-treated Cu deposited and without plasma-treated Cu deposited on ANFs. The results show that plasma treatment has a significant effect on the deposition of Cu on ANFs [45]. At the start, the influence of temperature was observed at a fixed time (30 min). Fig 8 (a) indicates a change in weight on ANFs due influence of temperature during Cu deposition. The weight is gradually increased with increasing temperature from 10 °C to 30 °C and thereafter decreased slowly. While Fig 8 (b) indicates a change in resistance on ANFs due to the influence of temperature during Cu deposition. It was observed that resistance is gradually decreased with increasing temperature 10 °C to 30 °C and thereafter increased slowly and this may be due to instability of solution caused by higher temperature which ultimately caused poor Cu deposition [37]. After analyzing the results, the 30 °C temperature was optimized for Cu deposition.

Deposition time has also a significant effect on weight and resistance in the ELD process, which needs to be optimized. Fig 8 (c) indicates a change in weight on ANFs due influence of time at constant temperature (30 °C) during Cu deposition. The weight is gradually increased with increasing time up to 20 mins and thereafter no obvious change in weight was observed. While Fig 8 (d) indicates a change in resistance on ANFs due to the influence of time during Cu deposition. It was observed that resistance is gradually decreased with increasing time up to 30 mins and thereafter it remained constant. This may be due to a saturation limit on functionalized ANFs and there are no more sites available after 30 mins [37]. Overall analyzing the results, the 30 °C temperature and 30 mins time were optimized for proper Cu deposition. At optimum electroless deposition, Cu deposited aramid nanofibers show low resistance of 1.5ohm Ω /cm^2.

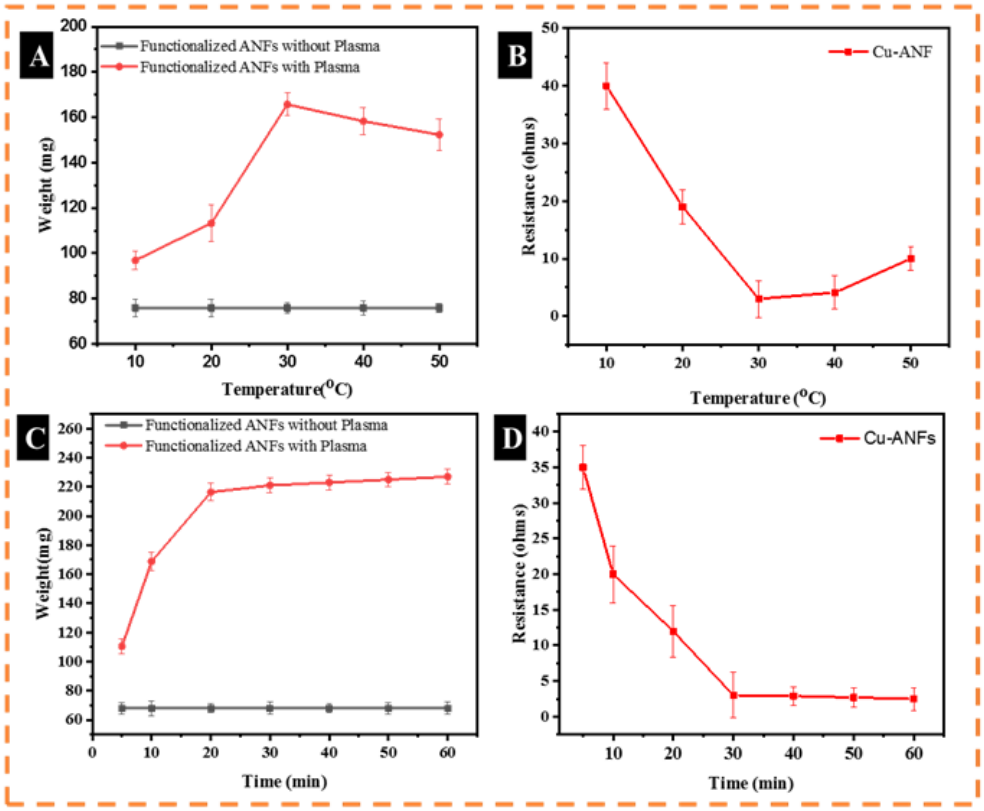

Figure 8. (A) Effect of ELD temperature on weight of ANFs, (B) Effect of ELD temperature on resistance of ANFs, (C) Effect of ELD time on weight of ANFs and (D) Effect of ELD time on resistance of ANFs.

2.4 **Conclusion**

We successfully prepared highly durable and electrically conductive aramid nanofibers (ANFs). Copper metal particles were deposited on aramid nanofibers by electroless deposition. The parameters including time and temperature were studied and optimized. The characterizations of prepared material including FE-SEM, EDX, XRD, XPS, FTIR and TGA were performed. Significantly, the deposition of Cu particles attained low electrical resistance about 1.5ohm/cm^2 and provided flexibility. The as-prepared Cu-ANFs has a good electrical conductance and could be used in various applications such as wearable electronics, flexible displays, and energy storage.

References

[1] White MS, Kaltenbrunner M, Głowacki ED, Gutnichenko K, Kettlgruber G, Graz I, Aazou S, Ulbricht C, Egbe DAM, Miron MC, Major Z, Scharber MC, Sekitani T, Someya T, Bauer S, Sariciftci NS (2013) Ultrathin, highly flexible and stretchable PLEDs. Nature Photonics 7 (10):811-816. doi:10.1038/nphoton.2013.188

[2] Kim R-H, Kim D-H, Xiao J, Kim BH, Park S-I, Panilaitis B, Ghaffari R, Yao J, Li M, Liu Z, Malyarchuk V, Kim DG, Le A-P, Nuzzo RG, Kaplan DL, Omenetto FG, Huang Y, Kang Z, Rogers JA (2010) Waterproof AlInGaP optoelectronics on stretchable substrates with applications in biomedicine and robotics. Nature Materials 9 (11):929-937. doi:10.1038/nmat2879

[3] Kaltenbrunner M, White MS, Głowacki ED, Sekitani T, Someya T, Sariciftci NS, Bauer S (2012) Ultrathin and lightweight organic solar cells with high flexibility. Nature communications 3 (1):770. doi:10.1038/ncomms1772

[4] Benight SJ, Wang C, Tok JBH, Bao Z (2013) Stretchable and self-healing polymers and devices for electronic skin. Progress in Polymer Science 38 (12):1961-1977. doi:https://doi.org/10.1016/j.progpolymsci.2013.08.001

[5] Hu L, Pasta M, La Mantia F, Cui L, Jeong S, Deshazer HD, Choi JW, Han SM, Cui Y (2010) Stretchable, Porous, and Conductive Energy Textiles. Nano Letters 10 (2):708-714. doi:10.1021/nl903949m

[6] Kim D-H, Rogers JA (2008) Stretchable Electronics: Materials Strategies and Devices. Advanced Materials 20 (24):4887-4892. doi:10.1002/adma.200801788

[7] Chen Z, Ren W, Gao L, Liu B, Pei S, Cheng H-M (2011) Three-dimensional flexible and conductive interconnected graphene networks grown by chemical vapour deposition. Nature Materials 10 (6):424-428. doi:10.1038/nmat3001

[8] Yeo W-H, Kim Y-S, Lee J, Ameen A, Shi L, Li M, Wang S, Ma R, Jin SH, Kang Z, Huang Y, Rogers JA (2013) Multifunctional Epidermal Electronics Printed Directly Onto the Skin. Advanced Materials 25 (20):2773-2778. doi:10.1002/adma.201204426

[9] Webb RC, Bonifas AP, Behnaz A, Zhang Y, Yu KJ, Cheng H, Shi M, Bian Z, Liu Z, Kim Y-S, Yeo W-H, Park JS, Song J, Li Y, Huang Y, Gorbach AM, Rogers JA (2013) Erratum: Ultrathin conformal devices for precise and continuous thermal characterization of human skin. Nature Materials 12 (11):1078-1078. doi:10.1038/nmat3779

[10] Pandey PA, Bell GR, Rourke JP, Sanchez AM, Elkin MD, Hickey BJ, Wilson NR (2011) Physical Vapor Deposition of Metal Nanoparticles on Chemically Modified Graphene: Observations on Metal–Graphene Interactions. Small (Weinheim an der Bergstrasse, Germany) 7 (22):3202-3210. doi:10.1002/smll.201101430

[11] Grodzicki A, Łakomska I, Piszczek P, Szymańska I, Szłyk E (2005) Copper(I), silver(I) and gold(I) carboxylate complexes as precursors in chemical vapour deposition of thin metallic films. Coordination Chemistry Reviews 249 (21):2232-2258. doi:https://doi.org/10.1016/j.ccr.2005.05.026

[12] Azzaroni O, Zheng Z, Yang Z, Huck WTS (2006) Polyelectrolyte Brushes as Efficient Ultrathin Platforms for Site-Selective Copper Electroless Deposition. Langmuir 22 (16):6730-6733. doi:10.1021/la060891

[13] Yu Y, Yan C, Zheng Z (2014) Polymer-Assisted Metal Deposition (PAMD): A Full-Solution Strategy for Flexible, Stretchable, Compressible, and Wearable Metal Conductors. Advanced Materials 26 (31):5508-5516. doi:10.1002/adma.201305558

[14] Liu X, Zhou X, Li Y, Zheng Z (2012) Surface-Grafted Polymer-Assisted Electroless Deposition of Metals for Flexible and Stretchable Electronics. Chemistry – An Asian Journal 7 (5):862-870. doi:10.1002/asia.201100946

[15] Garcia A, Polesel-Maris J, Viel P, Palacin S, Berthelot T (2011) Localized Ligand Induced Electroless Plating (LIEP) Process for the Fabrication of Copper Patterns Onto Flexible

Polymer Substrates. Advanced Functional Materials 21 (11):2096-2102. doi:10.1002/adfm.201100041

[16] Guo R, Yu Y, Zeng J, Liu X, Zhou X, Niu L, Gao T, Li K, Yang Y, Zhou F, Zheng Z (2015) Biomimicking Topographic Elastomeric Petals (E-Petals) for Omnidirectional Stretchable and Printable Electronics. Advanced Science 2 (3):1400021. doi:10.1002/advs.201400021

[17 Wang X, Hu H, Shen Y, Zhou X, Zheng Z (2011) Stretchable Conductors with Ultrahigh Tensile Strain and Stable Metallic Conductance Enabled by Prestrained Polyelectrolyte Nanoplatforms. Advanced Materials 23 (27):3090-3094. doi:10.1002/adma.201101120

[18] Huang Q, Liu L, Wang D, Liu J, Huang Z, Zheng Z (2016) One-step electrospinning of carbon nanowebs on metallic textiles for high-capacitance supercapacitor fabrics. Journal of Materials Chemistry A 4 (18):6802-6808. doi:10.1039/C5TA09309K

[19] Liu L, Yu Y, Yan C, Li K, Zheng Z (2015) Wearable energy-dense and power-dense supercapacitor yarns enabled by scalable graphene–metallic textile composite electrodes. Nature communications 6 (1):7260. doi:10.1038/ncomms8260

[20] Liu X, Chang H, Li Y, Huck WTS, Zheng Z (2010) Polyelectrolyte-Bridged Metal/Cotton Hierarchical Structures for Highly Durable Conductive Yarns. ACS Applied Materials Interfaces 2 (2):529-535. doi:10.1021/am900744n

[21] Wang X, Yan C, Hu H, Zhou X, Guo R, Liu X, Xie Z, Huang Z, Zheng Z (2014) Aqueous and Air-Compatible Fabrication of High-Performance Conductive Textiles. Chemistry – An Asian Journal 9 (8):2170-2177. doi:10.1002/asia.201402230

[22] “Goda, E. S., Gab-Allah, M. A., Singu, B. S., Yoon, K. R. (2019). Halloysite nanotubes based electrochemical sensors: A review. *Microchemical Journal*, *147*, 1083-1096.”

[23] Li K, Zhen H, Niu L, Fang X, Zhang Y, Guo R, Yu Y, Yan F, Li H, Zheng Z (2014) Full-Solution Processed Flexible Organic Solar Cells Using Low-Cost Printable Copper Electrodes. Advanced Materials 26 (42):7271-7278. doi:10.1002/adma.201403494

[24] Lee Y-H, Kim J-S, Noh J, Lee I, Kim HJ, Choi S, Seo J, Jeon S, Kim T-S, Lee J-Y, Choi JW (2013) Wearable Textile Battery Rechargeable by Solar Energy. Nano Letters 13 (11):5753-5761. doi:10.1021/nl403860k

[25] Goda, E. S., Lee, S., Sohail, M., Yoon, K. R. (2020). Prussian blue and their analogues as advanced supercapacitor electrodes. *Journal of Energy Chemistry*."

[26] Xue J, Wu T, Dai Y, Xia Y (2019) Electrospinning and Electrospun Nanofibers: Methods, Materials, and Applications. Chemical Reviews 119 (8):5298-5415. doi:10.1021/acs.chemrev.8b00593

[27] Oh HJ, Han SH, Kim SS (2014) A novel method for a high-strength electrospun meta-aramid nanofiber by microwave treatment. Journal of Polymer Science Part B: Polymer Physics 52 (12):807-814. doi:10.1002/polb.23486

[28] Paripovic D, Klok H-A (2011) Polymer Brush Guided Formation of Thin Gold and Palladium/Gold Bimetallic Films. ACS Applied Materials & Interfaces 3 (3):910-917. doi:10.1021/am101270f

[29] DEMİR A, Bozaci E, Gülümser T, Sarikanat M An ecological approach for the surface modification of aramid fibers. Tekstil ve Konfeksiyon 26 (3):256-261

[30] Wang C, Yang H, Chen F, Peng L, Gao H-f, Zhao L-p (2018) Influences of VTMS/SiO2 ratios on the contact angle and morphology of modified super-hydrophobic silicon dioxide material by vinyl trimethoxy silane. Results in Physics 10:891-902. doi:https://doi.org/10.1016/j.rinp.2018.08.007

[31] Politakos N, Azinas S, Moya SE (2016) Responsive Copolymer Brushes of Poly[(2-(Methacryloyloxy)Ethyl) Trimethylammonium Chloride] (PMETAC) and Poly(1H,1H,2H,2H-Perfluorodecyl acrylate) (PPFDA) to Modulate Surface Wetting

Properties. Macromolecular Rapid Communications 37 (7):662-667. doi:10.1002/marc.201500630

[32] Liu S, Hu M, Yang J (2016) A facile way of fabricating a flexible and conductive cotton fabric. Journal of Materials Chemistry C 4 (6):1320-1325. doi:10.1039/C5TC03679H

[33] Chen, G. S., Tau, R. J., Fang, J. S., Cheng, Y. L., Chen, Y. C. (2020). Mechanism of strengthening electroless plated copper films with extremely dilute oxide dispersion alloying: the optimal MnO addition. *Applied Surface Science*, 146816."

[34] Mahar FK, Mehdi M, Qureshi UA, Brohi KM, Zahid B, Ahmed F, Khatri Z (2017) Dyeability of recycled electrospun polyethylene terephthalate (PET) nanofibers: Kinetics and thermodynamic study. Journal of Molecular Liquids 248:911-919. doi:https://doi.org/10.1016/j.molliq.2017.10.116

[35] Afzali A, Mottaghitalab V, Motlagh MS, Haghi AK (2010) The electroless plating of Cu-Ni-P alloy onto cotton fabrics. Korean Journal of Chemical Engineering 27 (4):1145-1149. doi:10.1007/s11814-010-0221-8

[36] Patterson, B. A., Malakooti, M. H., Lin, J., Okorom, A., Sodano, H. A. (2018). Aramid nanofibers for multiscale fiber reinforcement of polymer composites. Composites Science and Technology, 161, 92-99.

[37] Wang, F., Wu, Y., Huang, Y., Liu, L. (2018). Strong, transparent and flexible aramid nanofiber/POSS hybrid organic/inorganic nanocomposite membranes. Composites Science and Technology, 156, 269-275.

[38] Yao, L., Lee, C., Kim, J. (2010). Fabrication of electrospun meta-aramid nanofibers in different solvent systems. Fibers and Polymers, 11(7), 1032-1040.

[39] Liu, X., Chang, H., Li, Y., Huck, W. T., Zheng, Z. (2010). Polyelectrolyte-bridged metal/cotton hierarchical structures for highly durable conductive yarns. ACS applied materials & interfaces, 2(2), 529-535.

[40] Liu, L., Yu, Y., Yan, C., Li, K., Zheng, Z. (2015). Wearable energy-dense and power-dense supercapacitor yarns enabled by scalable graphene–metallic textile composite electrodes. Nature communications, 6(1), 1-9.

[41] Gan X, Wu Y, Liu L, Shen B, Hu W (2007) Electroless copper plating on PET fabrics using hypophosphite as reducing agent. Surface and Coatings Technology 201 (16):7018-7023. doi:https://doi.org/10.1016/j.surfcoat.2007.01.006

[42] Yu D, Mu S, Liu L, Wang W (2015) Preparation of electroless silver plating on aramid fiber with good conductivity and adhesion strength. Colloids and Surfaces A: Physicochemical and Engineering Aspects 483:53-59. doi:https://doi.org/10.1016/j.colsurfa.2015.07.021

[43] Biesinger MC (2017) Advanced analysis of copper X-ray photoelectron spectra. Surface and Interface Analysis 49 (13):1325-1334. doi:10.1002/sia.6239

[44] Li X, Li Y, Guan T, Xu F, Sun J (2018) Durable, Highly Electrically Conductive Cotton Fabrics with Healable Superamphiphobicity. ACS Applied Materials & Interfaces 10 (14):12042-12050. doi:10.1021/acsami.8b01279

[45] Tai Y, Xu C, Chen H (2016) Silver-coated glass fabric composites prepared by electroless plating. Materials Letters 180:144-147. doi:https://doi.org/10.1016/j.matlet.2016.05.118

CHAPTER 3

Synthesis of Highly Conductive Electrospun Recycled Polyethylene Terephthalate Nanofibers Using the Electroless Deposition Method

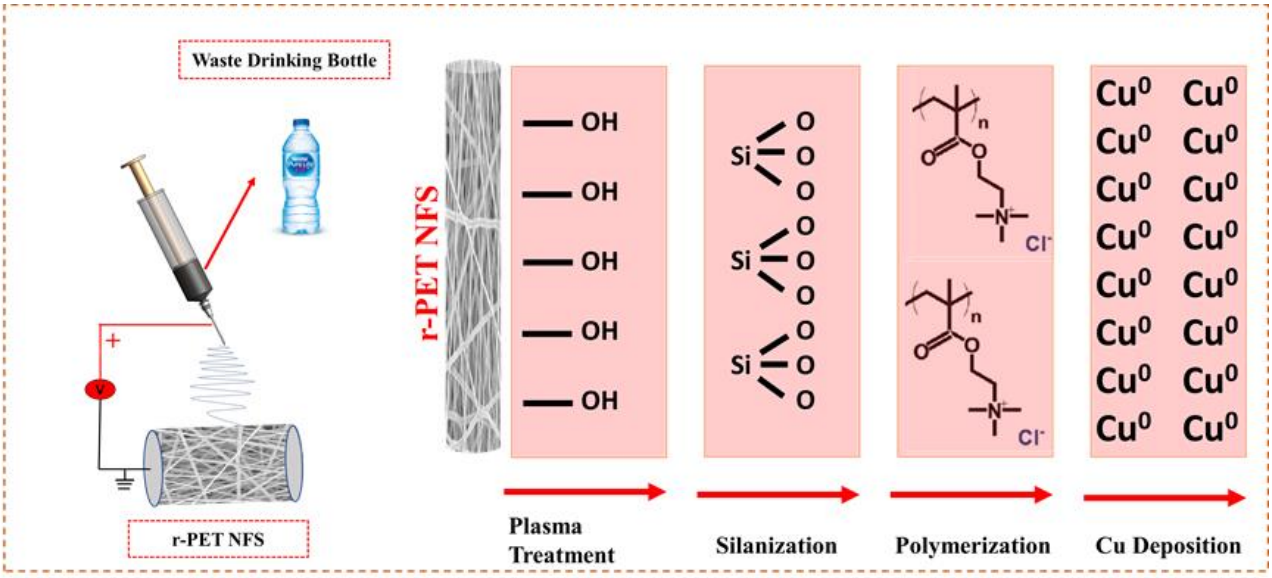

Figure 1. Schematic diagram of copper-coated r-PET NFS.

3.1. Introduction

Flexible electrically conductive materials have gained significant demand for electronics and telecommunication systems because of their capability to convey electrical properties in this century [1]. The increasing demand of materials for smart electronics that can work under mechanical deformation with high efficiency and the required conductivity has become a high stream/demanding field of research [2]. The polymer and metal composites have been extensively explored [3] with a variety of new applications including flexible displays, wearable electronics, energy devices, biological actuators, and smart electronic skin [4–8]. The parameters of these smart materials can work under mechanical deformation and interconnect with great mechanical flexibility (i.e., bending, stretching, twisting, and compressing) [1].

Wearable electronics rely heavily on metal-coated textiles to produce textile materials with special functional properties. In the previous research studies, textile based conductive materials were widely fabricated via various deposition methods [9,10]. Currently, some advanced techniques have been introduced to fabricate smart conductive textile materials such as atomic layer deposition [11], galvanic deposition, and electroless deposition (ELD) of metals [12,13]. Among the above techniques, ELD is the most utilized technique because of its low cost and easy process of fabrication at room temperature [14,15]. The ELD technique has been extensively explored in many advanced applications including electrically conductive textiles [16], EMI shielding [17,18], telecommunication frequencies, and electrostatic discharge [19]. Generally, the ELD method is carried out in three steps: the functional polymer anchoring layer by surface modification, the filling of catalyst on the polymer anchoring layer with ion exchange, and the deposition of site selective metals. Previously, ELD with different textile fabrics such as polyester, cotton, nylon, and Kevlar showed electrical properties with low cost at room temperature [20–23].

The previous textile based conductive fabrics contain a low surface area and high porous structure, which can limit the metal deposition rate. Electrospun nanofibers have gained much attraction in wide applications due to their high surface area and can create a high metal deposition rate [2]. Recently, polyester nanofibers have been achieved from waste drinking bottles having good mechanical strength and flexibility [24]. This is an alternate method to produce products from waste material and minimize solid waste in the environment. In 2019, the global market of recycled polyethylene terephthalate (r-PET) was valued at USD 7.34 billion, with a growth projection of 7.9% until 2027. These data show the importance of the r-PET market with consumers being more conscious about environmental sustainability [25].

Nanotechnology has deep roots in every field of life and in helping the research community to solve a wide a range of challenges [26]. Electrospinning is a simple technique to produce fibers with diameters in the range of a few tens to hundreds of nanometers. Electrospun nanofibers have a range of applications such as food packaging, wound dressings, tissue engineering, water filtration [27–30], air filtration, facemasks, flexible electronics, and sensors [31]. Keeping in the broad scope of electrospun nanofibers, the aim of this study is to investigate the ELD performance on electrospun nanofiber to fabricate flexible and conductive materials. The r-PET nanofibers were fabricated via the electrospinning technique, and copper metal was deposited by following the ELD method. The deposition of copper metal on r-PET nanofibers was characterized using scanning electron microscopy (SEM), energy dispersive X-ray spectroscopy (EDX), X-ray photoelectron spectroscopy (XPS), water contact angle, and tensile strength. Finally, the surface conductivity of metal deposited r-PET nanofibers was assessed using a four-point probe meter.

3.2. Experimental Section

*3.*2.1. Materials

Recycled polyethylene terephthalate (r-PET) was obtained from water bottles at a convenience store in Japan and were utilized directly without further purification. Trifluoracetic acid, chloroform, vinyltrimethoxysilane (98%), (2-(methacryloyloxy) ethyl) tri-methyl-ammonium chloride solution (METAC), ammonium tetra-chloro-palladate (II), and copper (II) sulfate pentahydrate were purchased from Sigma Aldrich USA (St. Louis, MI, USA). Chemical reagents, potassium sodium tartrate tetrahydrate, formaldehyde, potassium persulfate, and sodium hydroxide were purchased from Sinopharm Chemical Reagent Co., Ltd. (Huangpu, Shanghai, China).

*3.*2.2. Fabrication of r-PET Nanofibers

The r-PET nanofibers were fabricated by following the previous protocol [24]. Briefly, r-PET bottles were cut into small pieces (approximately 1 × 1 cm2) and dissolved in the TFA/chloroform with a ratio of 1:3 in order to make a 15% w/w polymer composition. Electrospinning was performed using a high-voltage power supply (Har − 100 × 12, Matsusada Co.; Tokyo, Japan) at room temperature. The prepared solution was poured into a syringe with a capillary tip attached having an internal diameter of 0.6 mm and keeping a 0.5 mL/h flow rate with a supplied voltage of 15 kV. The as-prepared r-PET nanofibers were collected on aluminum foil wrapped over a rotary collector system, and the capillary tip to collector distance was set as 15 cm. After electrospinning, the r-PET nanofibers were peeled off and dried overnight before further use.

3.2.3. Fabrication of Conductive r-PET Nanofibers

Graphical abstract represents the complete fabrication process to prepare conductive r-PET nanofibers and characterized by 4 steps (plasma treatment, silanization, polymerization, and electroless deposition). Each step is explained below.

3.2.3. Plasma Treatment

The obtained r-PET nanofibers were hydrophobic, and to create hydroxyl groups before the silanization process, plasma treatment was needed. Previously, plasma treatment was used to create hydroxyl groups on textile substrates [2]. The r-PET nanofibers were treated with air plasma using Harrick Plasma cleaner PDC-002, and the parameters for plasma treatment are listed below in Table 1.

Table 1

Table 1. Plasma treatment parameters.

Gas	Pressure (Pa)	Power (W)	Time (min)
Oxygen	30	45	5

3.2.4. Silanization

The plasma treated r-PET nanofibers were placed in an ethanol solution having 10% (v/v) vinyl-tri-methoxy-silane (VTMS) for 20 min. The VTMS-treated r-PET nanofibers were rinsed with DI water and immediately vacuum dried at 50℃. The successful VTMS treatment provided the hydrophobic surface of r-PET nanofibers due to the presence of dense vinyl groups.

3.2.5 Polymerization

The silanized-treated r-PET nanofibers were immersed into a polymerization solution, which contained a mixture of 20% (v/v) METAC aqueous solution (100 mL) and 60mg of potassium persulfate (KPS) for 60 min to carry out the polymerization of METAC (PMETAC) brushes

while stirring at 60℃. Finally, the polymerized r-PET nanofibers were washed with DI water and vacuum dried at 50℃ for 2 h.

3.2.6 Electroless deposition

The electroless deposition (ELD) of copper was carried out on PMETAC r-PET nanofibers by following previous protocols [20,22–24]. Briefly, the PMETAC r-PET nanofibers were immersed in a 5mM aqueous solution of ammonium tetra-chloro-palladate (II) (NH4)2PdCl4) for 20 min for the ion-exchange reaction. During the ion-exchange, [PdCl4]2- catalytic ions were immobilized onto the quaternary ammonium groups of PMETAC polymer chains, and the samples were gently washed with DI water. Further, an ELD bath was prepared to contain Solutions A and B (Table 2) with a ratio of 1:1, where Solution A consisted of 13 g/L copper sulfate pentahydrate, 12 g/L sodium hydroxide, and 29 g/L potassium sodium tartrate tetrahydrate, while Solution B contained formaldehyde 9.5 mL/L in DI water. A detailed summary of the chemicals used during the fabrication of the conductive r-PET nanofibers is given in Tables 2 and 3.

*Table 2*Table 2. Chemicals used for functionalization. VTMS, vinyl-tri-methoxy-silane; METAC, (2-(methacryloyloxy) ethyl) tri-methyl-ammonium chloride solution.

Chemicals	Formula	Process	Concentration
VTMS	C5H12O3Si	Salinization	20% (v/v in ethanol)
METAC	C9H18ClNO2	Polymerization	20%
Potassium persulfate	K2S2O8	Ion Exchanger	60 mg/100mL
Ammonium tetrachloropalladate(II)	(NH4)2PdCl4		5 mM

*Table 3*Table 3. Chemicals used for functionalization.

	Chemicals	Formula	Concentration
Solution A	Potassium sodium tartrate tetrahydrate	KNaC4H4O6·4H2O	29 g/L
	Sodium hydroxide	NaOH	12 g/L
Solution B	Copper(II) sulfate pentahydrate	CuSO4·5H2O	13 g/L
	Formaldehyde	HCHO	9.5 g/L

3.2.7. SEM Morphology

Scanning electron microscopy (S-3000N; Hitachi, Tokyo, Japan) with an acceleration voltage of 30 kV was used to observe the surface morphology of the neat r-PET nanofibers and copper-coated r-PET nanofibers. The EDX images and spectrum were obtained using an S-3000 N, Hitachi Ltd. X-ray spectroscopy, Japan. All samples of SEM and EDX were sputter coated with gold before analysis.

3.2.8. XPS Analysis

The X-ray spectroscopy (XPS) (S-3000 N, Hitachi, Tokyo, Japan) was performed to analyze the chemical composition of the neat r-PET nanofibers and copper-coated r-PET nanofibers.

3.2.9. Water Contact Angle

An OCA-40 contact angle instrument (Data physics Filderstadt Germany) was applied to determine the water contact angle of neat r-PET nanofibers and each process involved to fabricate the conductive r-PET nanofibers.

3.2.10. Tensile Strength Properties

The mechanical properties of neat r-PET nanofibers and copper-coated r-PET nanofibers after the ELD process were tested by a Titan Universal Tester 3-910, Titan Company Ltd., Germany. The tensile strength was measured according to the ASTM D-638 standard. During the test, the speed was set at 5.0 mm/min. The values of the stress-strain curves and Young's modulus were calculated by using the following Equations (1)–(3), respectively [29,31].

$$\varepsilon = \frac{\Delta l}{l} \quad (1)$$

$$\sigma = \frac{F}{A} \quad (2)$$

$$E = \frac{\sigma}{\varepsilon} \quad (3)$$

where Ɛ, σ, and E represents the stress, strain, and Young's modulus, respectively. Δl represent the change in length, and l shows the original length of the specimen. F is the applied force on the specimen, and A is the area of the specimen.

3.2.11. Shrinkage Test

The shrinkage test was performed by taking 5 × 5 cm2 r-PET nanofibers with an average thickness of 120 µm. The shrinkage of r-PET nanofibers after the ELD process was calculated by using Equation (4) for lengthwise shrinkage and Equation (5) for widthwise shrinkage, respectively.

$$Ls = \frac{L-\Delta L}{L} \times 100, \quad (4)$$

$$Ws = \frac{W-\Delta W}{W} \times 100, \quad (5)$$

$$Rs = \sqrt{Ls^2 + Ws^2} \quad (6)$$

In Equation (4), Ls is lengthwise shrinkage, L is the original length of the samples, and ΔL is the change in the original length after the ELD process. In Equation (5), Ws is widthwise shrinkage. W is the original width of the samples. Δw is the change in the original width after the ELD process. In Equation (6), Rs is the residual shrinkage after the ELD process.

3.3. Results and Discussion

*3.*3.1. Scanning Electron Microscopy

In this study, neat r-PET nanofiber samples were assessed by SEM (scanning electron microscopy) and analyzed to identify the surface morphology before and after the copper ELD process. The SEM images are shown in Figure 2A, which indicate that neat r-PET nanofibers have a smooth surface area and good morphology with an average diameter of 350 nm, whereas after electroless deposition of the copper, a conformal layer on the r-PET nanofibers was produced while retaining the smooth nanofiber surface texture, as shown in Figure 2C, with an average diameter of 700 nm. The copper-coated r-PET nanofibers had a diameter around 700 nm, which is slightly higher than the pristine r-PET nanofibers due to copper deposition on the nanofibers [24].

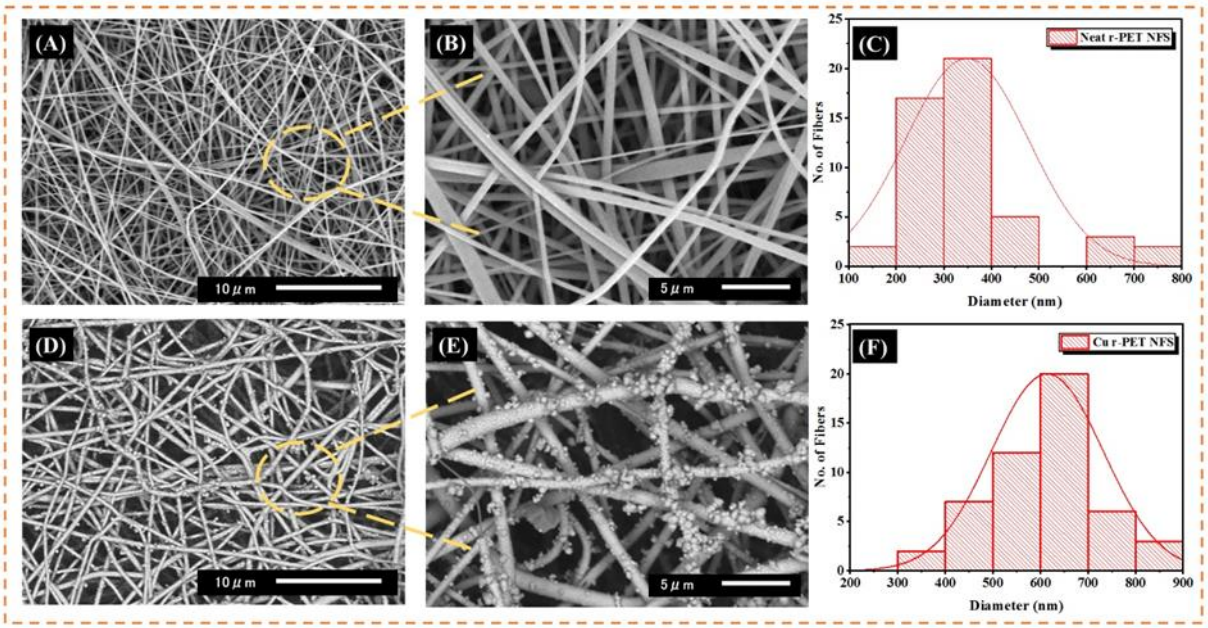

Figure 2. (A) SEM image of neat recycled polyethylene terephthalate (r-PET) nanofibers; (B) magnified SEM image of neat r-PET nanofibers; (C) diameter distribution of neat r-PET nanofibers; (D) SEM images of copper-coated r-PET nanofibers; (E) magnified SEM image of r-PET nanofibers; and (F) diameter distribution of copper-coated r-PET nanofibers.

3.3.2. EDX Analysis

The EDX elemental mapping was applied to verify the presence of copper metal in r-PET nanofibers as shown in Figures 3 and 4, respectively. Based on the characterization of the results, the r-PET nanofibers were composed of carbon and oxygen with no other impurities, as shown in Table 4. On the other hand, in Figure 4, the copper-coated r-PET nanofibers were composed of copper, carbon, and oxygen. As presented in Table 5, copper particles were uniformly distributed on the surface of r-PET nanofibers and contained 71% of copper by weight. r-PET nanofibers had a high surface area [31]; therefore, the deposition rate of copper nanoparticles was higher on the copper-coated r-PET nanofibers than the deposition on conventional textile [32].

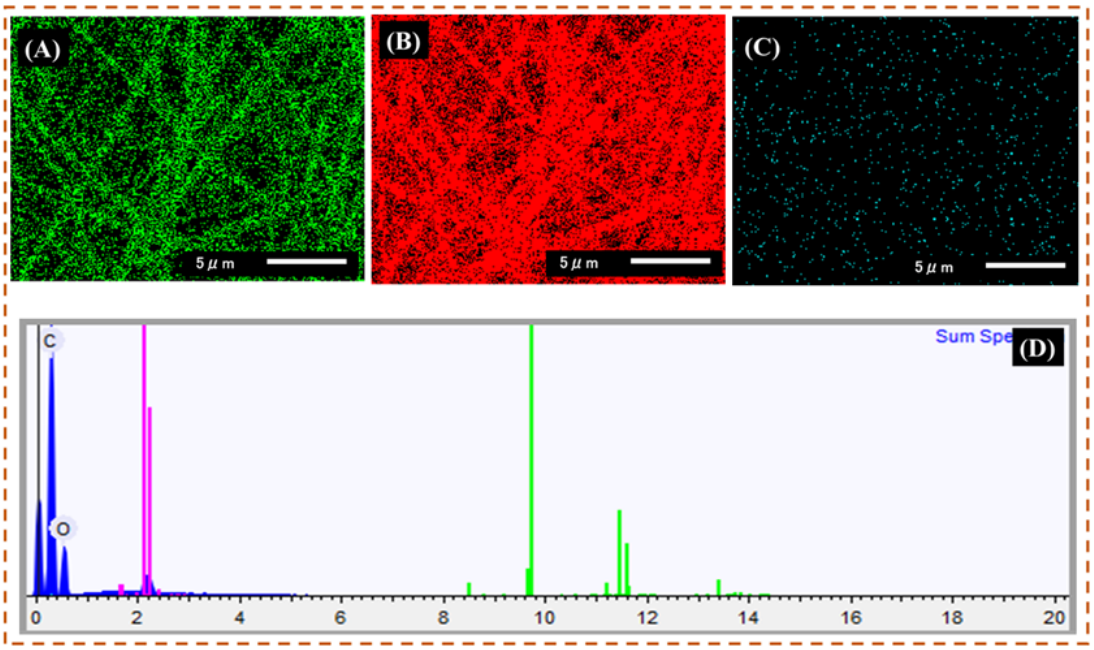

Figure *3*. EDX elemental mapping and spectrum of neat r-PET nanofibers. (A), (B), and (C) show the oxygen, carbon, and gold elemental mapping, respectively. (D) EDX full spectrum of neat r-PET nanofibers

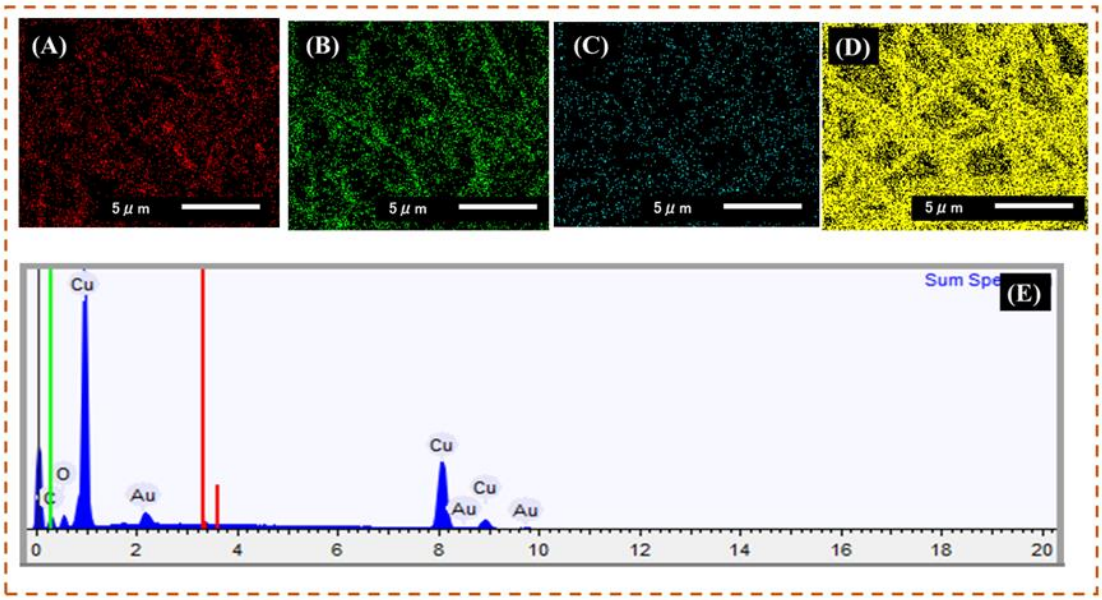

Figure 4. EDX elemental mapping and spectrum of copper-coated r-PET nanofibers. (A), (B), (C), and (D) show the oxygen, carbon, gold, and copper elemental mapping, respectively. And (E) EDX full spectrum of copper-coated r-PET nanofibers.

Table 4*Table 4. Summary if the results of elemental mapping.*

Element	Weight%	Weight% σ	Atomic%
Carbon	66.649	0.286	72.692
Oxygen	33.351	0.286	27.308

Table 5 Summary of the results of elemental mapping.

Element	Weight%	Weight% σ	Atomic%
Carbon	16.098	0.352	46.818
Oxygen	5.786	0.158	12.633
Copper	71.685	0.379	39.409
Gold	6.430	0.242	1.140

3.3.3. XPS Analysis

To investigate the specific elements and the presence of the chemical bonds, the XPS analysis was performed on neat r-PET nanofibers and copper-coated r-PET nanofibers to ensure the presence of copper elements after the ELD process, which was also confirmed by the EDX process. Figure 5 shows the spectrum peaks with a wide range for all samples of neat r-PET nanofibers and copper-coated r-PET. The XPS spectrum of copper-coated r-PET nanofibers revealed some additional peaks at a binding energy of (990.5–952eV), which could not be seen in the neat r-PET nanofibers. Furthermore, to ensure the presence of oxygen, nitrogen, sulfur, and carbon groups, along with their bond types, samples were investigated under XPS spectroscopy separately with the respective region and range of the spectrum of the specific elements. Figure 4 shows that the spectrum peaks at a binding energy of (529.4 – 286.3) in the region O1s, which revealed the same groups of C−O and C = O/O−C = O bonds for neat r-PET nanofibers and copper-coated r-PET nanofibers. As shown in Figure 4, copper-coated r-PET nanofibers revealed additional peaks at a binding energy of (990.5–952eV) in the region of 2p Cu 2p3/2 Cu 2p1/2, which led to the overlap of copper particles on the surface of nanofibers, which may show the presence of C-C double metallic bonds.

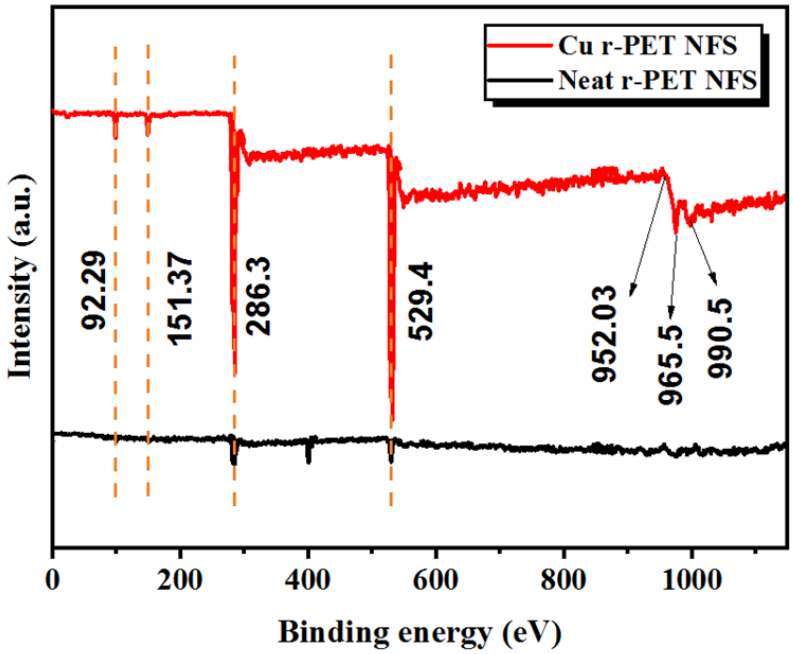

Figure 5. XPS analysis of neat r-PET nanofibers and copper-coated r-PET nanofibers.

3.3.4. Water Contact Angle Analysis

The water contact angle was used to examine each successful step required for the ELD process. Figure 6 indicates the water contact angle measurement for each step in the ELD process. The obtained r-PET nanofibers had a hydrophobic nature, and we needed to create hydroxyl groups before the silanization process. Plasma treatment was used to create the hydroxyl groups on the textile substrates, and the water contact angle of r-PET nanofibers changed from (140° ± 5)° to (14 ± 3)° [34]. This change showed that hydroxyl groups were created on the surface of the nanofibers, which were helpful for the VTMS process. r-PET nanofibers were impregnated in a 20% solution of the VTMS in ethanol, which reacted with the silane molecules and hydroxyl groups on the surface of the nanofibers, and the VTMS-treated r-PET nanofibers showed a hydrophobic property, yielding (138 ± 3)° due to the presence of dense vinyl groups, as shown in Figure 6 [37]. Furthermore, the solution was prepared containing the METAC monomer and potassium persulfate (KPS) initiator for polymerization. In the polymerization process, the VTMS based r-PET nanofibers were impregnated for a certain time, and the

chemical reaction happened in the meantime. After the polymerization, the water contact angle reached (80 ± 5)°, which might have happened due to the presence of some hydroxyl groups in METAC [38]. In the final process, PMETAC based r-PET nanofibers were impregnated in an ELD bath. After the ELD process, the r-PET nanofibers were fully covered with copper particles, and the water contact angle was (138 ± 5)°, which may be attributed mainly to the presence of copper nanoparticles on the surface of the r-PET nanofibers [20].

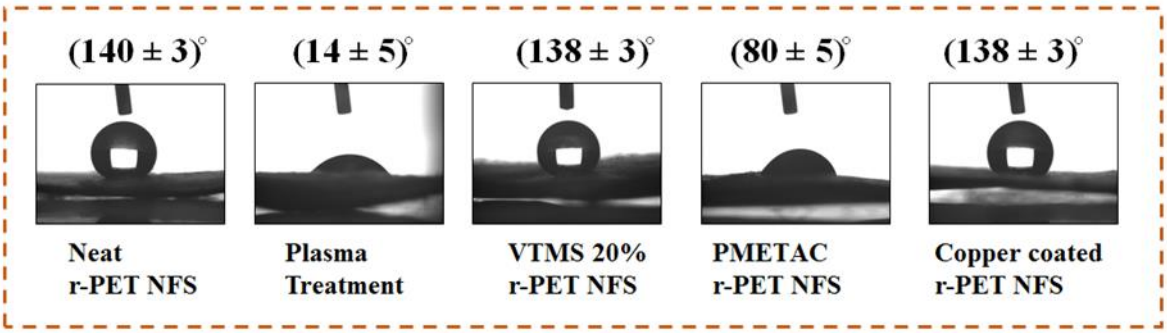

Figure 6. Water contact angle analysis of neat r-PET nanofibers and copper-coated r-PET nanofibers.

3.3.5. Optimum Temperature and Time Study

In the electroless deposition, temperature and time had significant effects on the deposition of copper on r-PET nanofibers. Figure 7 shows the results of the samples obtained with different deposition temperatures and times. The temperature for copper deposition on r-PET nanofibers was studied by keeping the time interval constant at 15 min. The effect on the masses at different temperatures in the ELD process is shown in Figure 7A. As the temperature increased, the mass of the r-PET nanofibers also increased and reached a maximum level of rapid increase at 40 °C. Further, with the increase of the temperature, the mass of the r-PET nanofibers was decreased, as shown in Figure 7A. Additionally, the change in the resistance at different temperatures in the ELD process is also shown in Figure 7B. It shows that as temperature increases, resistance decreases and reaches a minimum value at a temperature of 40 °C. By

further increasing the temperature, the resistance of the r-PET nanofibers increased, and this might be due to the instability of the solution caused by the higher temperature, which resulted in the poor deposition of the copper [39].

After the optimization of the temperature, for the deposition of copper on the r-PET nanofibers, time optimization was also equally important, as shown in Figure 7C,D. Figure 7C shows a notably higher increase in the deposition of copper from 3 min to 15 min with the deposition rate on the surface of the r-PET nanofibers, which gradually increased up to 30 min. As the deposition time was extended to 30 min, almost all of the surface of the r-PET nanofibers was covered with copper. Hence, in this study, fifteen minutes was the optimum time for the deposition of copper on the r-PET nanofibers. In addition, the mass of the r-PET nanofibers increased as the deposition time was prolonged, while the mass of the r-PET nanofibers remained constant. This might be due to there being no more available sites for copper deposition after 30 min. The plot of the resistance of the copper-coated r-PET nanofibers with different deposition times is shown in Figure 7D. As the deposition time increased, a uniform coating of the metal on the surface of the r-PET nanofibers was formed, which created a conducting path on the surface, and as a result, the resistance decreased. The sample obtained with a deposition time of 15 min showed minimum resistance.

According to the experimental results, continuous copper deposition could be obtained as the deposition time was extended up to 30 min, but the optimal time was observed as 15 min for the deposition of copper on the r-PET nanofibers at a temperature of 40 °C. In the optimum condition, the deposition of copper was good, showing the lowest resistance. Figure 8A,B displays the original photographs of an LED light on the surface of the prepared conductive r-PET nanofibers and the comparison of the r-PET nanofibers after the copper deposition, respectively. These results confirm that the copper was well deposited on the r-PET nanofibers and is highly recommended for use in wearable and flexible electronics applications.

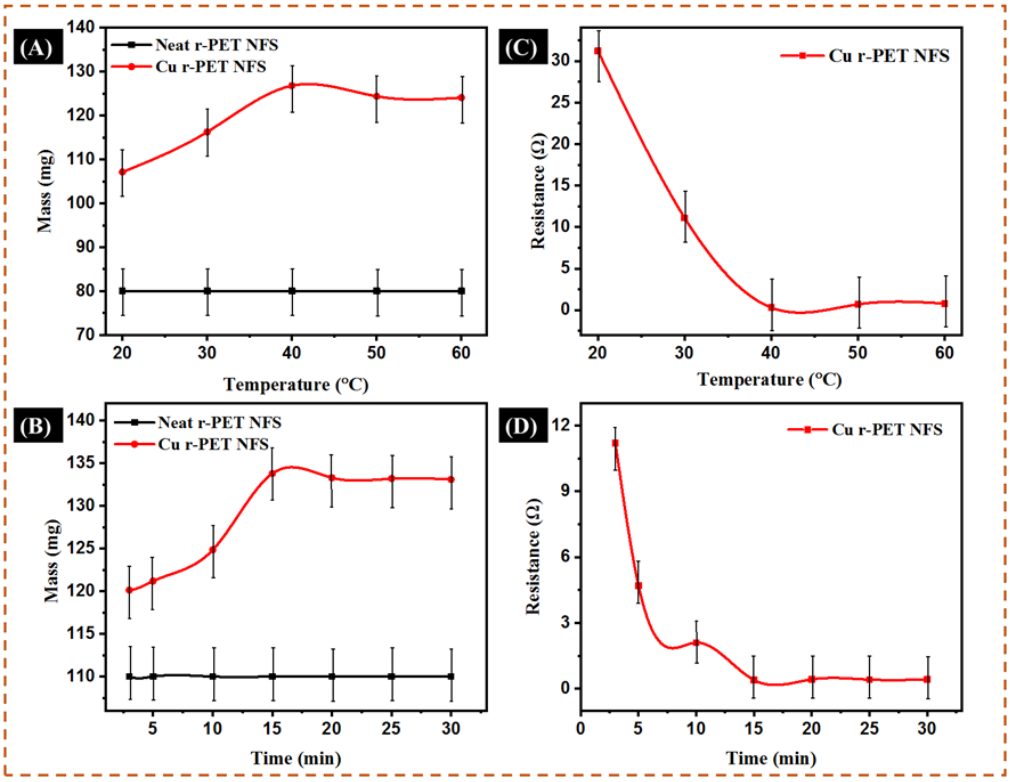

Figure 7. (A) The effect of the weight of the r-PET nanofibers as a function of temperature; (B) the effect of the resistance of the r-PET nanofibers as a function of temperature; (C) the effect of the weight of the r-PET nanofibers as a function of electroless deposition time; (D) the effect of the resistance of the r-PET nanofibers as a function of electroless deposition time.

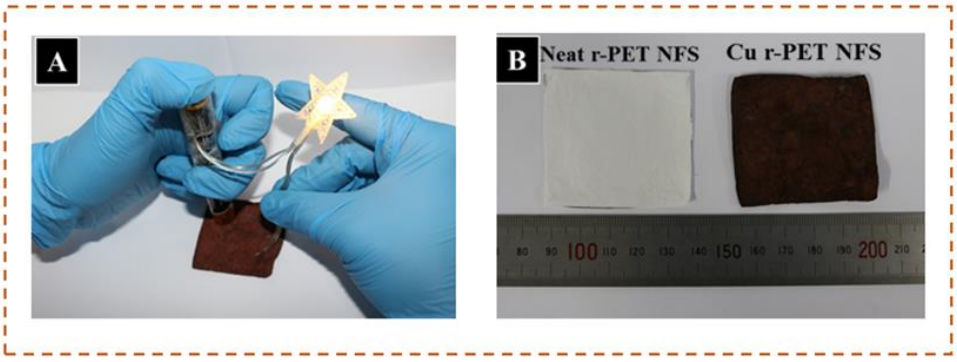

Figure 8. (A) Conductivity of r-PET NFS (B) results of copper-coated r-PET NFS after the ELD process.

3.3.6. Tensile Strength

The mechanical properties of the pristine r-PET nanofibers and copper-coated r-PET nanofibers were investigated. As shown in Figure 9, the tensile strength of pristine r-PET nanofibers was around 1.04 MPa with a deformation of about 1.2%. On the other hand, the tensile strength of copper-coated r-PET nanofibers was around 1.4 MPa with a deformation of about 1.3%. These results depict that there was stronger bonding between the copper particles and r-PET nanofibers. Young's modulus (elastic modulus) was calculated considering elastic regions of both types of nanofibrous mats. It was observed that the elastic modulus of Cu r-PET nanofibers was slightly increased. This may be because of the presence of metallic nanoparticles (Cu NPs).

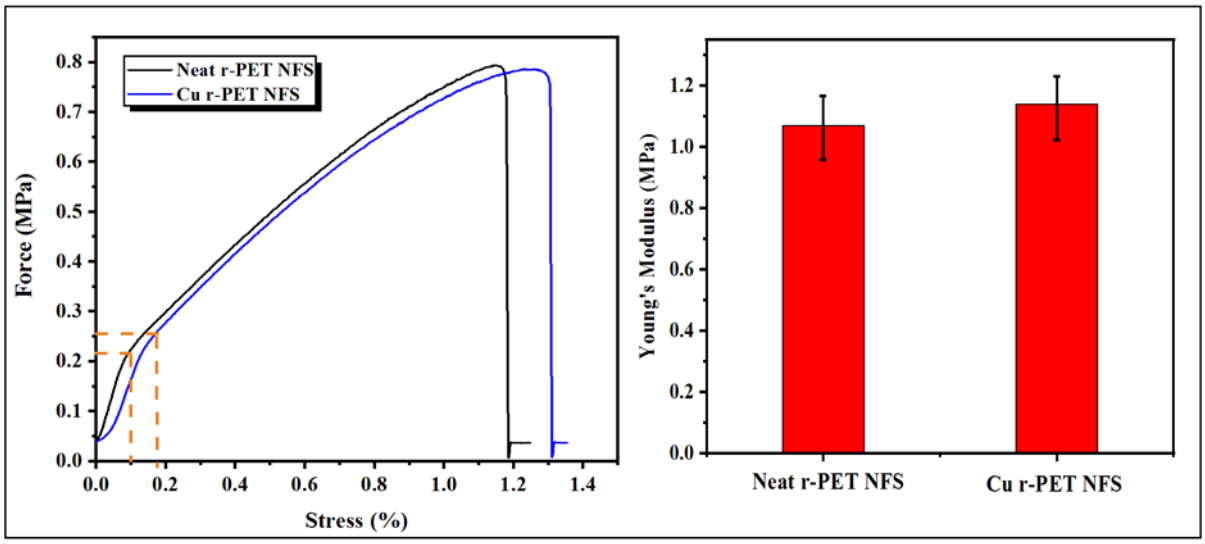

Figure 9. Stress–strain curve and Young's modulus values of neat r-PET nanofibers and copper-coated r-PET nanofibers after the ELD process.

3.3.7. Shrinkage Study

The r-PET nanofibers after being exposed to the salinization and the ELD process substantially shrunk, so it was necessary to analyze the shrinkage behavior in the r-PET nanofibers after the ELD process; there was exaggeration in documenting the finding. Table 6 shows the shrinkage

results, which show that the shrinkage behavior was also dependent on the medium used irrespective of the ELD process. In copper-coated r-PET nanofibers, the shrinkage percentage was higher than in the neat r-PET nanofibers. Salinization and temperature caused a maximum shrinkage within the copper-coated r-PET nanofibers after the ELD process. Ultimately, shrinkage was also the reason for the greater strength and attachment of the copper particles on the substrate compared to the neat r-PET nanofibers.

Table 6. Shrinkage of the r-PET nanofibers after the ELD process.

Shrinkage	Lengthwise	Widthwise
Cu r-PET NFS	11%	12%

a The shrinkage study was calculated by using Equations (4) and (5).

3.4. Conclusions

In this research study, copper-coated r-PET nanofibers were successfully fabricated by the process of electroless deposition. The optimized temperature was observed as 40 °C, and the optimized time of 15 min was set for proper copper deposition on the r-PET nanofibers. The SEM images evidently showed the fibrous morphology of the r-PET nanofibers with an average diameter of 350 nm, and the copper-coated r-PET nanofibers retained the fibrous morphology with a slight increase in the average diameter of 700 nm. The optimized copper-coated r-PET nanofibers were composed of 71.6% copper and showed a low electrical resistance of 0.1 Ω. Moreover, the r-PET nanofibers were flexible and showed good mechanical strength. As-prepared, conductive r-PET nanofibers have good potential and could be used in many applications such as wearable electronics, flexible sensors, and energy storage.

References

1. Wang, X.; Yan, C.; Hu, H.; Zhou, X.; Guo, R.; Liu, X.; Xie, Z.; Huang, Z.; Zheng, Z. Aqueous and air-compatible fabrication of high-performance conductive textiles. Chem. - An Asian J. 2014, 9, 2170–2177, doi:10.1002/asia.201402230.

2. Hussain, N.; Yousif, M.; Ali, A.; Mehdi, M.; Ullah, S.; Ullah, A.; Mahar, F.K.; Kim, I.S. A facile approach to synthesize highly conductive electrospun aramid nanofibers via electroless deposition. Mater. Chem. Phys. 2020, 255, 123614, doi:10.1016/j.matchemphys.2020.123614.

3. White, M.S.; Kaltenbrunner, M.; Głowacki, E.D.; Gutnichenko, K.; Kettlgruber, G.; Graz, I.; Aazou, S.; Ulbricht, C.; Egbe, D.A.M.; Miron, M.C.; et al. Ultrathin, highly flexible and stretchable PLEDs. Nat. Photonics 2013, 7, 811–816, doi:10.1038/nphoton.2013.188.

4. Verpoorten, E.; Massaglia, G.; Ciardelli, G.; Pirri, C.F.; Quaglio, M. Design and optimization of piezoresistive peo/pedot:Pss electrospun nanofibers for wearable flex sensors. Nanomaterials 2020, 10, 1–13, doi:10.3390/nano10112166.

5. Cui, J.; Zhou, Z.; Jia, M.; Chen, X.; Shi, C.; Zhao, N.; Guo, X. Solid polymer electrolytes with flexible framework of SiO2 nanofibers for highly safe solid lithium batteries. Polymers (Basel). 2020, 12, doi:10.3390/POLYM12061324.

6. Benight, S.J.; Wang, C.; Tok, J.B.H.; Bao, Z. Stretchable and self-healing polymers and devices for electronic skin. Prog. Polym. Sci. 2013, 38, 1961–1977, doi:10.1016/j.progpolymsci.2013.08.001.

7. Mokhtari, F.; Shamshirsaz, M.; Latifi, M.; Foroughi, J. Nanofibers-based piezoelectric energy harvester for self-powered wearable technologies. Polymers (Basel). 2020, 12, 1–15, doi:10.3390/polym12112697.

8. Hu, L.; Pasta, M.; La Mantia, F.; Cui, L.; Jeong, S.; Deshazer, H.D.; Choi, J.W.; Han, S.M.; Cui, Y. Stretchable, porous, and conductive energy textiles. Nano Lett. 2010, 10, 708–714, doi:10.1021/nl903949m.

9. Pandey, P.A.; Bell, G.R.; Rourke, J.P.; Sanchez, A.M.; Elkin, M.D.; Hickey, B.J.; Wilson, N.R. Physical vapor deposition of metal nanoparticles on chemically modified graphene: Observations on metal-graphene interactions. Small 2011, 7, 3202–3210,

doi:10.1002/smll.201101430.

10. Grodzicki, A.; Łakomska, I.; Piszczek, P.; Szymańska, I.; Szłyk, E. Copper(I), silver(I) and gold(I) carboxylate complexes as precursors in chemical vapour deposition of thin metallic films. Coord. Chem. Rev. 2005, 249, 2232–2258, doi:10.1016/j.ccr.2005.05.026.

11. Myndrul, V.; Vysloužilová, L.; Klápšt'Ová, A.; Coy, E.; Jancelewicz, M.; Iatsunskyi, I. Formation and photoluminescence properties of ZnO nanoparticles on electrospun nanofibers produced by atomic layer deposition. Coatings 2020, 10, 1–10, doi:10.3390/coatings10121199.

12. Leary, J.D.; Hamouda, F.; Mazé, B.; Pourdeyhimi, B. Preparation of pseudocapacitor electrodes via electrodeposition of polyaniline on nonwoven carbon fiber fabrics. J. Appl. Polym. Sci. 2016, 133, 1–8, doi:10.1002/app.43315.

13. Azzaroni, O.; Zheng, Z.; Yang, Z.; Huck, W.T.S. Polyelectrolyte brushes as efficient ultrathin platforms for site-selective copper electroless deposition. Langmuir 2006, 22, 6730–6733, doi:10.1021/la060891+.

14. Yu, Y.; Yan, C.; Zheng, Z. Polymer-assisted metal deposition (PAMD): A full-solution strategy for flexible, stretchable, compressible, and wearable metal conductors. Adv. Mater. 2014, 26, 5508–5516, doi:10.1002/adma.201305558.

15. Garcia, A.; Polesel-Maris, J.; Viel, P.; Palacin, S.; Berthelot, T. Localized ligand induced electroless plating (LIEP) process for the fabrication of copper patterns onto flexible polymer substrates. Adv. Funct. Mater. 2011, 21, 2096–2102, doi:10.1002/adfm.201100041.

16. Liu, X.; Chang, H.; Li, Y.; Huck, W.T.S.; Zheng, Z. Polyelectrolyte-bridged metal/cotton hierarchical structures for highly durable conductive yarns. ACS Appl. Mater. Interfaces 2010, 2, 529–535, doi:10.1021/am900744n.

17. Irfan, M.S.; Gill, Y.Q.; Hashmi, M.; Ullah, S.; Saeed, F.; Qaiser, A.A. Long-term stress relaxation behavior of Polyaniline-EPDM blends using the time-temperature-strain superposition method. Mater. Res. Express 2018, 6, 025318, doi:10.1088/2053-1591/aaf06a.

18. Irfan, M.S.; Gill, Y.Q.; Ullah, S.; Naeem, M.T.; Saeed, F.; Hashmi, M. Polyaniline-NBR blends by in situ polymerization: application as stretchable strain sensors. Smart Mater. Struct. 2019, 28, 095024, doi:10.1088/1361-665X/ab1df3.

19. Huang, X.; Dai, B.; Ren, Y.; Xu, J.; Zhu, P. Preparation and study of electromagnetic interference shielding materials comprised of Ni-Co coated on web-like biocarbon nanofibers via electroless deposition. J. Nanomater. 2015, 2015, doi:10.1155/2015/320306.

20. Liu, S.; Hu, M.; Yang, J. A facile way of fabricating a flexible and conductive cotton fabric. J. Mater. Chem. C 2016, 4, 1320–1325, doi:10.1039/C5TC03679H.

21. Mu, S.; Xie, H.; Wang, W.; Yu, D. Electroless silver plating on PET fabric initiated by in situ reduction of polyaniline. Appl. Surf. Sci. 2015, 353, 608–614, doi:10.1016/j.apsusc.2015.06.126.

22. Yu, D.; Mu, S.; Liu, L.; Wang, W. Preparation of electroless silver plating on aramid fiber with good conductivity and adhesion strength. Colloids Surfaces A Physicochem. Eng. Asp. 2015, 483, 53–59, doi:10.1016/j.colsurfa.2015.07.021.

23. Pang, H.; Bai, R.; Shao, Q.; Gao, Y.; Li, A.; Tang, Z. A novel Ag catalyzation process using swelling impregnation method for electroless Ni deposition on Kevlar ® fiber. Appl. Surf. Sci. 2015, 359, 280–287, doi:10.1016/j.apsusc.2015.10.100.

24. Mahar, F.K.; Mehdi, M.; Qureshi, U.A.; Brohi, K.M.; Zahid, B.; Ahmed, F.; Khatri, Z. Dyeability of recycled electrospun polyethylene terephthalate (PET) nanofibers: Kinetics and thermodynamic study. J. Mol. Liq. 2017, 248, 911–919, doi:10.1016/j.molliq.2017.10.116.

25. Bohaczuk, Venturelli, R,; Serafini, Immich, A. P,; MA, Guelli U de Souza, S,; & U, de, Souza, A, A.; Recycled polyester nanofiber as a reservoir for essential oil release. Journal of Applied Polymer Science, (2020) 50258.

26. Hashmi, M.; Ullah, S.; Ullah, A.; Akmal, M.; Saito, Y.; Hussain, N.; Ren, X.; Kim, I.S. Optimized Loading of Carboxymethyl Cellulose (CMC) in Tri-component Electrospun Nanofibers Having Uniform Morphology. Polym. 2020, Vol. 12, Page 2524 2020, 12, 2524, doi:10.3390/POLYM12112524.

27. Nadir Hussain, Sana Ullah, Muhammad Nauman Sarwar, Motahira Hashmi, Muzamil Khatri, Takumi Yamaguchi, Zeeshan Khatri, and I.S.K. Fabrication and Characterization of Novel Antibacterial Ultrafine Nylon-6 Nanofibers Impregnated by Garlic Sour Nadir. 2020, 21, 2780–2787, doi:10.1007/s12221-020-0031-5.

28. Ullah, S.; Hashmi, M.; Hussain, N.; Ullah, A.; Sarwar, M.N.; Saito, Y.; Kim, S.H.; Kim, I.S. Stabilized nanofibers of polyvinyl alcohol (PVA) crosslinked by unique method for efficient removal of heavy metal ions. J. Water Process Eng. 2020, 33, 101111, doi:10.1016/j.jwpe.2019.101111.

29. Mehdi, M., Mahar, F. K., Qureshi, U. A., Khatri, M., Khatri, Z., Ahmed, F., & Kim, I. S. Preparation of colored recycled polyethylene terephthalate nanofibers from waste bottles: Physicochemical studies. Advances in Polymer Technology, 37, 2018 2820-2827.

30. Wang, B., Zhao, M., Mehdi, M., Wang, G., Gao, P., & Zhang, K. Q. Biomolecule-assisted synthesis and functionality of metal nanoclusters for biological sensing: a review. Materials Chemistry Frontiers, 3, 2019 1722-1735.

31. Hashmi, M.; Ullah, S.; Ullah, A.; Khan, M.Q.; Hussain, N.; Khatri, M.; Bie, X.; Lee, J.; Kim, I.S. An optimistic approach “from hydrophobic to super hydrophilic nanofibers” for enhanced absorption properties. Polym. Test. 2020, 90, 106683, doi:10.1016/j.polymertesting.2020.106683.

32. Sereshti, H.; Amini, F.; Najarzadekan, H. Electrospun polyethylene terephthalate (PET) nanofibers as a new adsorbent for micro-solid phase extraction of chromium(VI) in enVIronmental water samples. RSC Adv. 2015, 5, 89195–89203, doi:10.1039/c5ra14788c.

33. Guo, R.H.; Jiang, S.X.; Yuen, C.W.M.; Ng, M.C.F.; Lan, J.W. Optimization of electroless nickel plating on polyester fabric. Fibers Polym. 2013, 14, 459–464, doi:10.1007/s12221-013-0459-y.

34. Demir, A.; Bozaci, E.; Gülümser, T.; Sarikanat, M. An ecological approach for the surface modification of aramid fibers. Tekst. ve Konfeksiyon 2016, 26, 256–261.

35. Hashmi, M.; Ullah, S.; Ullah, A.; Khan, M.Q.; Hussain, N.; Khatri, M.; Bie, X.; Lee, J.; Kim, I.S. An optimistic approach “from hydrophobic to super hydrophilic nanofibers”

for enhanced absorption properties. Polym. Test. 2020, 90, 106683, doi:10.1016/j.polymertesting.2020.106683.

36. Hashmi, M.; Ullah, S.; Kim, I.S. Electrospun Momordica Charantia Incorporated Polyvinyl Alcohol (PVA) Nanofibers for Antibacterial Applications. Mater. Today Commun. 2020, 101161, doi:https://doi.org/10.1016/j.mtcomm.2020.101161.

37. Wang, C.; Yang, H.; Chen, F.; Peng, L.; Gao, H. fang; Zhao, L. ping Influences of VTMS/SiO2 ratios on the contact angle and morphology of modified super-hydrophobic silicon dioxide material by vinyl trimethoxy silane. Results Phys. 2018, 10, 891–902, doi:10.1016/j.rinp.2018.08.007.

38. Politakos, N.; Azinas, S.; Moya, S.E. Responsive Copolymer Brushes of Poly[(2-(Methacryloyloxy)Ethyl) Trimethylammonium Chloride] (PMETAC) and Poly(1H,1H,2H,2H-Perfluorodecyl acrylate) (PPFDA) to Modulate Surface Wetting Properties. Macromol. Rapid Commun. 2016, 37, 662–667, doi:10.1002/marc.201500630.

39. Tai, Y.; Xu, C.; Chen, H. Silver-coated glass fabric composites prepared by electroless plating. Mater. Lett. 2016, 180, 144–147, doi:10.1016/j.matlet.2016.05.118.

CHAPTER 4

Electroless Deposition: A Superficial Route to Synthesis of Highly Conductive Electrospun Nylon 6 Nanofibers

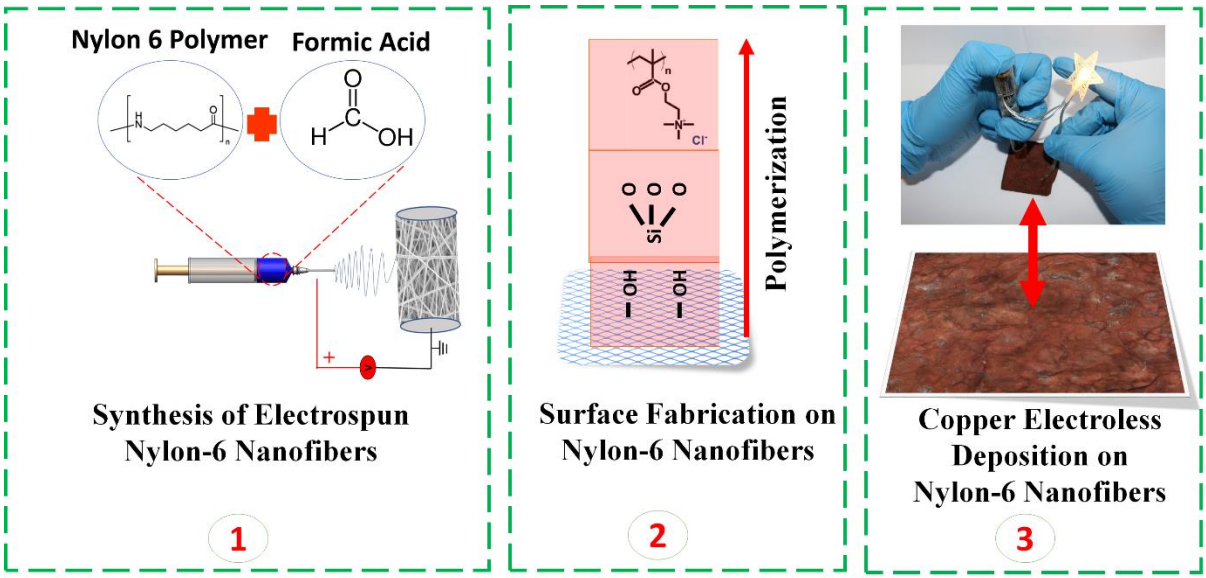

Figure 1. Schematic diagram of copper-coated N6 NFs.

4.1. Introduction

Recently, the characteristics and synthesis of flexible and wearable conductive materials have received much attention in potential applications in electronic devices [1]–[3]. Because of their incredibly high conductivity, suitable price, and comparatively outstanding stability, metal materials remain a primary choice in this regard. Metal is flexible when it is well decorated in a few layers on a polymeric substrate [4]. However, the metal may stretch or fold when appropriately formed [5], [6]. For the advancement of electronics devices, numerous processes have been reported for depositing metal nanoparticles on polymer-based substrates. Some of these methods are atomic layer deposition [7], physical vapor deposition [8], electroless plating [9]–[11], and electroless deposition (ELD). [12]–[14]. In this regard, physical vapor deposition and atomic layer deposition need expensive equipment and complicated operation processes [5]. Also, in this process, a relatively high annealing temperature must be considered, which may bring severe damage to the polymeric substrates and metal delamination. Electroplating is a process that is widely utilized at the laboratory and industrial scale. Nevertheless, for the ideal developments of conductive materials required to work under mechanical deformation for easy and economical processing, which is not applicable for most of the polymer-based substrate [10]. Among the above methods, ELD is an excellent alternative for metal deposition on polymer substrate regarding its low cost, easy process, and high conductivity. Furthermore, the ELD method is an autocatalytic redox reaction to deposit a thin coat metal layer on a catalyst-preloaded surface comprising almost all the versatile and rigid substrates. ELD is carried out at low temperatures without the need for costly equipment and with a minimum, or even no, substrate disruption. To date, ELD has been extensively studied on several versatile substrates such as cotton [1], polyethylene terephthalate [6], paper [15], polyvinylidene fluoride [16] and polyvinylpyrrolidone [17]. Besides, versatile devices built on textiles have several advantages over traditional conductive materials. Previously studies have reported

several problems, i.e., high porosity and low surface to volume ratio, which may cause a gap between metal deposition levels. Polymer-based nanofibers [8] can be considered as a solution to these problems. Polymer-based nanofibers have been promoting owing to their high surface area with low volume ratio, small pore size, and multifunctional surface properties. Smart electrically conductive materials are among the leading applications of nanofibers and have received considerable attention from scientists because of their commercial abilities to transport the electrical properties into polymer-based nanofibers [8], [16]–[18].

Among other polymer-based electrospun nanofibers, Nylon-6 (N6) polymer is one the alternative and widely explored nanofibers because of its ease of production, eco-friendly character, economic viability, unique molecular structure, suitable transition temperature, and mechanical properties [12], [19]. Therefore, the properties of nylon-6 nanofibers feasible for metal functionalization using electroless deposition technique for flexible and wearable electronics.

In this research, we attempt to fabricate the conductive Nylon 6 nanofibers (N6 NFs) by the electroless deposition technique. To this end, copper nanoparticles were deposited on the surface of the N6 NFs substrate. To analyze the deposition of copper metal on N6 NFs, characterizations such as scanning electron microscopy (SEM), energy-dispersive X-ray spectroscopy (EDX), X-ray photoelectron spectroscopy (XPS), water contact angle, and tensile test were performed. Finally, the surface conductivity of metal deposit N6 NFs was assessed using a four-point probe meter.

4.2. Experimental

4.2.1 Materials

Nylon 6 polymer with average MW 66000 and Formic acid, Vinyltrimethoxysilane (98%), [2-(Methacryloyloxy) ethyl] trimethylammonium chloride solution (PMETAC), Ammonium tetrachloropalladate (II), and Copper (II) sulfate pentahydrate were purchased from Sigma Aldrich USA. Potassium sodium tartrate tetrahydrate, Formaldehyde, Potassium persulfate, and Sodium hydroxide were purchased from Sinopharm Chemical Reagent Co. Ltd (China).

4.2.2 Electrospinning of N6 NFs

Electrospun Nylon 6 nanofibers (N6 NFs) were fabricated according to the method reported in [20]. Briefly, 20% w/w of Nylon 6 solution was prepared in formic acid and placed at a magnetic stirrer for 24 h until the solution was homogenized. Then, the prepared solution was poured into a 5 ml syringe and put on an electrospinning setup. Afterward, a 22 kV voltage was applied to the solution to produce N6 NFs, and the distance between the tip of the syringe and collector was kept at 14 cm. The flow rate was maintained at 1 ml/hour solution. The N6 NFs were collected at a rotating drum. Eventually, the prepared N6 NFs were dried and used for the ELD process.

4.2.3 Surface Treatment of N6 NFs

The surface treatment of N6 NFs was carried out in 3 steps, namely, plasma treatment, silanization, and polymerization. The previous prepared N6 NFs were electrospun and then treated with air plasma. Plasma was employed for 5 min on N6 NFs at constant pressure (30 Pa) and power (45 W). The prepared N6 NFs were silanized by immersing them in 10% vinyltrimethoxysilane (VTMS) for 20 min. Later, the silanized N6 NFs were used for polymerization after washing with double purified water and dried at 60℃. The silanized N6 NFs were immersed into a solution of 20% (v/v) PMETAC aqueous solution (100 mL) and

potassium persulfate (KSP; 60 mg) for 60 min while being continuously stirred at 60℃. In the next step, N6 NFs were treated with Ammonium tetrachloropalladate II (5 mM) for ion exchange reaction. The resulted N6 NFs were washed with double purified water and dried at 50℃ for the further ELD process.

4.2.4 Electroless Deposition on N6 NFs

Electroless deposition (ELD) was carried out according to the previously reported protocol [21]. Briefly, to prepare the copper ELD bath, two solutions 'A' and 'B' were prepared and mixed with a 1:1 ratio. Solution 'A' contains 13 g/L copper sulfate pentahydrate, 12 g/L sodium hydroxide, and 29 g/L potassium sodium tartrate tetrahydrate. In contrast, solution 'B' contains formaldehyde 9.5 mL/L in double purified water. The mentioned surface treated N6 NFs were immersed in a freshly prepared ELD bath. The effect of time, temperature, pH, and volume on the ELD process was observed and optimized.

4.2.5 Material Characterization

Scanning electron microscopy (S-3000N; Hitachi, Japan) with a high voltage of 30 kV was used to observe the surface morphology of electrospun N6 NFs and copper-coated N6 NFs.

The chemical structure of neat N6 NFs and copper-coated N6 NFs was analyzed using Fourier transform infrared spectroscopy (FTIR) on an IRPrestige-21 device by Shimadzu, Japan. From all nanofiber samples, 1-2 mg was ground with 0.1g KBr and pressed into a pellet to measure its transmission FTIR spectrum. The X-ray spectroscopy (EDX) (S-3000N; Hitachi, Japan) was performed to analyze the chemical composition of the neat N6 NFs and copper-coated N6 NFs.

Electrical resistance of copper-coated N6 NFs was measured using ST-225*C multifunctional Digital 4 Probe meter. The following equation was used to calculate the values of conductivity as gives below:

$$R = \frac{pl}{Wt} \quad (1)$$

Where R is resistance, p denotes the resistivity of the material and I is the length, W is the width and t is the thickness of the nanofibers.

The mechanical properties of neat N6 NFs and copper-coated N6 NFs were measured by Titan Universal Tester 3-910 Company Ltd, Germany. The tensile strength was measured according to the ASTM D-638 standard. During the test, speed was set at 5.0 mm/min. The following equations were used to calculate the values of stress-strain curves and Young's modulus [22].

$$\varepsilon = \frac{\Delta l}{l} \quad (2)$$

$$\sigma = \frac{F}{A} \quad (3)$$

$$E = \frac{\sigma}{\varepsilon} \quad (4)$$

where Ɛ and σ is strain and stress, respectively, E is Young's modulus, Δl is length change, l denotes the original length of the specimen, and F and A is for applied force and area of the specimen, respectively.

4.2.6. **Shrinkage test**

The copper deposition is an ambitious chemical process. For the ELD process, a heating study also was performed on the N6 substrate to examine the shrinkage. Afterward, the shrinkage study was measured by taking N6 NFs with a sample size of 5×5 cm2 and a constant average thickness of 110 µm. After the ELD process, lengthwise shrinkage and widthwise shrinkage of N6 NFs were calculated respectively.

4.3 Results and Discussions

4.3.1 Surface Morphology

The surface morphology of neat N6 NFs and copper-coated N6 NFs was examined via SEM at different magnifications (Fig. 2). As can be seen from Fig. 2, neat N6 NFs have smooth morphology and an average diameter of 100-200 nm [20]. After ELD, as copper particles were deposited on the surface of N6 NFs, the diameter of the nanofibers increased to 300-400 nm. In general, the diameter of copper-coated N6 NFs was larger than that of neat N6 NFs, suggesting the connection between copper nanoparticles around the nanofibers during the ELD process. EDX results further confirm the copper deposition on the surface of N6 NFs.

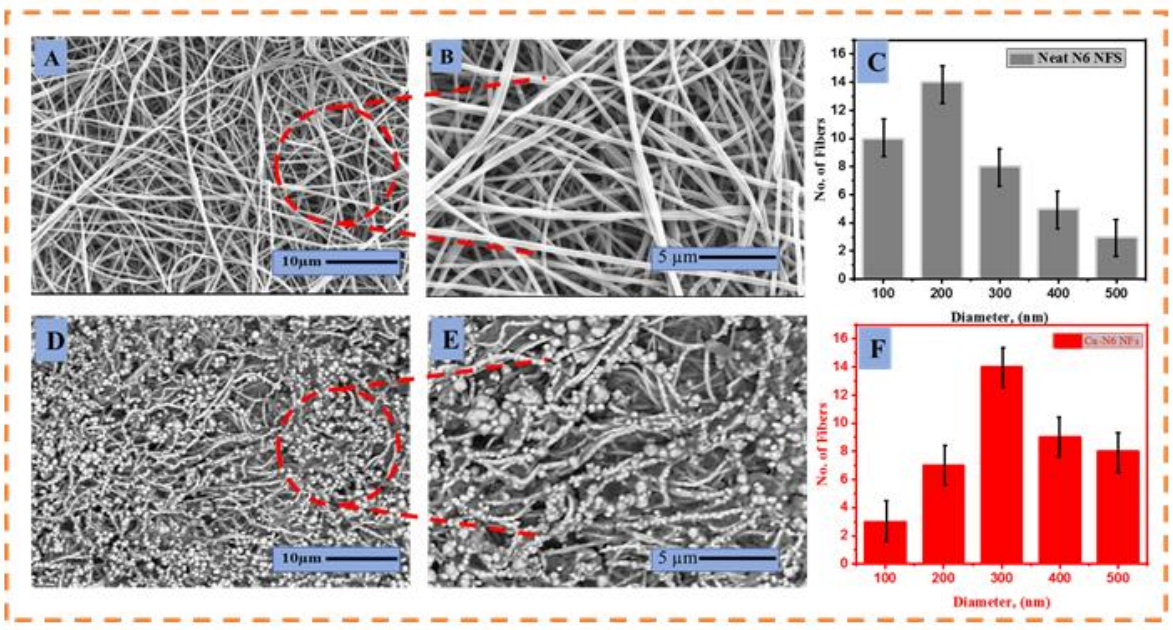

Figure 2. A SEM images of neat N6 NFs, 2B SEM images at different magnification and 2C diameter distribution of neat N6 NFS. Figure 2D SEM images of copper-coated N6 NFs, 2E SEM images at different magnification and 2F diameter distribution of copper-coated N6 NFs.

4.3.2 EDX analysis

EDX spectrum was employed on neat N6 NFs and copper-coated N6 NFs to ensure the qualitative and quantitative presence of copper nanoparticles. EDX spectrum was produced for

both neat N6 NFs and copper-coated N6 NFs. Fig 3 showed the presence of oxygen, carbon, and gold in neat N6 NFS. In comparison, Fig 4 showed, a certain amount of copper particles (73.438 % of total weight) was observed in copper-coated N6 NFs. Moreover, the central panel of the EDX image shows the rich and uniform deposition of copper particles on the surface of the N6 NFs. Therefore, uniform deposition of copper particles was confirmed by SEM and EDX spectrum (Fig. 3 and 4).

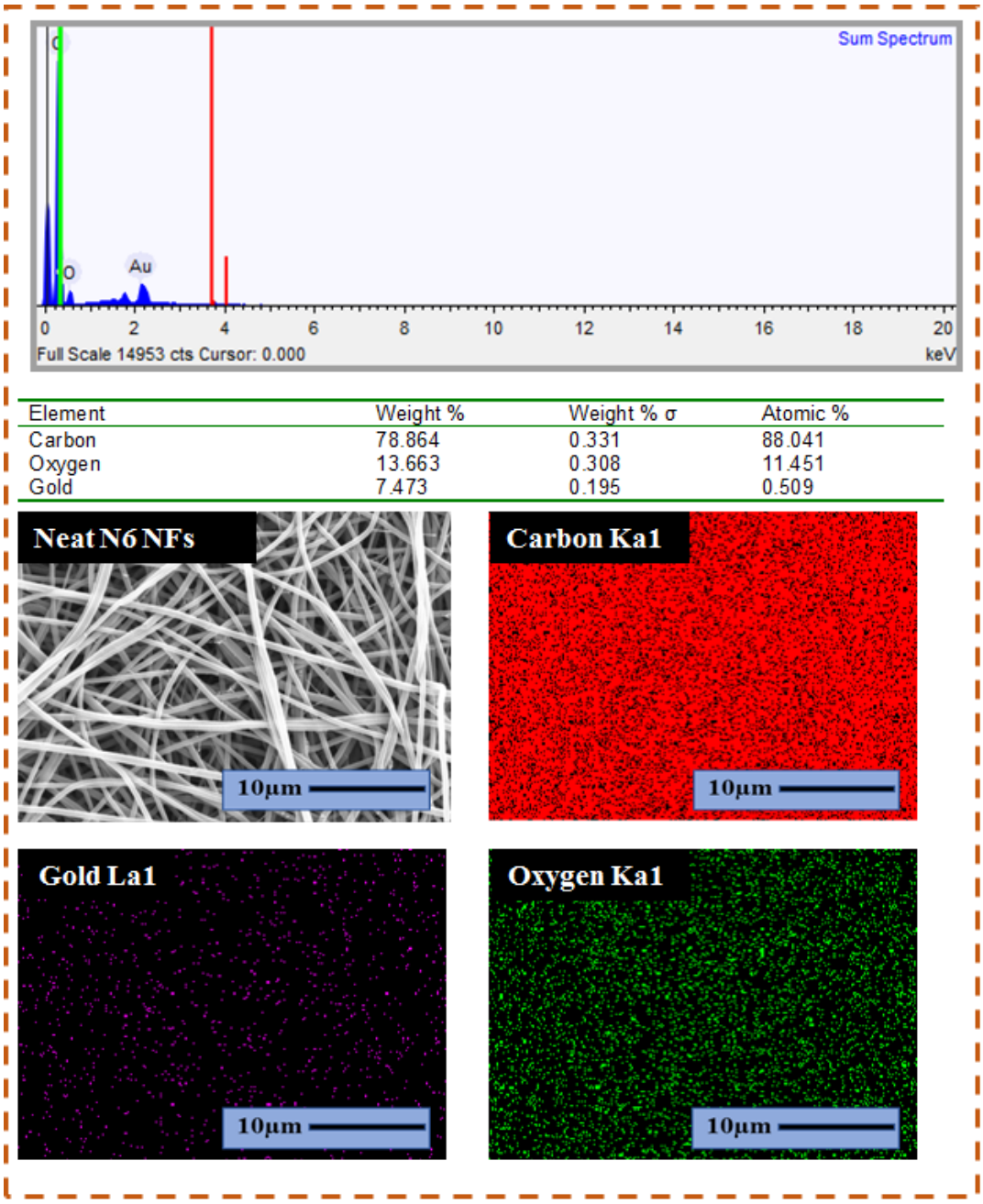

Figure *3*. EDX analysis of neat N6 NFs.

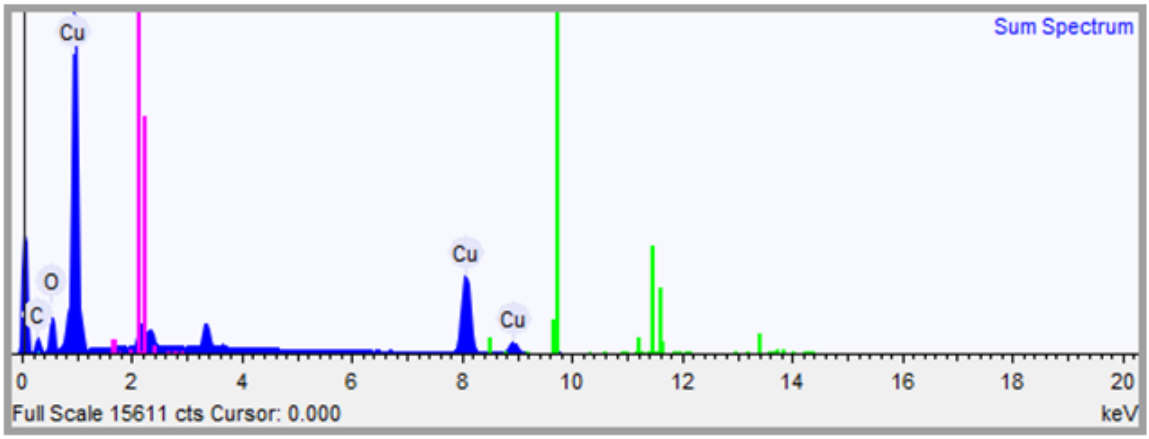

Element	Weight %	Weight % σ	Atomic %
Carbon	14.533	0.391	38.810
Oxygen	12.029	0.202	24.117
Copper	73.438	0.382	37.073

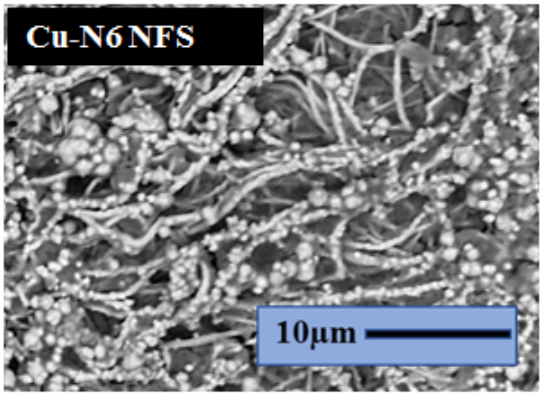

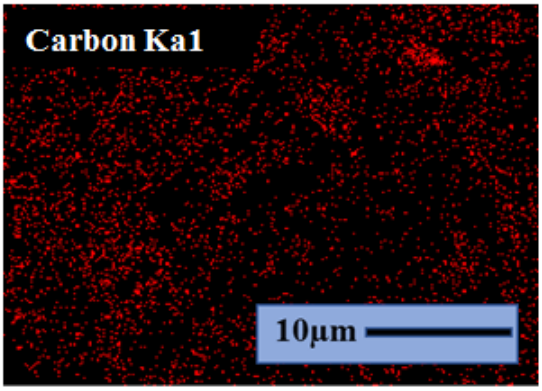

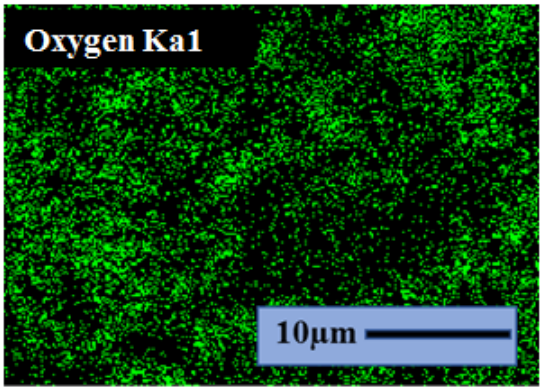

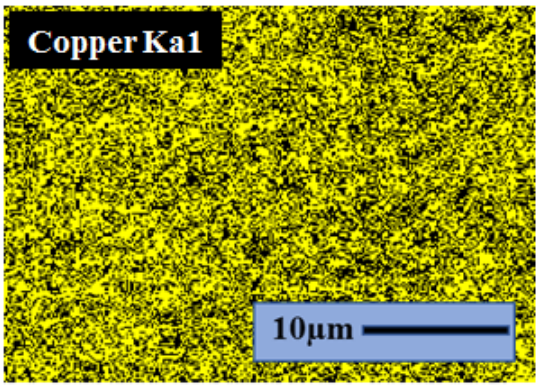

Figure 4. EDX analysis of copper-coated N6 NFs.

4.3.3 Optimum temperature, time, pH, and Volume study for copper-coated N6 NFs

The parameters including temperature, time, pH, and volume were optimized on the ELD for copper deposition. First, the influence of time was observed at a fixed temperature (40℃), pH (13), and volume (500 ml) during the ELD process. Fig. 5A shows the weight gain of copper particles and changes in resistance caused by the effect of time during the ELD process. The weight of copper particles gradually increased with increasing time from 2 min to 10 min and became constant thereafter. Meanwhile, the resistance was decreased with increasing time from 2 to 10 min. The time for the ELD process was optimized at 10 min for copper particles. The effect of temperature on copper deposition via the ELD process was optimized at 40℃, the time (10 min), pH (13), and volume (500 ml). Fig. 5B shows the weight gain of copper particles and the change in resistance caused by temperature during the ELD process. The weight of copper particles frequently raised with increasing temperature from 20 to 40℃ and decreased thereafter. The resistance was decreased with increasing temperature from 20 to 40℃ and then start to decline. The weight loss of copper particles may be attributed to the uncertainty of the solution due to higher temperatures (50℃) [21]. Hence, the temperature for the ELD process was optimized at 40℃ for copper particles. Furthermore, the influence of pH during the ELD process was observed and optimized. It can be inferred from Fig. 5C that the acidic range is not suitable for the ELD process and a better copper deposition can be achieved at a higher alkaline range. The explanation for this result is that alkaline pH balances the charges on PMETAC polymerized N6 NFs and attracts copper particles. The highest weight gain of copper particles and the lowest resistance was observed at 13 pH [22], [23]. Finally, the influence of volume during the ELD process was followed and optimized. Fig. 5D presents the weight gain of copper particles and changes in resistance caused by volume during the ELD process. The weight of copper particles gradually increased with increasing volume from 25 ml to 500 ml, and become constant onward. Meanwhile, the resistance was decreased with increasing volume

from 25 ml to 500 ml and continued to increase with the same trend. Fig. 6 displays the original photographs for the flexibility in N6 NFs and resistance of copper-coated N6 NFs after the ELD process. The results show that copper-coated N6 NFs have the highest weight gain for copper particles of 12 mg/cm^2 and the lowest resistance 0.6 Ω.

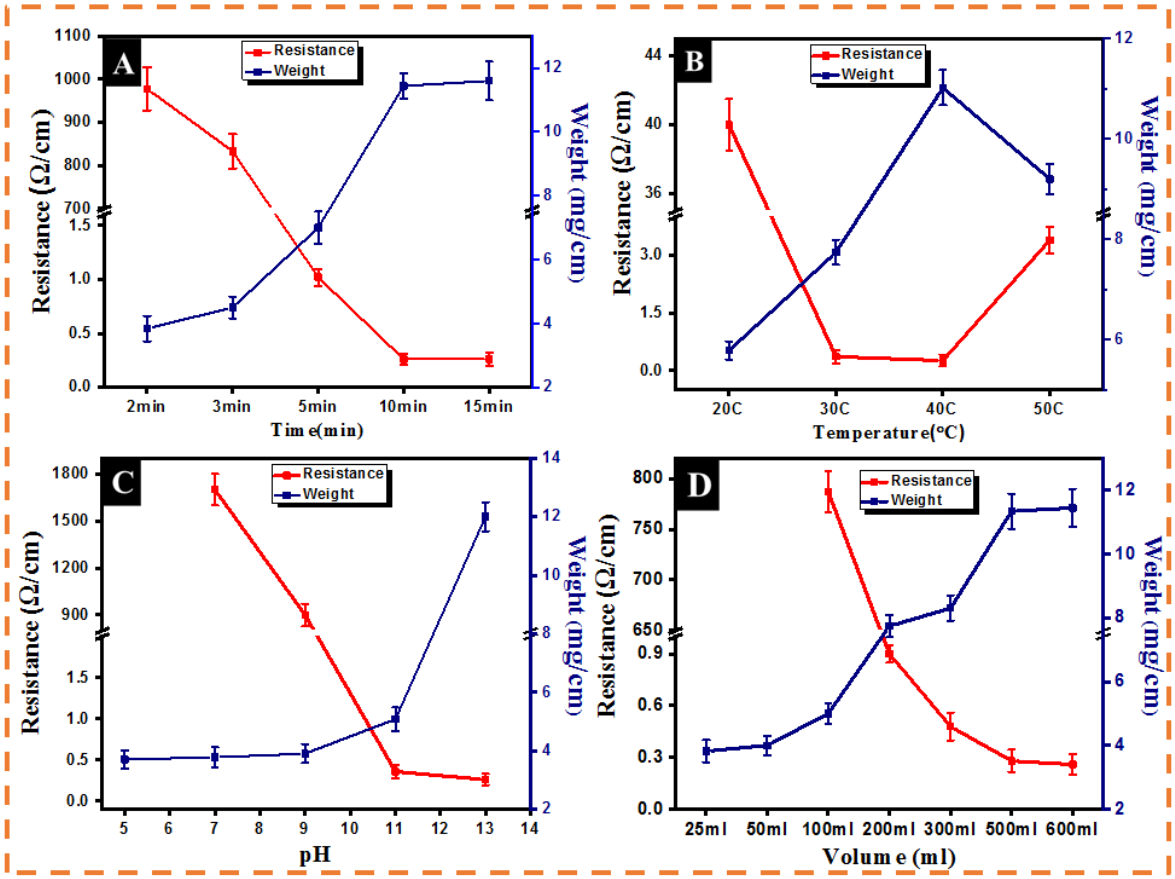

Figure 5. The effect of ELD parameters on resistance and weight gain over N6 NFs **(A)** effect of time, **(B)** effect of temperature, **(C)** effect of pH, and **(D)** effect of volume.

Figure 6. (A) Flexible N6 NFs (B) resistance measurement of copper-coated N6 NFs after ELD process (C) conductivity of N6 NFs.

Moreover, we have obtained 961.5 S/cm optimized conductivity of as prepared copper-coated N6 NFs and results are presented in table 1. We have also performed a series of experiments to know the effect of PMETAC for copper deposition and compare the result between copper-coated N6 NFs with PMETAC polymerization and copper-coated N6 NFs without PMTAC. Table 1 evidently shows that there is no conductivity 1.5 S/cm was found in copper-coated N6 NFs without PMETAC. The results validate the copper deposition due to surface polymerization with PMETAC.

Table 2 shows the comparative studies between copper-coated N6 NFs with ELD and previously reported methods. As shown in Table S2 that copper-coated N6 NFs not only offers less resistivity but also have improved electrical conductivity and mechanical properties.

Table 6

Table 1. Conductivity of copper-coated N6 NFs with PMETAC and without PMETAC

Samples	**Optimization of Time**		**Optimization of Temperature**		**Optimization of pH**		**Optimization of Volume**	
Cu N6 NFs with PMETAC	**min**	Conductivity S/cm^2	**(℃)**	Conductivity S/cm^2	**pH**	Conductivity S/cm^2	**(mL)**	Conductivity S/cm^2
	2	**0.3**	**20**	**7.1**	**7**	**0.3**	**100**	**0.4**
	3	**0.4**	**30**	**694.4**	**9**	**0.3**	**200**	**326.7**
	5	**225.4**	**40**	**961.5**	**11**	**771.6**	**300**	**578.8**
	10	**961.5**	**50**	**77.4**	**13**	**961.5**	**500**	**961.5**
	15	**769.2**					**600**	**939.2**
Cu N6 NFs without PMETAC	**2**	**0.1**	**20**	**1.0**	**7**	**0.1**	**100**	**0.4**
	3	**0.1**	**30**	**1.4**	**9**	**0.1**	**200**	**0.7**
	5	**0.2**	**40**	**1.5**	**11**	**1.5**	**300**	**0.8**
	10	**0.3**	**50**	**1.4**	**13**	**1.4**	**500**	**1.5**
	15	**0.2**					**600**	**1.2**

Table 7

Table 2. Comparative study of copper-coated N6 NFs with ELD method

Substrate	Metal	Method	Resistance	References
Nylon 6 NFs	Cu	Electrospinning & Electroless deposition	0.6 Ω/cm	This study
Nylon 6 NFs	O-SWCNTs	Electrospinning & dip coating method	950 Ω/sq	[36]
Nylon 11 NFs	MWCNTs	Self-assembled & Electrospinning	440 Ω/sq	[37]
Nylon 6,6 NFs	PVP-GO	Self-assembled & Electrospinning	8.6 Ω/sq	[38]
Nylon 6,6 NFs	Ag	Force spinning & Thermal evaporation	3–5 Ω/sq	[39]

Bending Test

To quantitatively demonstrate the flexibility and durability, the bending cycle test was performed up to 1000 cycles, as shown in Fig 07. The copper-coated N6 NFs exhibit superior bending durability. The resistance was measured by using a 4-point probe method with a Keithley 2400 source meter with initial resistance 1.5 ohm/cm. After 1000 cycles, we have found copper-coated N6 NFs retain 1.7 ohm/cm resistance with minor change of 0.2 ohm/cm.

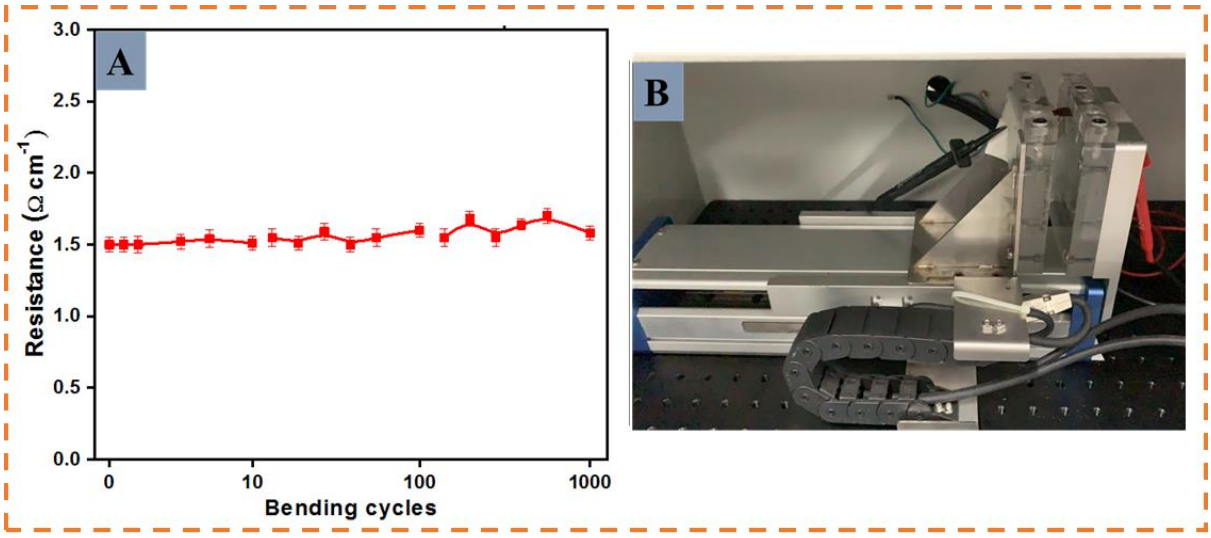

Figure 7. A Bending test of copper-coated N6 NFs. B. Original picture of Bending machine.

4.3.5 Chemical Analysis

The surface treatment of N6 NFs and copper-coated N6 NFs is further supported by FTIR investigation, as given in Fig. 08. In the FTIR spectra of neat N6 NFs, the bands at 3300 cm^{-1}, 1460 cm^{-1}, and 750 cm^{-1} are attributed to the stretching, deformation, and wagging vibrations of N–H bonds, respectively. The bands at 2935 cm^{-1} and 2860 cm^{-1} are associated with the CH_2 stretching vibrations. The band at 694 cm^{-1} is indexed to the bending of O-C-N [24], [25]. As can be seen, the plasma-treated sample has a similar spectrum as N6 NFs except for higher intensity at 3500 cm^{-1}, which represents the OH groups. In the silanization process, an additional peak at 1014 cm^{-1} was observed, which can be due to the plane vibration in C-H vibration. N6 NFs after polymerization was ensured with C=O stretching group at 1656 cm^{-1} Peak [24]. The polymerized sample also has a characteristic peak of the N-H group, suggesting the successful polymerization of N6 NFs [26]. Finally, copper-coated N6 NFs did not show any of the above-described peaks probably due to the smooth overlapping of copper deposition on the surface of the sample.

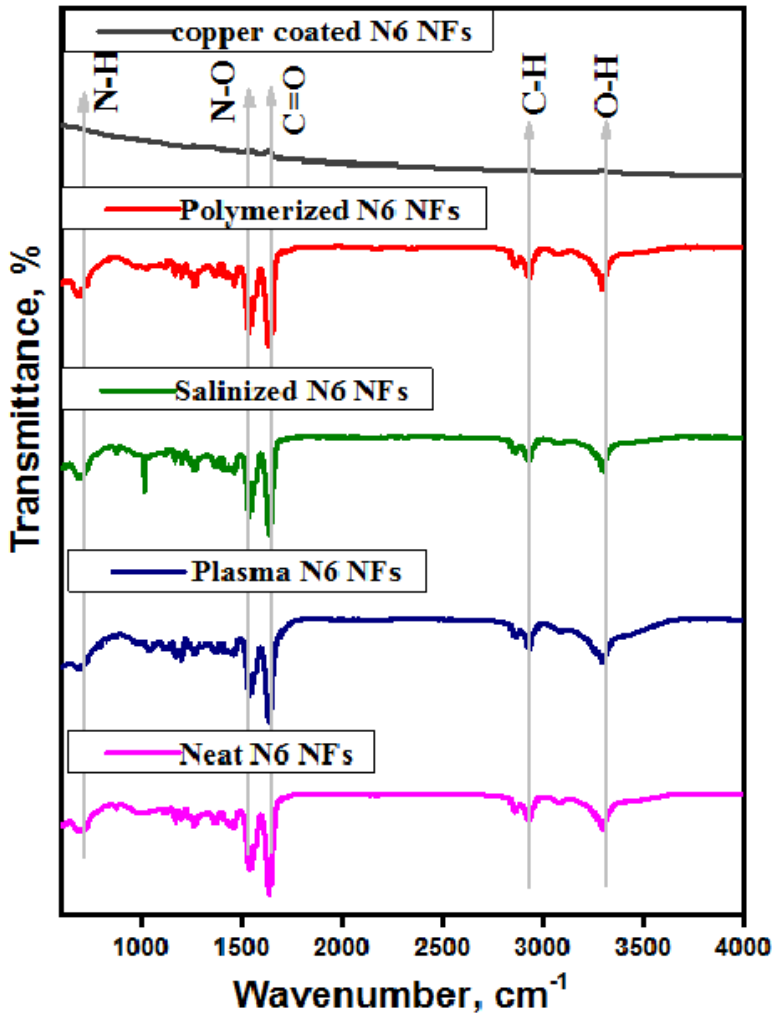

Figure 8. TIR spectrum of N6 NFs for each process (1. neat N6 NFs 2. Plasma N6 NFs 3. Salinized N6 NFs 4. Polymerized N6 NFs 5. Copper N6 NFs)

XPS analysis

The XPS study was examined to analyze the chemical structure of neat N6-NFs and copper-coated N6 NFs. Fig. 9A shows the XPS spectrum of neat N6 NFs and the deconvolution of each spectrum. The results reveal the neat N6 NFs containing carbon, nitrogen, and oxygen peaks at 282 eV, 400 eV, and 531 eV, respectively. After deconvolution of the C1s spectrum, a peak at 284 eV revealed three chemical conditions for carbon atoms. The peaks that appeared at 284.7 eV, 285.97 eV, and 287.4 eV show CH2-CH2, C-O, and CH 2 -C=O, respectively.

The high-resolution XPS spectrum of N1s at 400 eV can be attributed to N-C=O (amide bond). The O1s region was deconvoluted into two chemical states, i.e., 531 eV and 533.8 eV, which are attributable to O=C-N and the terminal OH group, respectively [26]. Fig. 9B illustrates the XPS spectrum and deconvolution of copper-coated N6 NFs. XPS spectra results confirm the presence of the same components of N6 NFs with the addition of Cu2p peaks. The deconvoluted Cu2p XPS spectra indicate three peaks at 934.36 eV, 944.66 eV, and 954.22 eV, classified as the Cu2p3/2 signal, the Cu2p satellites, and the Cu2p1/2 signal, respectively. These results confirm the presence of Copper particles on N6 NFs [27].

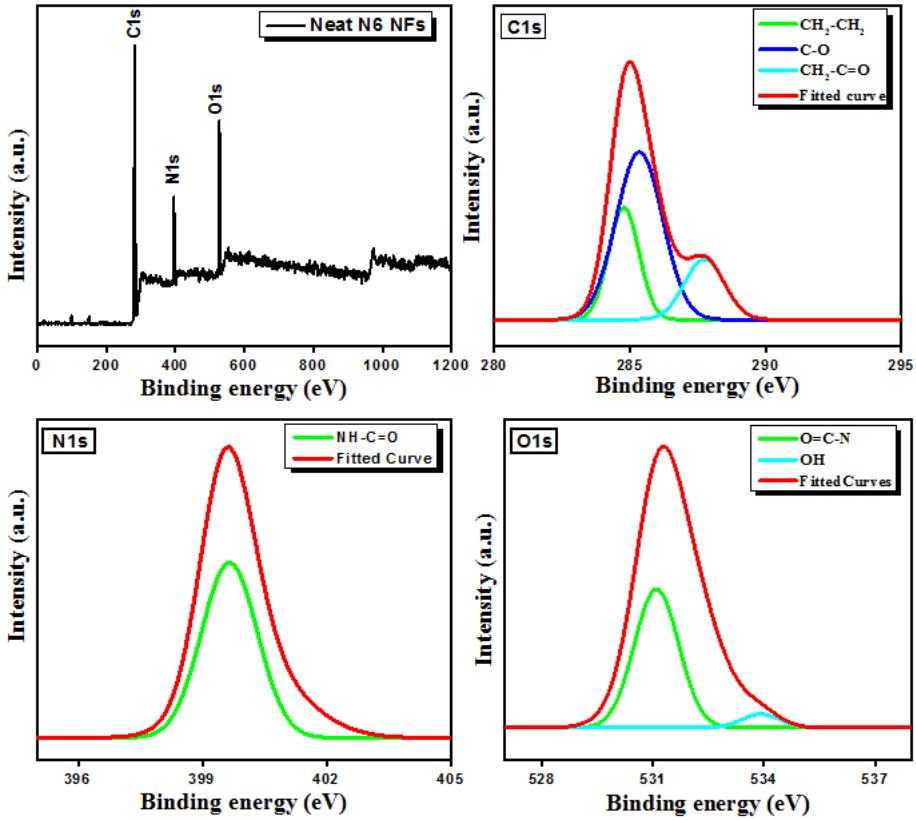

Figure 9. (A). XPS analysis of neat N6 NFs

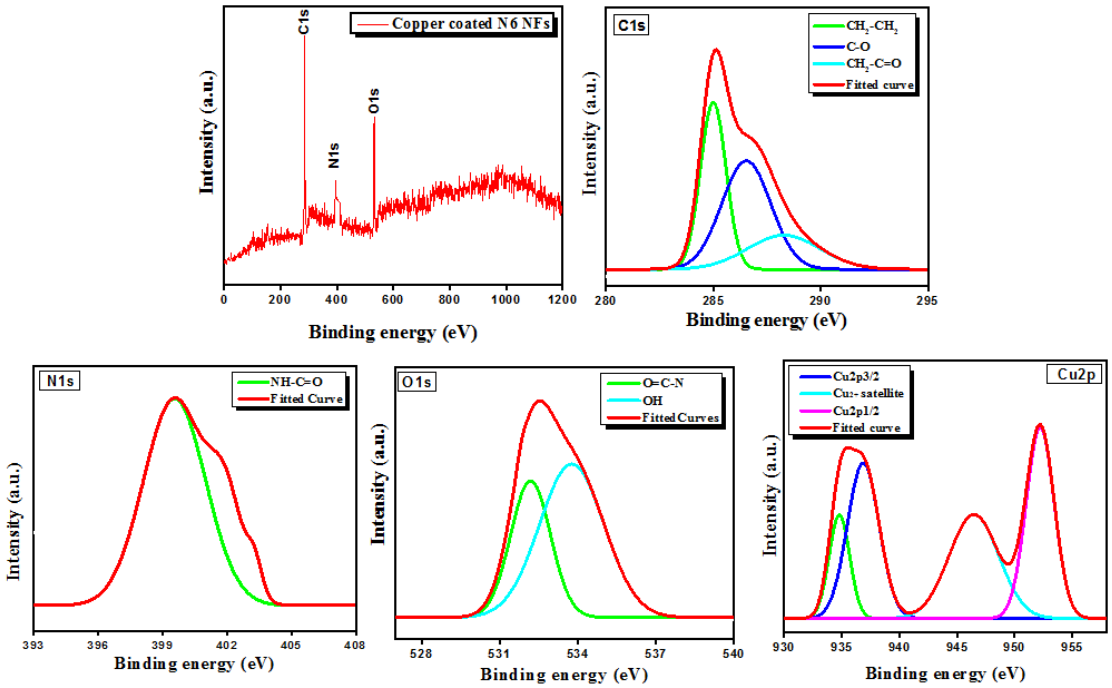

Figure 9. (B) XPS analysis of copper-coated N6 NFs.

4.3.6 Water Contact Angle

Water contact angle measurements show a significant variation in surface wettability of each fabrication process and validate the effective ELD procedure. The water droplets employed on each step, including neat N6 NFs, plasma-treated, silanized, polymerized, and copper-coated N6 NFs, are presented in Fig. 10. Neat N6 NFs are hydrophobic in nature, but hydroxyl groups (hydrophilic nature) may be required for surface functionalization of VTMS on N6 NFs [28]. Previously, plasma treatment has been used for generating hydroxyl groups. The neat N6 NFs showed an angle of 128° in our studies. Also, the successful use of plasma treatment led to a dramatic reduction in water droplet value at a water contact angle of 0°. This super formation of hydrophilicity in N6 NFs suggests successful plasma treatment and usefulness of producing OH groups for the silanization. After the silanization process, silane molecules are attached to OH groups of plasma-treated N6 NFs. Due to the attachment of dense silane molecules, N6 NFs were again become hydrophobic, having a contact angle of 138°. This successful

formation of hydrophobicity ensures that the presence of vinyl groups in VTMS on N6 NFs [29]. Moreover, after getting a reaction in polymerization, the PMETAC monomer and potassium persulfate (KPS), contribute to the successful fabrication of PMETAC (cation polymerization) on the surface of N6 NFs. The OH groups present in PMETAC polymer help polymerized N6 NFs to attain hydrophilic nature by showing a water contact angle of 72° [30]. Successful surface treatment of N6 NFs enables Cu particles to densely attach to the surface of N6 NFs during the ELD process. The copper-coated N6 NFs displayed a water contact angle of 140°, which is mostly attributed to the smooth deposition of copper particles on the surface of N6 NFs [31], [32]. Resultant water droplet analysis ensured that each step has a significant role for successful fabrication of copper deposition on N6 NFs.

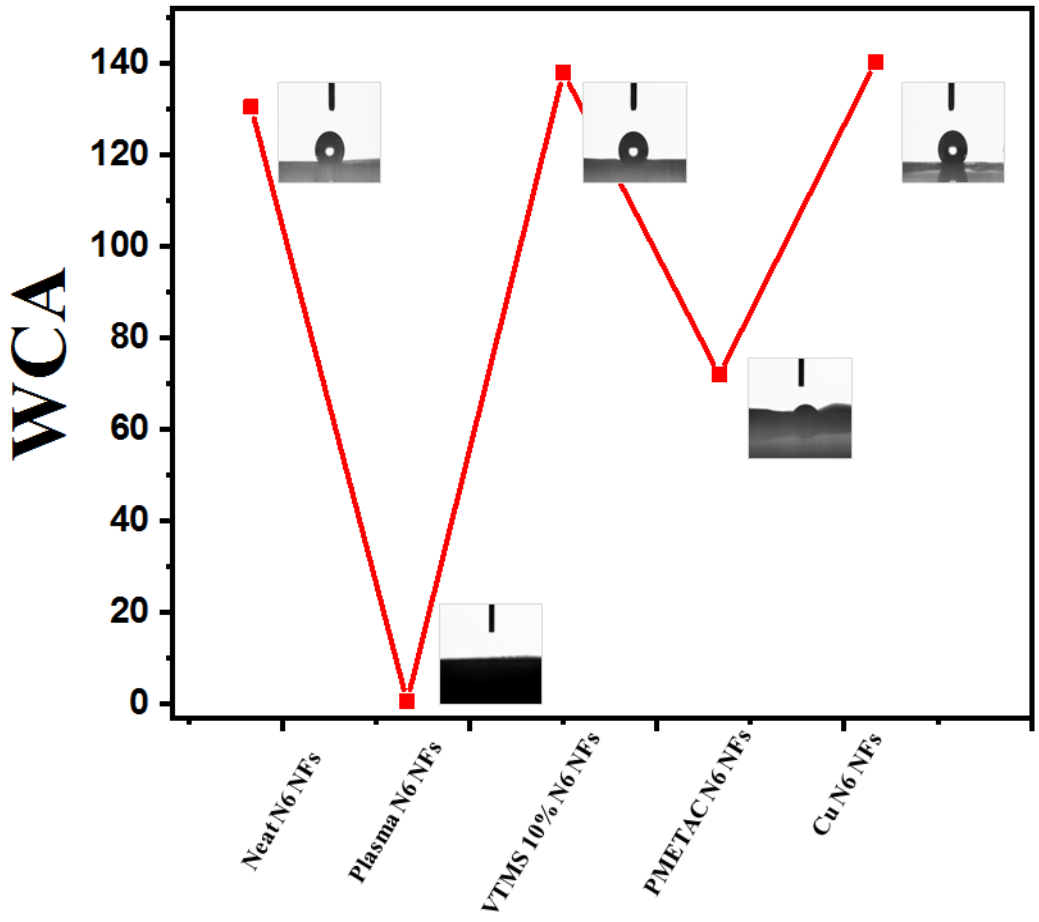

Figure 10. Water contact angle analysis of neat N6 NFs and copper-coated N6 NFs.

4.3.7 Mechanical Properties

Fig. 11A and 11B present the stress-strain curve and Young's Modulus of neat N6 NFs and copper-coated N6 NFs, respectively. The neat N6 NFs present an average value of 1.02 MPa for Young's modulus with 1.1% elongation at break. Meanwhile, the copper-coated N6 NFs show the value of 1.4 MPa for Young's modulus with 1.3 % elongation at break. These results reveal that copper deposition on N6 NFs has slightly higher mechanical strength and this may be due to various temperature treatments during surface functionalization of copper-coated N6 NFs [34].Thus, copper-coated N6 NFs can be suitable in many electrical applications such as flexible and wearable electronics electronic devices.

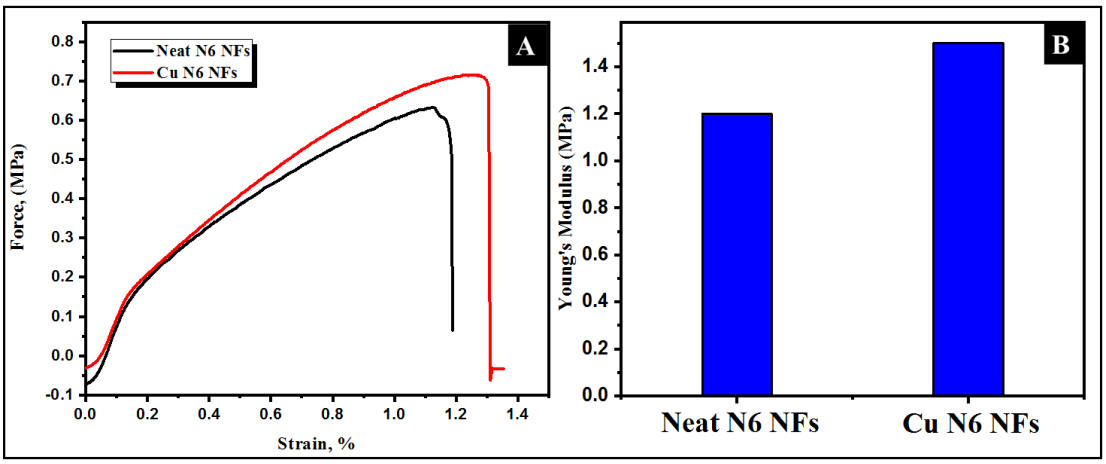

Figure 11. 'A' stress – strain curve and 'B' Young's Modulus of neat N6 NFs, and copper-coated N6 NFs

4.3.9 Thermal Gravimetric Analysis

Thermal deterioration rate and total combustion were employed to examine the change in the thermal behavior of neat N6 NFs and copper coated N6 NFs. Fig. 12 presents the thermogravimetric analysis graph obtained from TGA curves. TGA graph was studied with two phases to determines the temperature range and weight percentage. The temperature range of the initial phase was determined to be from ambient to 201℃ for pure N6 NFs. This phase indicates small weight increases and a temperature range increase up to 355.40℃, for copper-

coated N6 NFs. This result can be attributed to the presence of moisture in both neat N6 NFs and copper coated samples. Furthermore, the degradation rate for copper-coated N6 NFs presents the copper nanoparticle was attached on the surface of N6 web. Moreover, the temperature range for the thermal degradation rate of neat N6 NFs and copper coated N6 NFs was between 201℃ and 355℃. Although, the deterioration rate was keep followed up to total combustion at 438.51℃ for copper-coated N6 NFs. Resultant, Fig 12 shows the temperature range between 355℃ to 438.51℃ revealed that copper coated conductive N6 NFs is highly stable and can be used in many applications such as microelectronics and flexible sensors.

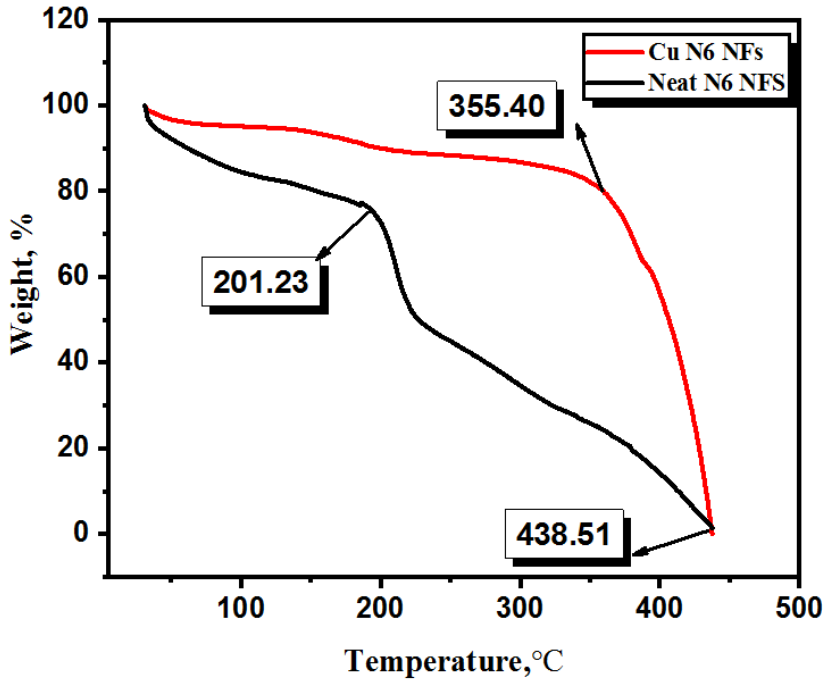

Figure 12. Thermal stability of pure N6 NFs, and copper-coated N6 NFs

4.4. Conclusion

In this study, highly conductive N6 NFs were successfully fabricated by the simple ELD technique. The SEM analysis showed bead-free neat N6 NFs with an average diameter of 200 nm. After ELD, the conductive N6 NFs showed an increase up to 400 nm. The EDX results showed that N6 NFs have densely covered with aggregates of copper nanoparticles. Moreover,

FTIR and XPS results confirm the copper deposition on N6 NFs. The water contact angle results indicate a significant change in hydrophilicity/hydrophobicity of N6 NFs in surface modification and the ELD processes, validating our successful copper deposition on N6 NFs. Parameters including time (10 min), temperature (40℃), pH (13), and volume (500 ml) were optimized for successful copper deposition on N6 NFs during the ELD process. The copper-coated N6 NFs showed a high 12 mg/cm weight gain of copper particles and the lowest resistance of 0.6 Ω. Furthermore, copper-coated N6 NFs obtained 961.5 S/cm conductivity. Thus, our proposed material copper-coated N6 NFs can be used in many electrical applications such as flexible and wearable devices.

References:

1. Y. Xu, K. Qian, D. Deng, L. Luo, J. Ye, H. Wu, and X. Feng. Carbohydrate Polymers, 250, 116915 (2020).
2. A. Schwarz, J. Hakuzimana, A. Kaczynska, J. Banaszczyk, P. Westbroek, E. McAdams, D. Tseles, *Surf. Coat. Technol.*, vol. 204, no. 9–**10**, 1412 (2010).
3. T. Kim, and D. Kwak., Fibers and Polymers, **13**, 471 (2012).
4. Y. Kim, Y. Song, H. Kim,. Fibers and Polymers, **20**, 466 (2019).
5. E. Gasana, P. Westbroek, J. Hakuzimana, K. De Clerck, G. Priniotakis, P, Kiekens, D. Tseles, S*urf. Coatings Technol.*, vol. 201, **no. 6**, 3547(2006).
6. J. Jang and S. K. Ryu, vol. **180**, 66(2006).
7. P. A. Pandey, G. R. Bell, J. P. Rourke, A. M. Sanchez, M. D. Elkin, B. J. Hickey, N. R. Wilson, no. **22**, 3202 (2011).
8. A. Ponti, M. H Raza, F. Pantò, A. M. Ferretti, C. Triolo, S. Patanè, & S. Santangelo, **36**, 1305 (2020).

9. Z. H. Ma, K. L. Tan, E. T. Kang, E. T., **114**, 17 (200).

10. R. H. Guo, S. X. Jiang, C. W. M. Yuen, M. C. F. Ng, J. W. Lan, G. H. Zheng, Fibers and polymers, **13**, 1037-(2012).

11. R. H. Guo, S. X. Jiang, C. W. M. Yuen, M. C. F. Ng, J. W. Lan, Y. L. Yeung, S. J. Lin, Fibers and polymers, **14**, 752 (2013).

12. S. Liang, Y. Li, T. Zhou, J. Yang, X. Zhou, T. Zhu, C. He, Advanced Science, vol. 4, no. 2, (2017).

13. Z. Liu, H. Hu, B. Yu, M. Chen, Z. Zheng, F. Zhou, *Electrochem. commun.*, vol. 11, no. **2,** 492 (2009).

14. X. Cauchy, J. E. Klemberg-Sapieha, and D. Therriault, *ACS Appl. Mater. Interfaces*, vol. 9, no. **34**, 29010 (2017).

15. Y. Yu, C. Yan, and Z. Zheng, 5508 (2014)

16. A. Morinaga, H. Tsutsumi, and Y. Katayama, Y. ChemPhysChem, 20 2973 (2019).

17. G. H. Kim, J. H. Shin, T. An, G. Lim. *Scientific reports*, **1** 8 (2018).

16. L. Petrik, Æ. P. Ndungu, and Æ. E. Iwuoha, 38 (2010).

17. N. A. M. Barakat, M. A. Kanjwal, F. A. Sheikh, H. Y. Kim, *Polymer (Guildf).*, vol. 50, no. **18,** 4389 (2009).

18. L. Sumin, D. Kimura, K. H. Lee, J. C. Park, I. S. Kim, *Text. Res. J.*, vol. 80, no. **2,** 99 (2010).

19. S. Ullah, M. Hashmi, D. Kharaghani, M. Q. Khan, Y. Saito, T. Yamamoto, I. K. Kim, In*t. J. Nanomedicine*, vol. **14**, 2693 (2019).

20. A. W. Jatoi, Jatoi, F. Ahmed, M. Khatri, A. Tanwari, Z. Khatri, H. Lee, I. K. Kim, I. S. Ultrason. Sonochem., vol. **39**, no. 34 (2017).

21. X. Wang, C. Yan, H. Hu, X. Zhou, R. Guo,X. Liu, Z. Zheng, Z. Chem. - An Asian J., vol. **9,** no. 8, 2170 (2014).

22. G. S. Chen, R. J. Tau, J. S. Fang, Y. L. Cheng, Y. C. Chen, *Applied Surface Science*, **146816** (2020).

23. Shacham-Diamand, Y., Dubin, V., & Angyal, M., **262,** 93 (1995).

24. U. A. Qureshi, Z. Khatri, F. Ahmed, A. S. Ibupoto, M. Khatri, F. K Mahar, I. S. Kim, J. Mo*l. Liq.*, vol. **244**, 478 (2017).

25. L. A. Díaz-Alejo, E. C. Menchaca-Campos, J. Uruchurtu Chavarín, R. Sosa-Fonseca, M. A. García-Sánchez,. International Journal of Polymer Science, (2013).

26. L. Liu, Y. Yu, C. Yan, K. Li, Z. Zheng, Nature communications, **6**, 1 (2015).

27. X. Gan, Y. Wu, L. Liu, B. Shen, W. Hu Surface and Coatings Technology **201,** 7018 (2007)

28. X. Li, Y. Li, T. Guan, F. Xu, J. Sun, J Durable, ACS Applied Materials & Interfaces **10**, 12042 (2018).

29. A. DEMİR, E. Bozaci, T Gülümser, M. Sarikanat, Tekstil ve Konfeksiyon **26,** 256 (2016).

30. C. Wang, H, Yang, F. Chen, L. Peng, H-F. Gao, L-p. Zhao, Results in Physics **10,** 891 (2018).

31. N. Politakos, S. Azinas, SE,. Moya. Macromolecular Rapid Communications **37,** 662 (2016).

32. S. Liu, M. Hu, J. Yang, Journal of Materials Chemistry C **4**, 1320 (2016).

33. A.J. Wagner, G.M. Wolfe, D.H. Fairbrother, Appl. Surf. Sci. **219**, 317 (2003).

34. F. K. Mahar, M. Mehdi, M., U. A. Qureshi, K. M. Brohi, B. Zahid, F. Ahmed, & Z. Khatri,. Journal of Molecular Liquids, 248, 911 (2017).

35. K. Wei, T. Ohta, B. S. Kim, K. W. Kim, K. H Lee, M. S. Khil, & I. S. Kim. Polymers for Advanced Technologies, 21, 746 (2010).

36. Bak, H., Cho, S. Y., Yun, Y. S., & Jin, H. J. (2010). Electrically conductive transparent films based on nylon 6 membranes and single-walled carbon nanotubes. Current Applied Physics, 10(3), S468-S472.

37. Havel, M., Behler, K., Korneva, G., & Gogotsi, Y. (2008). Transparent Thin Films of Multiwalled Carbon Nanotubes Self-Assembled on Polyamide 11 Nanofibers. Advanced Functional Materials, 18(16), 2322-2327.

38. Huang, Y. L., Baji, A., Tien, H. W., Yang, Y. K., Yang, S. Y., Ma, C. C. M., ... & Wang, N. H. (2011). Self-assembly of graphene onto electrospun polyamide 66 nanofibers as transparent conductive thin films. Nanotechnology, 22(47), 475603.

39. Mihut, D. M., Lozano, K., & Foltz, H. (2014). Fabrication and characterization of silver- and copper-coated Nylon 6 forcespun nanofibers by thermal evaporation. Journal of Vacuum Science & Technology A: Vacuum, Surfaces, and Films, 32(6), 061401.

CHAPTER 5

Conductive and antibacterial cellulose nanofibers decorated with copper nanoparticles for potential application in wearable devices.

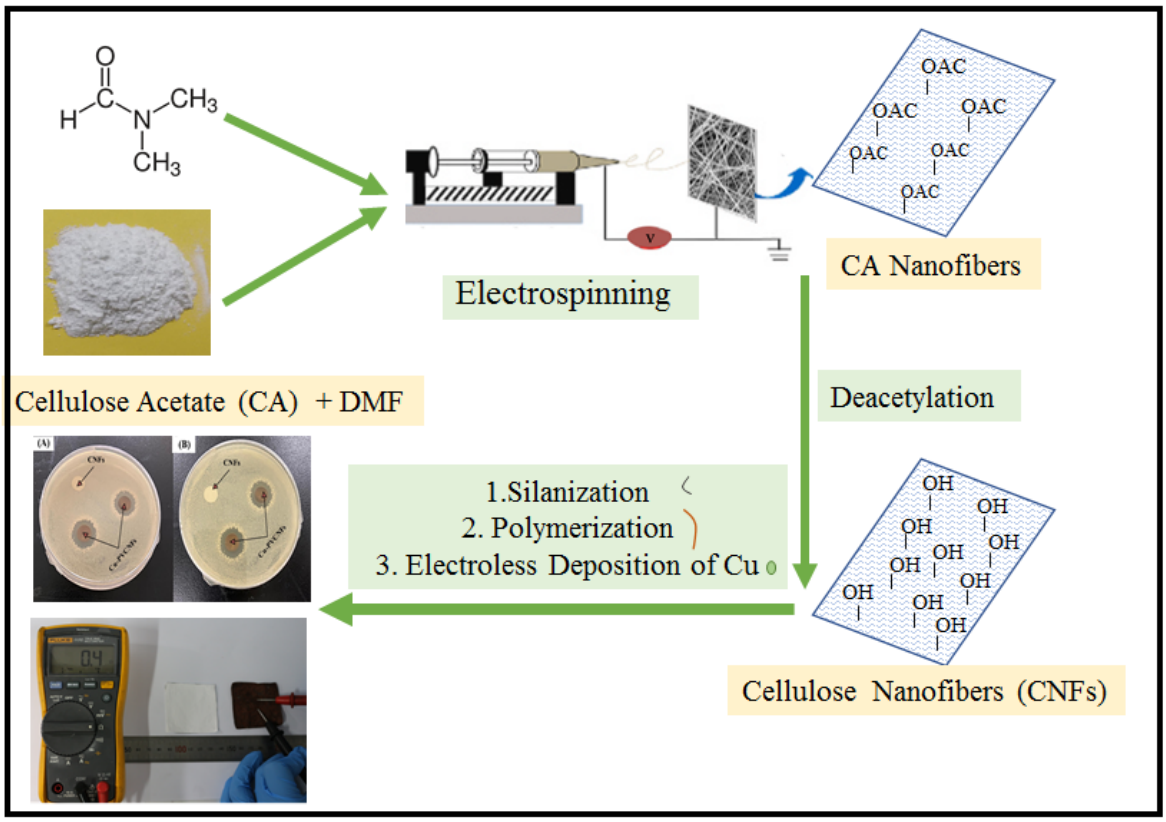

Figure 1. Scheme. Fabrication of conductive and antibacterial cellulose nanofibers.

5.1 **Introduction**

One of the smart textiles field is wearable electronics which have received a lot of interest [1]. Wearable electronics use to detect or observe the body conditions, or provide some tasks, such as energy storage and transmission of information. One of the main characteristics of these kind of products are their flexibility and comfort [1,2]. One of the significant characteristics in wearable electronics is conductivity[3]. Researchers have been focused on the application of the mixture of conventional polymeric fibers and conductive nanoparticles. So that, the combination of conductive nanoparticles with organic polymers can resolve the conductive materials lack of flexibility and comfort [4]. In this regard, the nanofibrous mats have attracted a huge interest because of high porosity and surface area which led to higher amount of metal deposition and accordingly yield higher conductivity [5]. In the past few years, Au, Ag, Pd, and Cu metals have been used as conductive coating. Among them, because of the outstanding conductivity to cost ratio, Cu would be a great choice to use as a conductive metal in a wearable electronics [6–8]. Among the various kind of polymers, one of the prevalent organic polymers is cellulose with permanent source, and biocompatible and environmentally friendly products [9]. In recent years, cellulose based materials have been used to prepare nanofibers by means of electrospinning technique [10]. So, cellulose nanofibers have been used as a substrate for electronics due to its outstanding features, such as low coefficient of thermal expansion, high optical transmittance, thermal stability, and mechanical strength [11–13]. Furthermore, it has a high compatibility with human skin, thus it can be used in wearable electronics[14]. The fabrication and design of flexible metal substrate has attracted a lot of attention and many improvement have been made by application of different metallization methods, includes physical deposition of vapors [15,16], chemical vapor deposition [17], electrochemical plating and electroless deposition (ELD) of metals [18,19]. ELD process is an attractive technique because of the lower cost, site-selectivity, simple process, versatility, and scalability, which made it a

proper method surface metallization of the soft materials [20–23]. In this research, we deposited copper nanoparticles on the cellulose nanofibers by electroless deposition (ELD) method as a functional composite with high conductivity. As wearable electronics frequently are close to users' daily lives, so they are vulnerable to be contaminated with different bacteria and made health problems for the users. In this regard, one of the important properties which can improve their performance is antibacterial activity [39]. Cellulose nanofibers have not any antibacterial activity, and it can promote microorganism's growth which may cause health concerns. Hence, the application of antibacterial materials in cellulose nanofibers can increase its safety. Many researchers have imported the antibacterial activity to the cellulose nanofibers through modifying surface [24,25], blending bactericides [26], and silver nanoparticles [27,28], etc. Copper (Cu) is a broad-spectrum biocide and can effectively inhibits the bacteria growth, fungi, and algae [29], [30,31], So, Cu containing surfaces may provide hospital requirements [32]. Accordingly, the application of Cu metal as a conductive material for coating on the cellulose nanofibers can improve its functionality and create a multifunctional nanofibrous structure with high conductivity and antibacterial performance. In this regard, we used electroless deposition of Cu on the cellulose nanofiber to prepare highly conductive antibacterial nanofibers.

5.2. Experimental

5.2.1 Materials

Cellulose acetate (CA) (39.8% acetyl content having average Mw = 30 kDa), acetone and dimethylformamide (DMF) were purchased from Sigma Aldrich USA. [2-(Methacryloyloxy) ethyl] trimethylammonium chloride solution (METAC), Ammonium tetrachloropalladate (II), and Copper (II) sulfate pentahydrate, were obtained from Sigma Aldrich USA. Potassium sodium tartrate tetrahydrate, Formaldehyde, Potassium persulfate, and Sodium hydroxide were bought from

5.2.2 Fabrication of cellulose acetate nanofibers

Preparation of cellulose acetate nanofibers (CANFs) was followed by previous methods [33,34] Briefly, CA polymer (17 % w/w) was dissolved in acetone and dimethylformamide (DMF) keeping ratio 2:1 stirring until a homogeneous solution formed. CA solution was poured into a 5ml plastic syringe and supplied a high voltage of 16.6 kV using a power supply (Har-100*12, Matsusada Co. Tokyo Japan) to the polymer solution. A capillary tip of ~0.6 mm diameter was used for electrospinning. The electrospun nanofibers were collected on an aluminum foil and capillary tip to collector distance was set 14 cm.

5.2.3 Surface Treatment of CANFs

The surface treatment of CANFs was carried out in 3 process, namely, deacetylation of cellulose acetate (CA), silanization, and polymerization. The prepared electrospun CA nanofibers were first deacetylated according to previous process [7]. Briefly, CA nanofibers dipped in NaOH (0.05 M) for 48 hours to get neat cellulose NFs. Then cellulose NFs web was washed with distilled water to reach the neutral pH. Finally, prepared cellulose NFs were dried and used for further process.

Silanization of the prepared cellulose NFs was done by immersing them in 10% vinyl trimethoxy silane (VTMS) for 20 minutes. Later, the silanized cellulose nanofibers (SCNFs) were used for polymerization after washing with double purified water and dried at 60℃. The silanized cellulose NFs were immersed into a 100 mL of 20% (v/v) METAC aqueous solution and potassium persulfate (KSP; 60 mg) for 60 min with continuous stirring at 60℃. After this, cellulose NFs were treated with Ammonium tetrachloropalladate II (5 mM) for ion exchange reaction. The resulted cellulose NFs (PSCNFs) were washed with DI water and dried at 50℃ for the ELD process.

5.2.4 Electroless Deposition Copper on the nanofibers

Electroless deposition (ELD) was carried out according to the previously reported protocol [7,23]. Briefly, to prepare the Copper ELD bath, we prepared two solutions, A and B. Both solutions were prepared and mixed with a 1:1 ratio. Solution 'A' contains 13 g/L copper sulfate pentahydrate, 12 g/L sodium hydroxide, and 29 g/L potassium sodium tartrate tetrahydrate. Solution 'B' contains formaldehyde 9.5 mL/L in Double purified. Above mentioned treated cellulose NFs were immersed into freshly prepared copper ELD bath in different condition to prepare the optimized Cu-coated nanofibers (Cu-PSCNFs). To investigate the effect of PMATAC on Cu deposition, ELD process has been done on the CNFs without polymer treatment (CuCNFs).

5.2.5. Characterization

Scanning electron microscopy (S-3000N; Hitachi, Japan) with a high voltage of 30 kV was used to observe the surface morphology of electrospun cellulose NFs and copper coated cellulose NFs. The Energy Dispersive X-Ray Analysis (EDX) (S-3000N; Hitachi, Japan) was performed to analyze the element mapping of the neat CNFs and copper-coated CNFs. The chemical structure of neat cellulose NFs and copper coated cellulose NFs were analyzed using Fourier transform infrared spectroscopy (FTIR) on an IR prestige - 21 by Shimadzu Japan. All nanofiber samples 1-2 mg were ground with 0.1g KBr and pressed into a pellet of which transmission FTIR spectrum was measured. An OCA-40 contact angle instrument (Data physics Germany) was applied to determine the water contact angle of neat CNFs and each process involved fabricating conductive CNFs. The electrical resistance of the nanofibers was measured using ST-225*C multifunctional Digital 4 Probe meter. The following equation was used to calculate the values of conductivity as gives below:

$$R = \frac{pl}{Wt} \qquad (1)$$

Where “R” is resistance, “p” denotes the resistivity of the material and “I” is the length, “W” is the width and “t” is the thickness of the nanofibers.

The bending cycle test was done up to 1000 cycles to show the durability and flexibility of the coating. The conductive CNFs exhibit superior bending durability. Sample size 5X3cm. The resistance was measured by using a 4-point probe method with a Keithley 2400 source meter Initial resistance 1.5 ohm/cm^2, After 1000cycles 1.7 ohm/sq.cm, Minor change 0.2 ohm/sq.cm up to 1000 cycles.

The mechanical properties of neat cellulose NFs and copper coated cellulose NFs were measured by Titan Universal Tester 3-910 Company Ltd, Germany. The tensile strength was measured according to the ASTM D-638 standard. During the test, speed was set at 5.0 mm/min.

The antibacterial performance of neat cellulose NFs and copper coated cellulose NFs were measured by disc diffusion method against gram positive *Staphylococcus aureus* and gram-negative *Escherichia coli* bacteria. Both bacteria Escherichia coli and Staphylococcus aureus were grown in nutrient broth at 37 ˚C for 24 h to reach the 1×10^9cfu/mL number of viable bacterial cells. By four serial dilution with 0.03mol/L PBS, the number of viable bacterial cells were adjusted to 3×105cfu/mL - 4×105cfu/mL. The copper coated and the neat cellulose nanofibers were soaked into a flask containing 5 mL suspension of prepared bacterial solution. The flask was then shaken at 150 rpm on a rotary shaker at 37.8℃ for 18h. After shaking, four serial dilutions of 1:10 of each sample with 0.3 mM PBS (monopotassium phosphate) were prepared. Finally, 1mL of each bacterial suspension dilutions poured onto an agar plate. After 24 h of incubation at 37.8℃, the number of created colonies on the agar plate were calculated.

Antibacterial efficacy was determined based on duplicated test results. Percentage of bacterial reduction was calculated according to the following equation:

$$R(\%) = \frac{B - A}{B} \times 100 \qquad (2)$$

Where R is the percentage bacterial reduction, B and A are the number of live bacterial cells in the flask of treated and untreated sample after shaking.

Disc diffusion method was used to evaluate the antibacterial activity of the nanofibers against Staphylococcus aureus and E coli bacteria. The sterile copper coated and un-coated nanofibers with a diameter of 8 mm were cut and placed in the plates, which cultured separately with each bacteria strain and incubated overnight (12 h) at 37℃.

5.3. Results and Discussions

5.3.1. Optimization of ELD process

The effect of time, temperature, volume, and pH on the deposition of copper onto the nanofibers' surface were optimized by measuring the conductivity and weight (mg/cm^2) of the treated nanofibers (Figure 2).

The influence of ELD process time was observed at a fixed temperature (40 °C), pH (13), and volume (500 ml). Figure 2A shows the changes of conductivity and weight of the nanofibers by increasing the time of ELD process. Whatever we continued the treatment, more Cu was coated on the fibers' surface and the weight and conductivity of the nanofiber become more. The effect of treatment temperature is shown in Figure 2B. By increasing the temperature up to 40 ^{0}C, the weight gaining, and conductivity increased. But at the temperature of 50 ^{0}C, the amount of Cu deposition as well as the conductivity decreased. A high temperature made the solution instable which caused ultimately less Cu deposition. Figure 2C revealed the effect of volume on the Cu deposition. By increasing the volume up to 500 ml, both the amount of Cu deposition and conductivity increased well. Changing the acidity of the solution influences Cu deposition. As shown in Figure 2D, at basic pH, the amount of Cu deposition increased significantly. The acidic and light basic pH is not suitable for the ELD process. So, the higher

Cu deposition can be obtained at a higher alkaline range (pH=13). This may because of the alkaline pH balanced PMETAC charges on CNFs to attract more Cu atoms [35,36].

Finally, the optimized condition for ELD process on PSCNFs was temperature: 40℃, time: 10 min, pH: 13, and volume: 600 ml to obtain a nanofiber with 983.5 S/cm conductivity. Comparing the results of ELD process on the polymer treated nanofibers and the nanofibers without polymer revealed the effect of PMATAC on Cu deposition. In the optimized condition the amount of Cu deposition on the PSCNFs (weight 14 mg/cm) were higher than the untreated one (weight 0.7 mg/cm). Accordingly, the conductivity of the Cu-CNFs was very low (conductivity 2.5 S/cm). This can be because of the ionic affinity of the Cu to the cationic PMATAC polymer. This test showed the necessity of the application of PMATAC polymer before ELD process.

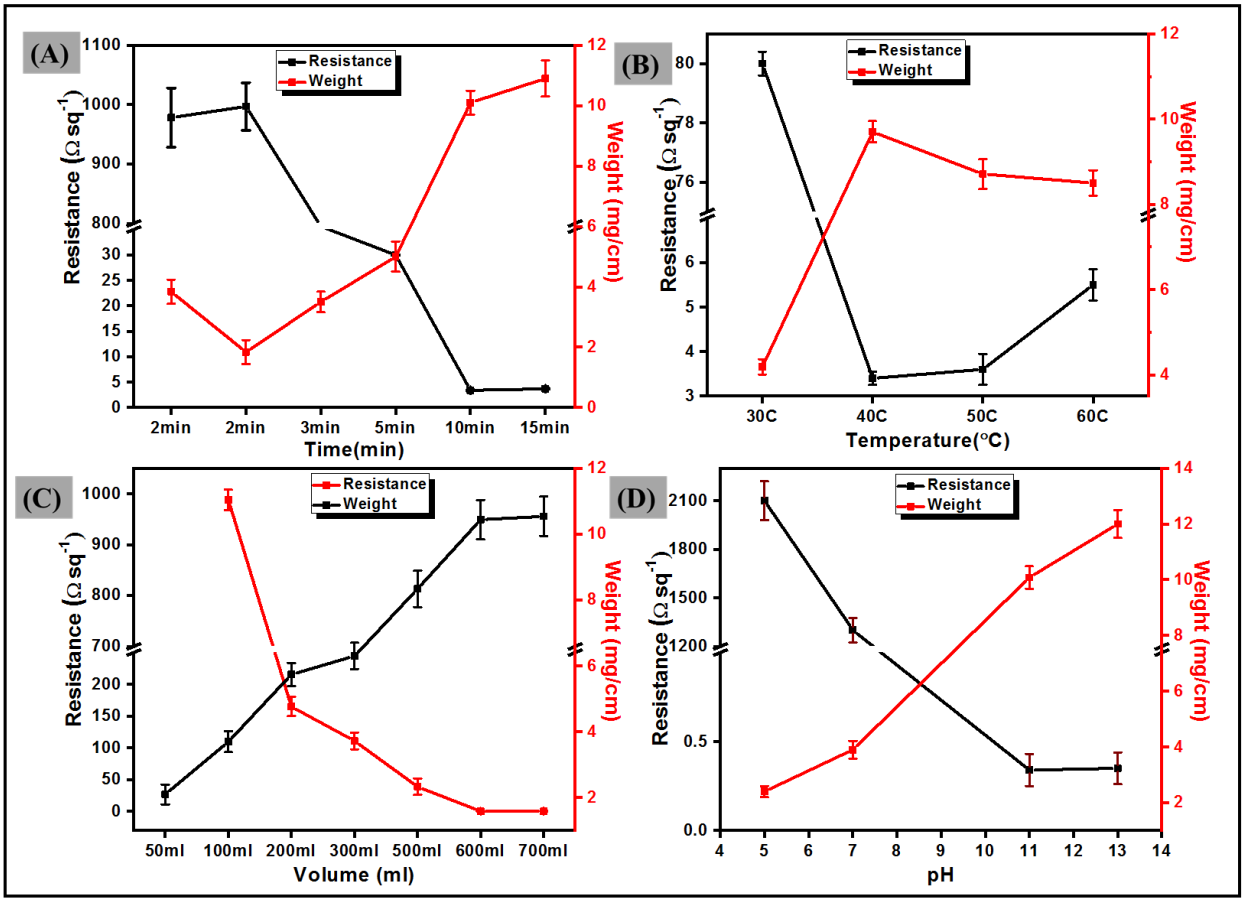

Figure 2 Figure 2. Effect of ELD (A) Time, (B) Temperature, (C) volume, and (D) pH on the conductivity and weight of the Cu-PSCNFs

5.3.2. Surface Morphology

Nanofibers microstructures were observed by SEM (Figure 3), showing that the CA, CNFs, PSCNFs, and Cu-PSCNFs have medium diameters of 200-300nm, 200-300nm, 300-400nm, and 500-600nm, respectively. CA nanofiber has a smooth and bead free morphology. Deacetylating process did not damage the structure and the CNFs has a smooth surface with ribbon like structure, which led to a little increase in nanofiber diameter. By introducing the silane and polymerization process the fibers were overlapping each other and the structure became denser accordingly the medium diameter of the nanofibers increased, confirming that the chemical modification has been done on the nanofiber surface without destroying the nanofibrous structure. It was observed that the nanofibers keep their fibrous structure even after Cu deposition. The increase in nanofibers diameter and roughness revealed the successful ELD process to create a flexible conductive membrane that can be used for wearable electronics.

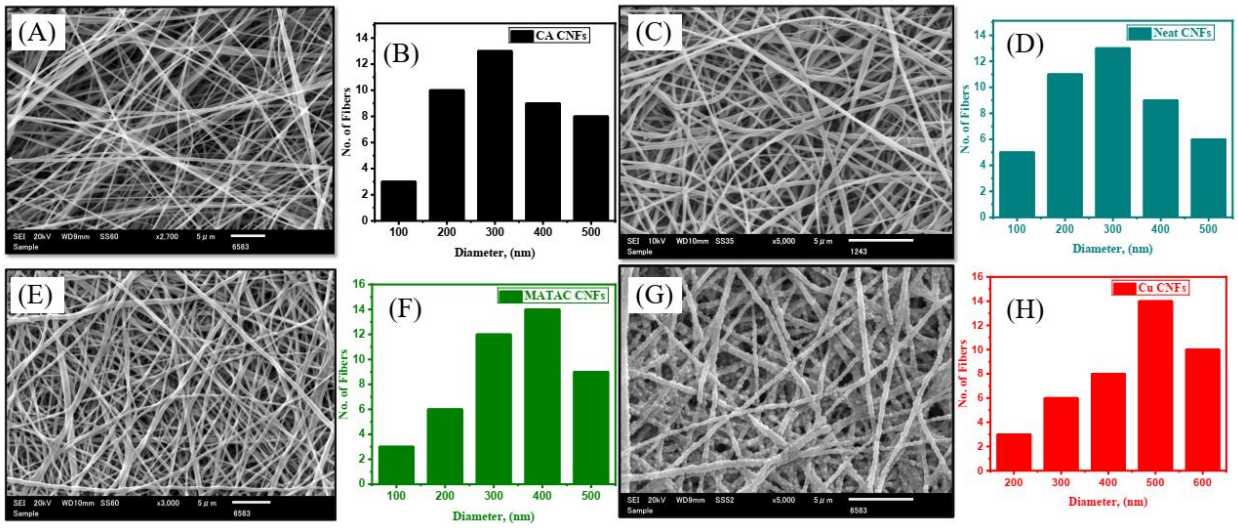

Figure 3. SEM images and diameter distribution of (A, B) neat CA, (C, D) CNFs, (E, F) PSCNFs, (G, H) Cu-PSCNFs.

5.3.3. EDS analysis

Elementary analysis of nanofibers was done using SEM-EDS, as shown in Figure 4. indicated that carbon, and oxygen were the principal elements of the cellulose nanofibers. EDS analysis of copper coated cellulose nanofibers indicated the presence of Cu on the Copper coated CNFs surface, which confirmed the successful ELD of Cu on the fiber surface. Because of the high surface area of the nanofibers, this method can yield a much content of Cu on the nanofiber membrane surface leading high performance nanofiber with conductivity [7]. Figure 4 surface leading high performance nanofiber with conductivity [7].

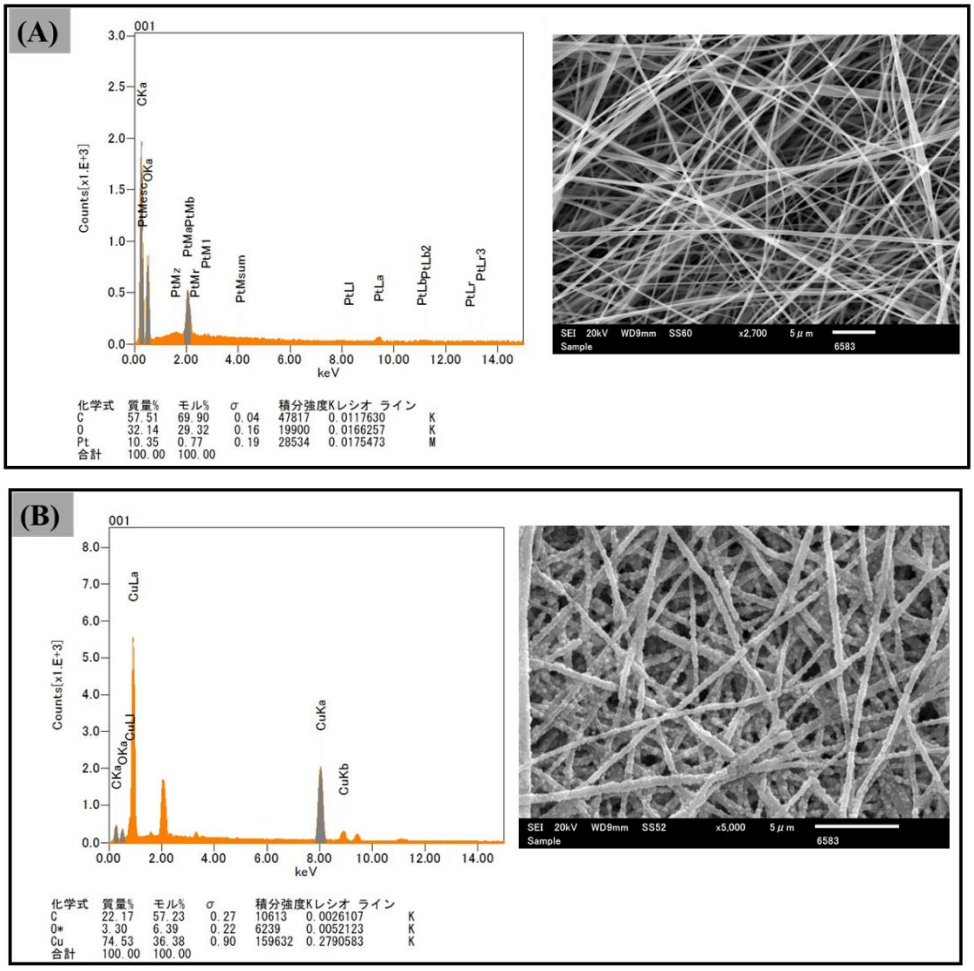

Figure 4. EDS analysis of (A) neat CNFs, and (B) Cu- PSCNFs

5.3.4 FTIR spectroscopy analysis

Figure 5 shows the FTIR spectra of the nanofibers. For neat CA nanofibers, there are the characteristic peaks of cellulose acetate attributed to the acetate groups' vibrations C-O at 1745 cm^{-1}, C-CH_3 at 1375cm^{-1}, -C-OH stretching vibration at 1049.28 cm^{-1} and C-O-C at 1235 cm^{-1}[134,37]. In the FTIR spectrum of the deacetylated nanofiber, the characteristic peaks of CA disappeared, and new absorption peaks appeared at 3500 cm^{-1} attributed to O-H groups. Moreover, cellulose nanofibers indicted the characteristic absorption peaks of cellulose structure at the 2917 cm^{-1} for C-H stretching at and at 1316 cm^{-1} for C-H wagging[38]. These changes confirmed the successful deacetylation process and synthesis of cellulose nanofibers.

The FTIR spectrum of the polymerized nanofiber revealed the extra peak at 1656 cm^{-1} that indicates C=O stretching vibration[35]. For Cu-PSCNFs the C=O and OH stretching vibration were disappeared, this can be because of high amount of Cu atoms on the nanofiber surface which reduce the intensity of the other peaks.

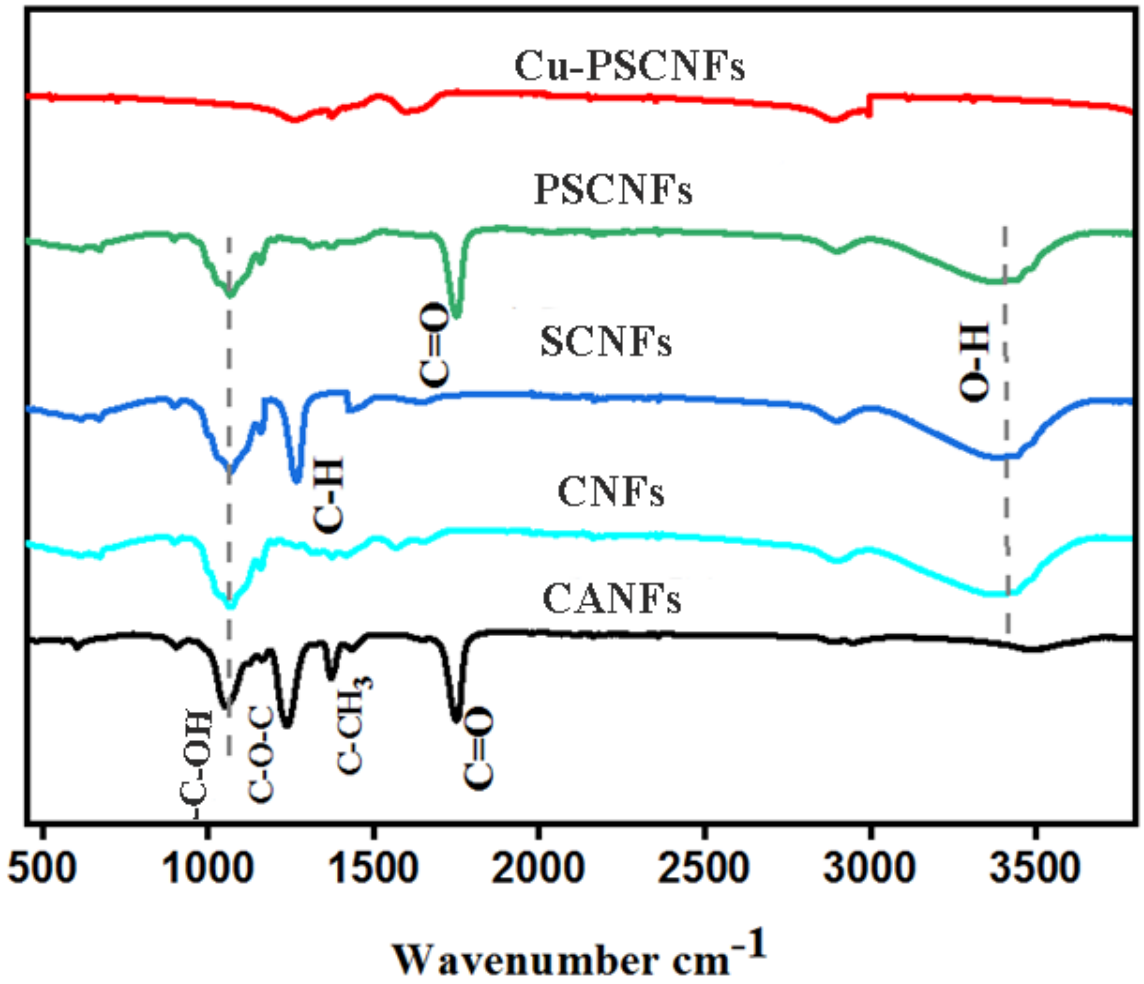

Figure 5. FTIR analysis of CANFs, CNFs, VCNFs, PSCNFs, Cu-PSCNFs.

5.3.5. Antibacterial performance

Conductive nanofibers have great potential to be applied in the next generation of sensors, energy conversion, and storage devices in wearable electronics[3]. As wearable electronics mostly exposed to daily-life environments, so they can be contaminated frequently with different bacteria. Furthermore, wearable electronics can be used in biomedical applications. In this manner, one of the important properties which can improve their performance is antibacterial activity[39]. The anti-bacterial properties of the CNFs and Cu-PSCNFs were

examined against S. aureus and B. subtilis as model bacteria [40]. Cellulose nanofiber did not show any antibacterial performance (Figure 6A). The Cu coated nanofibers (Cu-PSCNFs) showed clear bacterial inhibition rings against both bacteria (Figure 6B). So, it had a promising antibacterial performance. For centuries, metallic copper has been used as an efficient antimicrobial agent for water disinfection and wound treatment. The antibacterial activity mechanism is the strong affinity of Cu to carboxyl and amine groups on bacteria wall[41]. Accordingly, the prepared nanofibers can be an appropriate candidate for application in wearable devices, especially in the medical field.

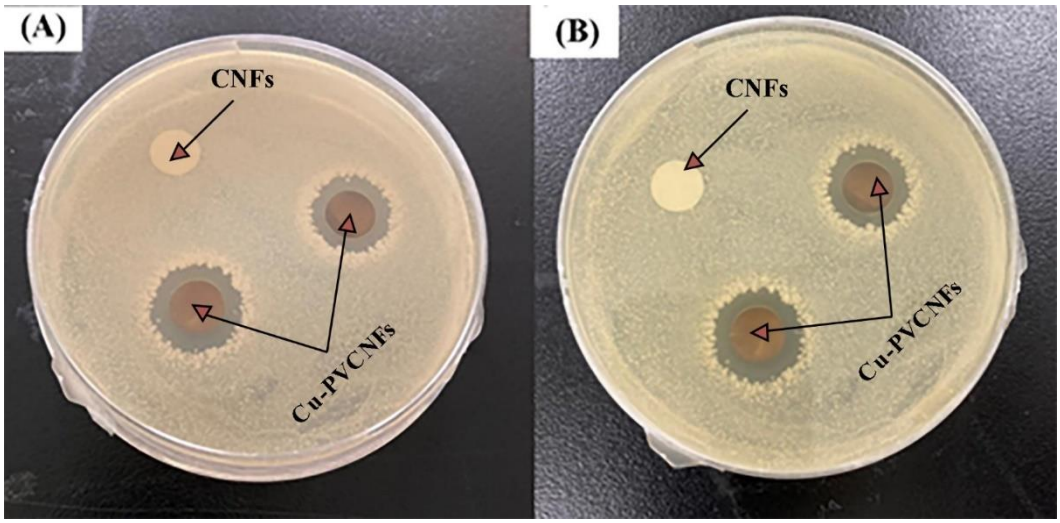

Figure 6. Antibacterial properties of the CANFs, and Cu-PSCNFs against (A) S. aureus and (B) B. subtilis

5.3.6. Tensile strength

The mechanical properties of the prepared nanofibers were studies through stress-strain test (Figure 6). The CNFs approximately showed an elastic mechanical behavior with the tensile stress of 1.92 MPa, breaking elongation of (6.8%), and Young modulus of 0.96. Cu deposition increased the tensile stress (2.1MPa), strain (7.1%) and decreased the Young modulus to 1.3. This may attributed to the interaction of Cu and the CNFs interactions which resulted in the mechanical strength improvement [1].

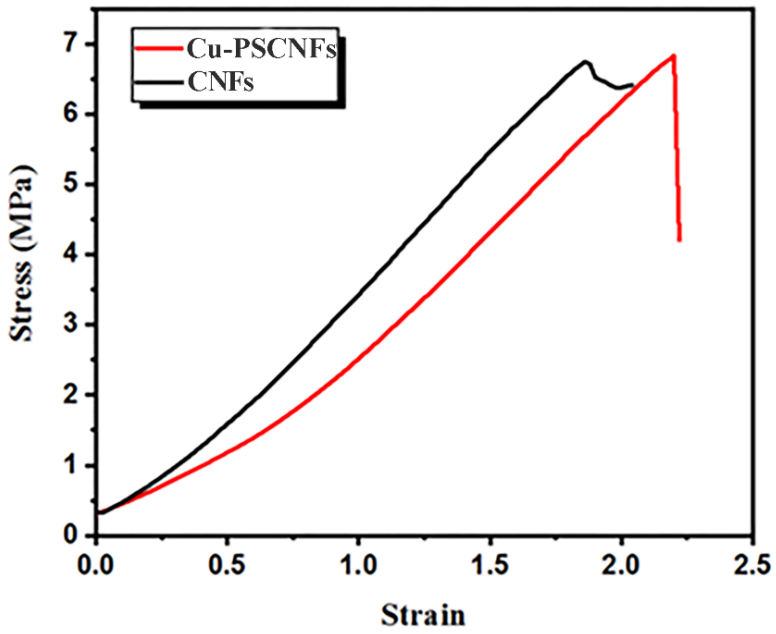

Figure 7. Tensile strength of the (A) CNFs, and (B) Cu-PSCNFs

5.3.7. Water contact angle (WCA)

Water contact angle determines that how each process can change the surface hydrophilicity and wettability and thus it can confirm the successful ELD process. Figure 8 indicated the WCA of the CANFs, CNFs, SCNFs, PSCNFs, and Cu-PSCNFs. In cellulose acetate at least one of the OH groups per hexose unit is substituted by an acetate group. Accordingly, cellulose acetate is hydrophobic whereas cellulose is more hydrophilic. The cellulose acetate showed an angle of 137° in our studies. As shown in Figure 8, the water contact angle of the CNFs (10.5°) was much lower than the CANFs, which confirmed that the deacetylation process has been done properly. However, the application of VTMS led to decreasing the hydrophilicity by increasing the WCA to 135°. This can be because of the reaction between silane groups with the hydroxy groups of the cellulose and the presence of the vinyl group on the surface of the nanofibers[42]. So, the increase of WCA confirmed the successful attachment of VTMS to the nanofiber surface. After polymerization step, the WCA decreased by showing a WCA of 64.3° because of the PMETAC ionic structure [43]. The successful surface coating of CNFs with

PMETAC led to deposition of Cu particles on the surface of the nanofibers and covering them properly. The Cu-coated nanofibers had a WCA of 134.5°, which was due to the Cu presence on the fabric surface[44]. Changes of the WCA after each process was a good evidence for successful ELD process.

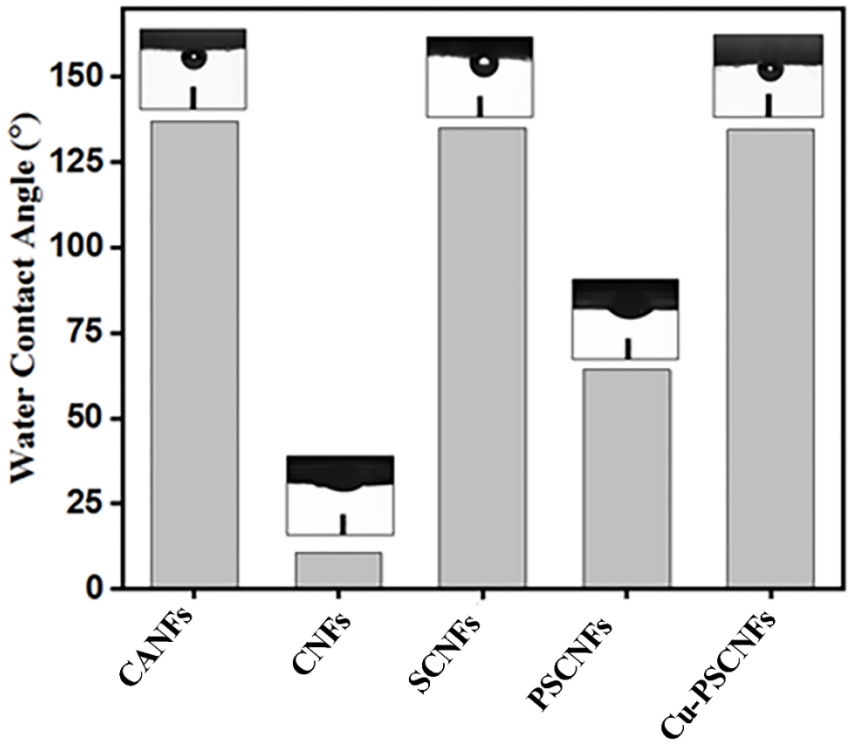

Figure 8. Water contact angle of the nanofibers after each process

5.3.8. Effect of bending cycle on resistance

Electronic devices are usually constructed on rigid substrates. Nowadays, change of the substrate to soft materials lead to flexible wearable electronics. Accordingly, the effect of bending cycles on resistance of the metal coated fabric is a very important factor [45]. Figure 9 reveled the effect of bending cycles on the Cu coated nanofibers resistance (Cu-PSCNFs). The sample's resistivity did not change significantly even after 1000 bending cycle. It has been shown theoretically that if the conductive layer is attached to the polymer substrate properly,

the elongation is suppressed by the polymer layer and the metal layer can deform evenly without change in resistivity. Accordingly, the results of bending test revealed that the copper coating was uniform and the attachment between metal and substrate is good enough to maintain its conductivity during the application [45,46].

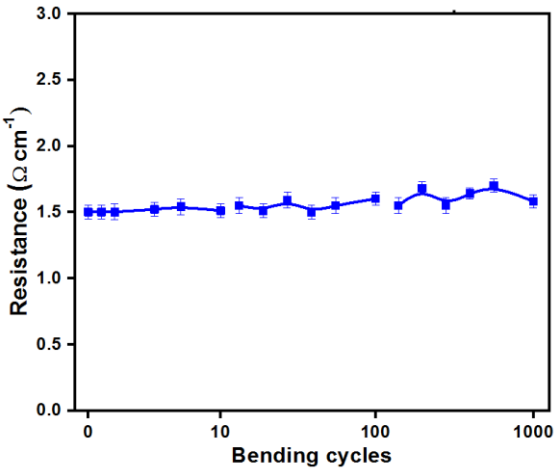

Figure 9. The effect of bending cycles on the Cu-PSCNFs resistance

5.4. Conclusion

Cellulose acetate nanofibers were successfully electrospun. The deacetylation process has been done with NaOH to prepare cellulose nanofibers. Electrically conductive cellulose nanofibers were prepared by deposition of Cu on the nanofibers by means of ELD process. The ELD process parameters were optimized, and then Cu deposition was done at the optimized condition. SEM images revealed the nanofibrous structure even after ELD process. FTIR and contact angle analysis showed the deacetylation process, and Cu coating has been done properly. The Cu coated cellulose nanofiber had a good antibacterial performance against S. aureus and B. subtilis as model bacteria. Cu deposition improved the mechanical performance of the nanofibers. The Cu-coated cellulose nanofibers demonstrated a high conductivity (amount of 983.5 S/cm conductivity) which was stable even after 1000 cycles of bending. Accordingly, the results demonstrated that the Cu-coated cellulose nanofibers could be a great candidate for wearable electronics for biomedical application.

References

1. Gan, L.; Geng, A.; Wu, Y.; Wang, L.; Fang, X.; Xu, L.; Mei, C. *Polymers (Basel)* **2020**, *12*.

2. Tang, J.; Zhao, R.; Yin, X.; Wen, Y.; Shi, Y.; Zhu, P.; Chen, Z.; Zeng, R.; Tan, L. *Journal of Biomedical Nanotechnology* **2019**, *15*, 1432.

3. Chinnappan, A.; Baskar, C.; Baskar, S.; Ratheesh, G.; Ramakrishna, S. *J. Mater. Chem. C* **2017**, *5*, 12657.

4. Heo, J. S.; Eom, J.; Kim, Y.-H.; Park, S. K. *Small* **2018**, *14*, 1703034.

5. Seyedin, S.; Zhang, P.; Naebe, M.; Qin, S.; Chen, J.; Wang, X.; Razal, J. M. *Mater. Horiz.* **2019**, *6*, 219.

6. Chen, P.; Li, H.; Hu, S.; Zhou, T.; Yan, Y.; Pan, W. *J. Mater. Chem. C* **2015**, *3*, 7272.

7. Hussain, N.; Yousif, M.; Ali, A.; Mehdi, M.; Ullah, S.; Ullah, A.; Khan, F.; Soo, I. *Materials Chemistry and Physics* **2020**, *255*, 123614.

8. Li, K.; Zhen, H.; Niu, L.; Fang, X.; Zhang, Y.; Guo, R.; Yu, Y.; Yan, F.; Li, H.; Zheng, Z. *Advanced Materials* **2014**, *26*, 7271.

9. Tu, H.; Xie, K.; Ying, D.; Luo, L.; Liu, X.; Chen, F.; Duan, B.; Fu, Q.; Zhang, L. *ACS Sustainable Chem. Eng.* **2020**, *8*, 14927.

10. Gopiraman, M.; Jatoi, A. W.; Hiromichi, S.; Yamaguchi, K.; Jeon, H.-Y.; Chung, I.-M.; Ick Soo, K. *Carbohydrate Polymers* **2016**, *149*, 51.

11. Greish, Y. E.; Meetani, M. A.; Al Matroushi, E. A.; Shamsi, B. A. *Carbohydrate Polymers* **2010**, *82*, 569.

12. Lee, H.; Kim, S.; Shin, S.; Hyun, J. *Carbohydrate Polymers* **2021**, *253*, 117238.

13. Phan, D.-N.; Dorjjugder, N.; Khan, M. Q.; Saito, Y.; Taguchi, G.; Lee, H.; Mukai, Y.; Kim, I.-S. *Cellulose* **2019**, *26*, 6629.

14. Hou, M.; Xu, M.; Li, B. *ACS Sustainable Chemistry & Engineering* **2018**.

15. Pandey, P. A.; Bell, G. R.; Rourke, J. P.; Sanchez, A. M.; Elkin, M. D.; Hickey, B. J.; Wilson, N. R. *Small* **2011**, *7*, 3202.

16. Grodzicki, A.; Łakomska, I.; Piszczek, P.; Szymańska, I.; Szłyk, E. *Coordination Chemistry Reviews* **2005**, *249*, 2232.

17. Yu, Y.; Yan, C.; Zheng, Z. *Advanced Materials* **2014**, *26*, 5508.

18. Liu, X.; Zhou, X.; Li, Y.; Zheng, Z. *Chemistry – An Asian Journal* **2012**, *7*, 862.

19. Garcia, A.; Polesel-Maris, J.; Viel, P.; Palacin, S.; Berthelot, T. *Advanced Functional Materials* **2011**, *21*, 2096.

20. Huang, Q.; Liu, L.; Wang, D.; Liu, J.; Huang, Z.; Zheng, Z. *J. Mater. Chem. A* **2016**, *4*, 6802.

21. Liu, L.; Yu, Y.; Yan, C.; Li, K.; Zheng, Z. *Nat Commun* **2015**, *6*, 1.

22. Liu, X.; Chang, H.; Li, Y.; Huck, W. T. S.; Zheng, Z. *ACS Appl. Mater. Interfaces* **2010**, *2*, 529.

23. Wang, X.; Yan, C.; Hu, H.; Zhou, X.; Guo, R.; Liu, X.; Xie, Z.; Huang, Z.; Zheng, Z. *Chemistry - An Asian Journal* **2014**, *9*, 2170.

24. Das, M.; Goswami, U.; Kandimalla, R.; Kalita, S.; Ghosh, S. S.; Chattopadhyay, A. *ACS Appl. Bio Mater.* **2019**, *2*, 5434.

25. Qin, F.; Fang, Z.; Zhou, J.; Sun, C.; Chen, K.; Ding, Z.; Li, G.; Qiu, X. *Biomacromolecules* **2019**, *20*, 4466.

26. Becherini, S.; Mitmoen, M.; Tran, C. D. *ACS Appl. Mater. Interfaces* **2019**, *11*, 44708.

27. Das, M.; Goswami, U.; Ghosh, S. S.; Chattopadhyay, A. *ACS Appl. Bio Mater.* **2018**, *1*, 2153.

28. Li, J.; Kang, L.; Wang, B.; Chen, K.; Tian, X.; Ge, Z.; Zeng, J.; Xu, J.; Gao, W. *ACS Sustainable Chem. Eng.* **2019**, *7*, 1146.

29. Tang, L.; Zhu, L.; Tang, F.; Yao, C.; Wang, J.; Li, L. *Langmuir* **2018**, *34*, 14570.

30. Wang, Y.; Li, J.; Li, B. *J. Agric. Food Chem.* **2016**, *64*, 5736.

31. Neufeld, M. J.; Harding, J. L.; Reynolds, M. M. *ACS Appl. Mater. Interfaces* **2015**, *7*, 26742.

32. Bunge, M. A.; Ruckart, K. N.; Leavesley, S.; Peterson, G. W.; Nguyen, N.; West, K. N.; Glover, T. G. *Ind. Eng. Chem. Res.* **2015**, *54*, 3821.

33. Khatri, Z.; Mayakrishnan, G.; Hirata, Y.; Wei, K.; Kim, I.-S. *Carbohydrate Polymers* **2013**, *91*, 434.

34. Ahmed, F.; Ayoub Arbab, A.; Jatoi, A. W.; Khatri, M.; Memon, N.; Khatri, Z.; Kim, I. S. *Ultrasonics Sonochemistry* **2017**, *36*, 319.

35. Hussain, N.; Yousif, M.; Ali, A.; Mehdi, M.; Ullah, S.; Ullah, A.; Mahar, F. K.; Kim, I. S. *Materials Chemistry and Physics* **2020**, *255*, 123614.

36. Hussain, N.; Mehdi, M.; Yousif, M.; Ali, A.; Ullah, S.; Hussain Siyal, S.; Hussain, T.; Kim, I. S. *Nanomaterials* **2021**, *11*, 531.

37. Sudiarti, T.; Wahyuningrum, D.; Bundjali, B.; Arcana, I. M. *IOP Conf. Ser.: Mater. Sci. Eng.* **2017**, *223*, 012052.

38. Khatri, Z.; Ahmed, F.; Jhatial, A. K.; Abro, M. I.; Mayakrishnan, G.; Kim, I.-S. *Cellulose* **2014**, *21*, 3089.

39. Kweon, O. Y.; Lee, S. J.; Oh, J. H. *NPG Asia Materials* **2018**, *10*, 540.

40. Hashemikia, S.; Hemmatinejad, N.; Ahmadi, E.; Montazer, M. *Materials Science and Engineering: C* **2016**, *59*, 429.

41. Phan, D.-N.; Dorjjugder, N.; Saito, Y.; Khan, M. Q.; Ullah, A.; Bie, X.; Taguchi, G.; Kim, I.-S. *Materials Today Communications* **2020**, *25*, 101377.

42. Wang, C.; Yang, H.; Chen, F.; Peng, L.; Gao, H.; Zhao, L. *Results in Physics* **2018**, *10*, 891.

43. Sun, G.; Zhang, M.; He, J.; Ni, P. *Journal of Polymer Science Part A: Polymer Chemistry* **2009**, *47*, 4670.

44. Liu, S.; Hu, M.; Yang, J. *J. Mater. Chem. C* **2016**, *4*, 1320.

45. Korzeniewska, E.; De Mey, G.; Pawlak, R.; Stempień, Z. *Scientific Reports* **2020**, *10*, 8310.

46. Li, T.; Huang, Z. Y.; Xi, Z. C.; Lacour, S. P.; Wagner, S.; Suo, Z. *Mechanics of Materials* **2005**, *37*, 261.

CHAPTER 6

Conclusion

In this dissertation, flexible and highly conductive electrospun nanofibers were successfully fabricated by the simple ELD technique. Different types of polymers including aramide recycled polyethylene terephthalate, nylon 6 were used to prepared nanofibers mats using electrospinning technique.

Considering results and discussions of ELD technique, successfully prepared highly durable and electrically conductive aramid nanofibers (ANFs). Copper metal particles were deposited on aramid nanofibers by electroless deposition. The parameters including time and temperature were studied and optimized. The characterizations of prepared material including FE-SEM, EDX, XRD, XPS, FTIR and TGA were performed. Significantly, the deposition of Cu particles attained low electrical resistance about 1.5ohm/cm^2 and provided flexibility. The as-prepared Cu-ANFs has a good electrical conductance and could be used in various applications such as wearable electronics, flexible displays, and energy storage.

In this research study, copper-coated r-PET nanofibers were successfully fabricated by the process of electroless deposition. The optimized temperature was observed as 40 °C, and the optimized time of 15 min was set for proper copper deposition on the r-PET nano-fibers. The SEM images evidently showed the fibrous morphology of the r-PET nanofibers with an average diameter of 350 nm, and the copper-coated r-PET nanofibers retained the fibrous morphology with a slight increase in the average diameter of 700 nm. The opti-mized copper-coated r-PET nanofibers were composed of 71.6% copper and showed a low electrical resistance of 0.1 Ω. Moreover, the r-PET nanofibers were flexible and showed good mechanical strength. As-prepared, conductive r-PET nanofibers have good potential and could be used in many applications such as wearable electronics, flexible sensors, and energy storage.

In this study, highly conductive N6 NFs were successfully fabricated by the simple ELD technique. The SEM analysis showed bead-free neat N6 NFs with an average diameter of 200 nm. After ELD, the conductive N6 NFs showed an increase up to 400 nm. The EDX results showed that N6 NFs have densely covered with aggregates of copper nanoparticles. Moreover, FTIR and XPS results confirm the copper deposition on N6 NFs. The water contact angle results indicate a significant change in hydrophilicity/hydrophobicity of N6 NFs in surface modification and the ELD processes, validating our successful copper deposition on N6 NFs. Parameters including time (10 min), temperature (40℃), pH (13), and volume (500 ml) were optimized for successful copper deposition on N6 NFs during the ELD process. The copper-coated N6 NFs showed a high 12 mg/cm weight gain of copper particles and the lowest resistance of 0.6 Ω. Furthermore, copper-coated N6 NFs obtained 961.5 S/cm conductivity. Thus, our proposed material copper-coated N6 NFs can be used in many electrical applications such as flexible and wearable devices.

Cellulose acetate nanofibers were successfully electrospun. The deacetylation process has been done with NaOH to prepare cellulose nanofibers. Electrically conductive cellulose nanofibers were prepared by deposition of Cu on the nanofibers by means of ELD process. The ELD process parameters were optimized, and then Cu deposition was done at the optimized condition. SEM images revealed the nanofibrous structure even after ELD process. FTIR and contact angle analysis showed the deacetylation process, and Cu coating has been done properly. The Cu coated cellulose nanofiber had a good antibacterial performance against S. aureus and B. subtilis as model bacteria. Cu deposition improved the mechanical performance of the nanofibers. The Cu-coated cellulose nanofibers demonstrated a high conductivity (amount of 983.5 S/cm conductivity) which was stable even after 1000 cycles of bending. Accordingly, the results demonstrated that the Cu-coated cellulose nanofibers could be a great candidate for wearable electronics for biomedical application.

Acknowledgments

All praises to almighty Allah, the most gracious and the most merciful.

and Durood o Salam to Muhammad PBUH wa All e Muhammad a.s. First and foremost,

I would like to praise and thank God, the almighty, who has granted countless blessing, knowledge, and opportunity to the writer. so that I have been finally able to accomplish the thesis.

I would like to praise and thank to Imam Mahdi (atfs). Our belief is that Imam (a.s) knows about all our affairs and is always ready to help us. He is aware of our action & he helps us even if we don't ask or seek His help. Imam Mahdi (atfs)

I would like to express my special appreciation and thanks to my advisor Professor Ick Soo Kim, you have been a tremendous mentor for me. I would like to thank you for encouraging my research and for allowing me to grow as a research scientist. Your advice on both research as well as on my life have been invaluable.

My sincere appreciation is for Prof. Zeeshan Khatri, who has remained my mentor from my University life, Prof. Zeeshan guided and supported me to enter Japan and encouraged me to go for higher studies and helped me to take right decision on right time.

I would also like to thank Prof. Kobayashi Shunichi, Prof. Zhu Chunhong, Prof. Lieva Van Langenhove, Prof. Kai Wei, Prof. Tanweer Hussain, Prof. Farooq Ahmed Arain and Prof. Najma Memon for their guidance, counselling and help.

I would like appreciate Ms. Katayama yukari, Ms. Tomoko Ikeda and Ms saito yuki, from secretariat office Shinshu University, they supported me in all my difficult conditions and helped like family members during my studies at Shinshu University.

I am thankful to my friends, Mr. Muzamil Khatri, Mr. Mujahid Mehdi, Mr. Aizaz Ali, Mr. Abdul Gaffar Abro, Mr. Hader Shah, Mr. Safdar Ali, Mr. Umair Sarwar, Mr. Akhtiar Hussain, Mr. Mola Bux, and Mr. Muhammad Yousaf.

A special thanks to my family. Words cannot express how grateful I am to my mother, father (late), and siblings for all of the sacrifices that you have made on my behalf. Your prayer for me was what sustained me thus far. I would also like to thank Benazir Muhammad. Thank you for supporting me for everything.

Special thanks to Mr. Yamashita Kentaro who assisted me to prepare necessary documentation at Shinshu University and Kim lab members (Mr. Sanaullah, Ms. Motahira Hashmi, Mr. Azeemullah, Mr. Muhammad Nauman Sarwar, Mr. Yusuke Saito, Mr. Phan Duy Nam, Mr. Dawood Kharaghani, Mr. Mohammad Qamar Khan, Mr. Yuji Suzuki, Mr. Yuki Kikuchi, Mr. Takami Yamaguchi, Mr. Kousei Wada, Ms. Wang Feifei, Mr. Sun Lei, Mr. Md. Kaiser Haider) for spending such a great time for 3 years.

At the last but not least, I am very thankful to Rotary Yoneyama Memorial Foundation for thier financial support during my studies. The Rotary Yoneyama Memorial Foundation has paid for my study expense and allowing me to focus on my academic pursuits. Without your donationtion, I couldn't be able to complete my studies.